



Suspended Load Estimation in Data Scarce Rivers

Nikolaos Efthimiou¹

Received: 10 July 2024 / Accepted: 2 September 2024
© The Author(s) 2024

Abstract

Sediment rating curves (SRCs) are tools of satisfactory reliability in the attempt to describe the sediment regime in catchments with limited or poor-quality records. The study valorised the most suitable SRC development method for the estimation of the coarse suspended sediment load at the outlet of nine Mediterranean sub-watersheds. Four established grouping techniques were assessed, to minimize the uncertainty of the results, namely simple rating curve, different ratings for the dry and wet season of the year, hydrographic classification, and broken line interpolation, at three major Greek rivers (Aliakmon, Acheloos – upper route, Arachthos). The methods' performance was benchmarked against sediment discharge field records, utilizing statistical measures and graphical analyses. The necessary observations were conducted by the Greek Public Power Corporation. The results were site/station dependent, and no methodology emerged as universally accepted. The analysis designated that the simple rating curve performs best at the cross-sections Moni Ilarion, Moni Prodromou, and Arta bridge, the different ratings for the dry and wet season of the year at Grevena bridge and Gogo bridge, the hydrographic classification at Velventos and Plaka bridge, and the broken line interpolation at Avlaki dam and Tsimovo bridge. In this regard, the study advocates the use of multiple SRC methods. Despite its limitations, the method merits a rather simple and cost-effective generation of a (continuous, detailed, sufficiently accurate) synthetic suspended sediment discharge timeseries, with high interpolating, extrapolating and reproducibility potential. The success of the application could benefit, among others, water quality restoration and dam management operations.

Keywords Northwestern Greece · Suspended sediment discharge · Sediment rating curves · Empirical sediment load equations

✉ Nikolaos Efthimiou
efthimiou@fzp.czu.cz; efthimiounik@yahoo.com

¹ Fac Environ. Sci., Czech Univ. Life Sci. Prague, Prague, Czech Republic

1 Introduction

Detached soil fragments enter a watershed's hydrographic network as the 'byproduct' of the ongoing soil surface; riverbed; bank erosion processes. Based on their origin, fluvial sediments are categorized as wash load and bed load material. Wash load is produced only during flood events. It is the result of erosional processes that take place exclusively at the catchment surface, i.e., outside the drainage network, and is usually in suspension. Bed load on the other hand consists of streambed material, it is either in traction or suspension, and is the only source of sediments during the dry season.

Bed load is typically estimated using the methodologies of Gilbert (1914), Schoklitsch (1930), Einstein (1948; 1950), Meyer-Peter and Müller (1948), which are based on the tractive force theory¹ (Lane 1937, 1955). Gilbert's research (1914) made foundational contribution to the study of bed load transfer in watercourses. He investigated the laws that govern bed load movement, and the interrelation of load quantity with the stream's slope and discharge, and the debris' comminution level. He introduced the term 'traction' to describe sediment movement along the riverbed, where larger particles like gravel (2–80 mm) and pebbles (4–64 mm) are rolled, slid, or bounced (saltated) by the force of flowing water. His work laid the groundwork for understanding sediment transport dynamics and the development of modern fluvial geomorphology. Schoklitsch (1930) developed an empirical formula to estimate the bed load transport rate based on water discharge and sediment size. His work introduced the concept of a critical shear stress or threshold that must be exceeded for bed material to start moving, refining earlier models of sediment transport. The formula became widely used in hydraulic engineering and river management, as it provided a practical tool for calculating sediment movement in natural streams. Einstein's 1948 work provided a mathematical framework for estimating the rates at which sediment particles are transported along the riverbed, influenced by factors such as water flow, sediment size, and channel characteristics. His 1950 publication introduced the 'bed-load function', a tool used to calculate the rate at which sediment particles are carried by flowing water, influenced by the same factors. Meyer-Peter and Müller (1948) developed the empirical Meyer-Peter-Müller (MPM) equation, to predict bed load transport in rivers. Their work focused on how sediment is transported along the riverbed by the force of water flow. The MPM equation introduced the concept of shear stress as the driving factor for particle movement, with bed load transport occurring only when shear stress exceeds a certain critical threshold. Suspended load is estimated by the equations of Lane and Kalinske (1941), and Einstein (1964), in which suspension is described by the diffusion and dispersion concept². Lane and Kalinske (1964) developed a model that described how finer particles, such as

¹ It was developed for marginal sediment transport conditions. It assumes that along a watercourse and its surrounding area critical shear forces occur – for an alluvial stream (its bed can be eroded or aggregated) it's a force sufficient enough to cause the mobilization of particles otherwise stable at its banks or shores. Most research has been conducted in laboratory conditions.

² Diffusion occurs as individual sediment particles move randomly due to turbulence, spreading from areas of higher concentration to lower concentration within the water. This random (molecular) movement helps distribute the particles evenly across the flow. It's a molecular-scale process driven by the kinetic energy of particles. Dispersion refers to the spread of particles or solutes in a fluid due to variations in velocity or flow conditions in addition to molecular diffusion. It's a larger-scale process often observed in fluid flows. Faster currents carry sediment farther, while slower currents cause particles to settle or spread less. Together, these processes ensure the sediment is distributed and transported throughout the river system, influencing its overall sediment load and deposition patterns.

silt and clay, are transported in suspension by the flow of water. Their work emphasized the role of turbulent flow in keeping sediment particles suspended and how sediment concentration depends on water velocity and turbulence. They also highlighted the distinction between bed load and suspended load, providing a more comprehensive framework for analysing sediment transport in river systems. In 1964, Einstein expanded on his earlier work by addressing suspended sediment load transport in rivers. He developed a more detailed theory that explained how sediment particles are carried in suspension by the turbulence of flowing water. Einstein's model considered the vertical distribution of sediment concentration, showing that finer particles remain suspended longer while coarser ones settle more quickly. His work emphasized the complex interaction between flow velocity, turbulence, and particle size, contributing significantly to the theoretical understanding and prediction of suspended sediment transport in river systems. Other empirical methods (calibration required; natural watercourse conditions need to be considered) are the Leopold and Maddock (1953), Fleming (1969), and Kennedy (1895) formulas, which are based on the regime theory³ (Lindley 1919).

Suspended load estimation has gained increasing attention by the scientific community over the last decades. Researchers focus on the impact (level, means) of soil erosion (Sui et al. 2005), riparian zone characteristics (Steiger et al. 2001; Nicholas 2003), specific sources of sediment, e.g., landslide debris, riverbanks (Prestegard 1988; Laubel et al. 2000) on a watercourse's budget, and the negative effects of high sediment supply on the natural and anthropogenic environment. Regarding the latter, the chemical, physical, and biological properties of aquatic ecosystems are degraded by excessive nutrient; trace metal; organic compound; pesticide volumes (Lloyd et al. 1987; Paul et al. 2024) attached to displaced fragments that enter the fluvial network through runoff (Neal et al. 2006; Singh and Stenger 2018). Eutrophication, water temperature rise, decrease of photosynthesis rates, drop of dissolved oxygen levels, fish kills (lack of oxygen, clogged gills), migration of sensitive species are indicative consequences. Furthermore, flood risk soars due to canal silting caused by deposition build-up (Kavian et al. 2016). Besides, the proper function of infrastructure is tampered. In the case of hydroelectric dams (Fig. 9), their reservoirs gradually lose their active storage capacity – the Sanmenxia (China) and Mead (Hoover Dam, USA) reservoirs lose annually approximately 1.7% and 0.3%, respectively (Sloff 1991) – flood storage capacity is reduced, equipment is damaged, and pressure is exerted on the base of the dam (Schleiss et al. 2016; Paschalidis et al. 2021). Moreover, irrigation and drainage networks suffer from equipment clogging and silting, harbour services are affected by silting, drinking water quality declines requiring increased treatment costs (Waters 1995), recreational activities are restricted. In this regard, the United States Environmental Protection Agency (USEPA) classified suspended sediment concentration (SSC) as one of the major causes of river impairment (USEPA 1996, 2017).

At worldwide scale circa 14×10^9 t of suspended load and 1×10^9 t of bed load ends up in the oceans (Walling 1984), and the fertile surface soil layer is reduced by 57.5 mm/1000 y. Soil loss (by extension sediment deposition) does not only depreciate the natural capital, but is also a severe monetary threat. Brown (1948) estimated the annual cost of sedimenta-

³ An alluvial channel can regulate its features (depth, width, gradient) creating a dynamic state of equilibrium, in which it can transport a certain amount of water containing a given amount of material. During a climatic cycle it is assumed that the sum of net sedimentation and erosion is zero. Most research has been conducted in the field.

tion in the USA at circa \$175 M, an amount exceeding several billion dollars in today's prices. Clark et al. (1985) raised the cost (1980 prices) to \$6.1 B, \$2.2 B of which are owed to farmlands. Mahmood (1987) estimate the annual reservoir remediation cost due to active storage depletion at approximately \$6 B, globally. The annual sediment removal cost from the reservoirs of the EU and UK is circa €2.3 B for sediment volumes produced by water erosion; including all other soil loss processes, i.e., gullies, landslides, quarrying, etc., the cost elevates to €5–8 B per year (Panagos et al. 2024).

Hence, the accurate quantification of suspended load becomes essential for the design of appropriate watershed; river management (Kuhnle and Simon 2000) and pollution control strategies (Gao et al. 2007). Systematic sediment discharge measurements, however, are costly and time-consuming, they require specialized personnel and/or well-maintained gauging stations to perform them, and they depend on natural conditions during the sampling. To this end, approximations of different theoretical background and complexity are implemented (Wren et al. 2000; Gao 2008), depending on resources availability. These span from simple deterministic methods such as the sediment rating curves (SRC) (Asselman 2000; Moradinejad 2024) to comprehensive ones, including watershed modelling (Arnold et al. 1993; Mariani et al. 2024), turbidity monitoring (Lewis 1996; Rasmussen et al. 2009), artificial intelligence techniques like fuzzy logic (Lohani et al. 2007; Buyukyildiz and Kumcu 2017) and Artificial Neural Networks (ANNs) (Jain 2001; Sharma et al. 2015), automated pumping samplers (Herman et al. 2008; Gettel et al. 2011), etc. The applicability of some (turbidity monitoring, automated samplers) is limited by high operational costs (installation, calibration, functioning, maintenance), while the validity of others (models) is questioned by the scarcity and/or poor quality of field data that hinder the validation of the simulated results.

In Greece, a country that faces similar limitations, a long-term national-scale sampling program could only be realized by a public agency – in this case the Greek Public Power Corporation (PPC). The apparent merits of the compiled database, comprising Q_s and simultaneous discharge-suspended sediment discharge records ($Q-Q_s$) at several cross-sections nationwide, were offset by the program's deficiencies that affected the quality of outputs. In brief, (i) some stations display rather fragmented Q_s timeseries, (ii) bed load measurements were disregarded due to high cost and technical difficulties, (iii) the $Q-Q_s$ pairs recording was temporally infrequent, non-systematic, and with long non-recording intervals, and (iv) Q_s , $Q-Q_s$ data refer to past decades and they are considered obsolete, since they largely describe the designing period of dam development projects (recording continues to this day, yet the processing of raw data has stopped after their completion). The latter underline the need for a contemporary high-quality Q_s timeseries, able to accurately represent the sedimentary regime of the surveyed watercourse(s) and support modern research efforts.

In this context, the study aims to evaluate the performance of four established SRC methodologies on Mediterranean type watercourses, with specific reference to Greek rivers. The goal is to provide insight on the selection of the most suitable method per gauging station for the accurate quantification of suspended sediment discharge. The 'simple rating curve' (Asselman 2000), 'different ratings for the dry and wet season of the year' (Rovira and Batalla 2006; Walling 1977; Hu et al. 2011), 'hydrographic classification' – influenced by the 'different ratings for the rising and falling limb of the runoff hydrograph' (Glysson 1987; Jansson 1996; De Girolamo et al. 2015) – and 'broken line interpolation' (Koutsoyiannis 2000) [also known as 'piecewise linear regression' (Ryan and Porth 2007; Yang et al. 2016)]

methods were employed. Nine cross-sections of three major rivers of north-western Greece, namely Aliakmon, Acheloos (upper route), and Arachthos were surveyed. The evaluation was based on statistical and graphical analyses. To the best of the author's knowledge, this is the first time that such an extensive and manifold dataset concerning Greece is investigated in international literature. The novelty of this research lies in the sample size processed (consisted of 36 time series in total), the diversity of the watercourses (natural and modified canals), the high sedimentation rates and the impending siltation risk (catchments susceptible to erosion) that require in-depth knowledge and effective management, and the use of observed sediment discharge records as benchmark values.

2 Materials and methods

2.1 Study area

The study focuses on nine cross-sections of three major rivers of north-western Greece, namely Aliakmon, upper Acheloos (delimited by the Avlaki Dam), and Arachthos (Fig. 1). Their gauging network consists of four; one; four hydrometric stations, respectively, each

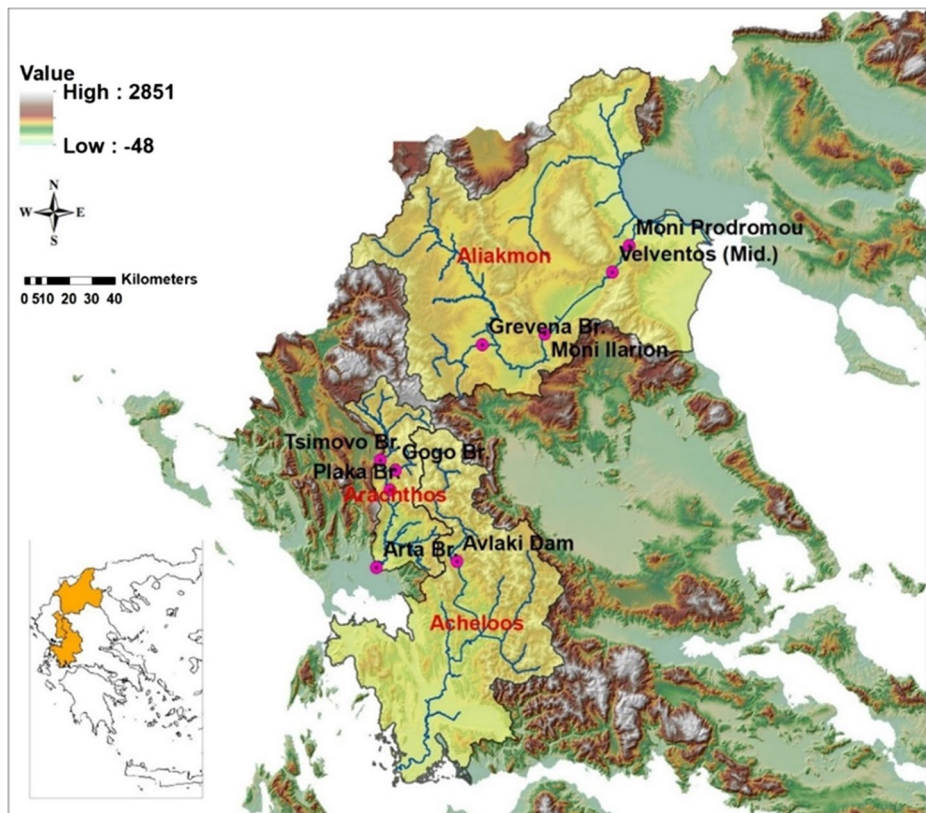


Fig. 1 Study area

demarcating the outlet of the homonym sub-watershed (Table 1). The rivers' selection was based on (i) the availability of reliable, detailed, long-term data that can underpin simulations and their validation, (ii) their subdivision potential into smaller clusters, allowing the expansion and amplification of conclusions, (iii) the diversity of flow conditions, comprising natural and modified canals (Aliakmon's route comprises a cascade of five dams that regulate its flow), (iv) the high sedimentation rates, impact of the local geological, geomorphological, climatic, hydrological conditions, and anthropogenic practices (Poulos et al. 1996), (v) their importance as key financial and development drivers, contributing to the regional water supply, irrigation, and power supply needs, and (vi) their vital role as aquatic ecosystems, promoting environmental sustainability. The watersheds' characteristics were described in previous research efforts, e.g., by Efthimiou (2019), Efthimiou et al. (2020; 2022), etc.

In brief, the climate is Mediterranean (Kottek et al. 2006), manifesting in hot, dry summers with frequent thunderstorms and mild, rainy winters. Grouped in this general category, various climatic types are met, influenced by the complex orographic and topographic configuration, i.e., strong altitudinal differences, dryland-to-sea transition, etc. For example, the Mediterranean type is prevalent at the coastal zones, the Continental type at the mountainous areas, and the Alpine type at very high altitudes (Livadas 1976; Balafoutis 1977).

Table 1 Study area attributes (retrieved from Efthimiou et al. 2022)

	Grevena br.	Moni Ilarion	Moni Prodromou	Velventos (Mid)	Avlaki Dam	Arta br.	Plaka br.	Tsimovo br.	Gogo br.
Catchment	Aliakmon	Aliakmon	Aliakmon	Aliakmon	Ache-loos	Arachthos	Arachthos	Arachthos	Arachthos
District	Western Macedonia	Western Macedonia	Central Macedonia	Central Macedonia	Thessaly	Thessaly	Thessaly	Thessaly	Thessaly
Water District	»	»	Western Macedonia	Western Macedonia	Western Central Greece	Western Central Greece	Western Central Greece	Western Central Greece	Western Central Greece
A (km ²)	855.23	4,755.11	187.49	891.92	1,354.92	1,889.69	1,000.54	646.21	204.75
Q ^a (m ³ s ⁻¹)	18.46 ^d	52.20 ^d	72.86 ^d	72.88 ^d	52.40 ^e	64.60 ^e	41.80 ^e	18.10 ^e	10.74 ^d
Period	1962-87	1962-82	1962-71	1962-70	1950-94	1962-75	1961-79	1964-01	1965-75
Qs ^b (kg s ⁻¹)	1.96	74.41	83.12	79.54	26.22	239.75	60.59	10.98	4.70
Period	1962-81	1962-81	1962-73	1962-70	1965-83	1962-75	1961-77	1964-77	1966-75
Q-Qs ^c	47	93	79	61	30	47	122	104	77
Period	1965-83	1965-83	1965-73	1965-71	1967-70	1965-73	1965-90	1966-76	1966-74

^a Discharge

^b Sediment discharge

^c Discharge-suspended sediment discharge pairs

^d Mean daily records

^e Mean monthly records

Precipitation is determined by the mountain range of Pindos, the dominant morphological element of the study area, and of Greece in general. The thrust is the extension of the Alpine system that stretches through Central and Southern Europe (Everett et al. 1986). It descends from Epirus to Peloponnese parallel to the eastern coastline of continental Greece, forming a natural barrier that demarcates western from eastern Greece in terms of climate (and water abundance) regime. Specifically, the western windward side (where the Acheloos, and Arachthos watersheds are) receives far higher precipitation depths than the eastern leeward one (where Aliakmon is), because of the rain shadow effect (Hatzianastassiou et al. 2008).

Regarding lithology, the upper Acheloos and Arachthos watersheds, part of the external Hellenides (Pindos, Ionian) geotectonic zones, comprise (mainly) erosion-prone sedimentary formations, i.e., limestones, sandstones, marls, hornstones, ophiolites, flysch, clay schists and Quaternary alluvial deposits (conglomerates, terraces, talus cones and scree, etc.). The bedrock of the Aliakmon watershed, laying over the Pindos and Sub-Pelagonian zones (western; eastern part of the basin, respectively), roughly consists of erosion-resistant material, i.e., crystalline formations, granites, volcanic rocks, ophiolites, limestones, sedimentary and volcano-sedimentary formations (Migiros et al. 2008; Karalis et al. 2018).

Besides, the upper Acheloos and Arachthos watersheds share similar topographic (mountainous terrain, steep slopes, diversification between morphological elements) and land use (extensive vegetation cover; limited plains and croplands) features. Conversely, the Aliakmon basin's relief is milder.

2.2 Datasets and Instruments

The PPC provided the Q - Q_s pair (Fig. 10), daily; monthly Q ($\text{m}^3 \text{s}^{-1}$) (Fig. 11), and monthly Q_s (kg s^{-1}) (Fig. 12) records per cross-section. The mean monthly Q , Q_s patterns are displayed in Figs. 13; 14, respectively.

The Q - Q_s pairs sampling program was hydrologically (not calendar-) based, with most measurements taken in low flow conditions. Daily Q calculations required the development of stage-discharge curves, using concurrent water stage and Q observations. Q is the average value of the nQ_i measured at the (n) sub-sectors every cross-section was divided to. Subsequently, mean daily Q was estimated by implementing the respective water stage value on each section's specific formula. Monthly Q_s derived from a fixed-interval sampling schedule, with PPC estimating total Q_s using Eqs. 1, 2.

$$G_s = K \times S_c \times Q \times 10^{-8} \quad (1)$$

$$S_c = \frac{\sum S_s Q_s}{\sum Q_s} \quad (2)$$

where, G_s (T s^{-1}) is the total sediment discharge, K a rating coefficient equal to 2.792, Q ($\text{m}^3 \text{s}^{-1}$) the cross-section's mean discharge, S_c (ppm) the cross-section's mean concentration, S_s (ppm) the sub-sector's mean concentration, Q_s ($\text{m}^3 \text{s}^{-1}$) the sub-sector's mean discharge, $S_s \times Q_s$ ($\text{m}^3 \text{s}^{-1}$) the sub-sector's partial discharge.

Q_s measurements were conducted using a Delft bottle sampler (Fig. 15) (Dijkman 1978, 1981) taking one average sub-sectoral value per section. The instrument considers coarse ($> 100 \mu\text{m}$) suspended sediment from a range of 0 (water surface) to 0.1 m depth above the

riverbed. Its operation is an application of the flow-through principle, according to which water enters the intake nozzle, flows through the chamber, and deposits the material at its ‘tail’. Sedimentation (settling) is caused by the notable reduction of flow velocity within the vessel due to its bottle-like shape (at the entry, is equal to that of the undisturbed flow). The Delft method estimates (in situ) in sufficient accuracy the volumetric quantity of the local sand transport, limiting laboratory analysis. At least 5 min of sampling time is necessary for the acquisition of statistically reliable records.

2.3 Sediment Rating Curves (SRC)

A power function (Eq. 3) is the most common SRC form (Mimikou 1982; Asselman 2000).

$$Q_s = aQ^b e \quad (3)$$

where, Q_s (kg s^{-1}) is the sediment discharge, Q ($\text{m}^3 \text{s}^{-1}$) the discharge, a (kg s^{-1}) the rating coefficient, b (dimensionless) the rating exponent, and e the multiplicative error term. The exponent values range between 0.5 and 3, and the error term follows – in theory at least – a Gaussian (log-normal) distribution (Walling 1977).

Several researchers attempted a physical interpretation of the role of a , b . Morgan (2005) correlated the high values of a with large volumes of suspended (fine) material, an easily routed load that can increase sediment transport rates. According to Peters-Kümmerly (1973) a reflects (proportionally) the watershed’s erodibility, i.e., low values indicate the presence of non-susceptible formations and vice versa. Arguably, the coefficient merely represents the value of Q_s when Q is equal to 1, hence, it cannot serve as erodibility measure since its magnitude will be largely ‘controlled’ by the catchment size. This means that unit discharge in a small catchment could classify as very high flow, whereas, in a large one as very low – well beneath the minimum record.

On the other hand, Ellison et al. (2014) correlated b with the flow’s erosive potential [so did Peters-Kümmerly (1973), Asselman (2000), and Gao (2008)] and sediment transport capacity. As its values increase, transport capacity becomes more efficient (at steeper slopes, i.e., higher b values, even low flows can ‘carry’ sediment load), reaching its full potential near the coefficient’s upper threshold. At this highly sensitive state, even a small increase of Q can affect Q_s disproportionately. Specifically, as streamflow increases, a steep positive gradient denotes rapid SSC rise, a low or level gradient designates moderate SSC rise, and a negative gradient signifies dilution due to limited sediment supply (Ellison et al. 2014). The exponent can also interpret storm event dynamics (Tanaka et al. 1983), upland sediment supply and transport within the watershed (the rate is supply limited; the degree depends on the seasonality of land cover) (Gao and Puckett 2012), variations of the rising and falling limb of hydrographs or the erodibility of different (dry, wet) regions (Park 1992), the extend of new sediment sources (Syvitski et al. 2000), etc.

2.4 Statistical Measures

2.4.1 Statistical Bias Correction Factor (BCF)

The non-parametric bias correction factor (BCF) (Eq. 4) or ‘smearing’ estimator of Duan (1993) is used for the correction of the back-transformation bias from logarithmic to arithmetic space.

$$BCF = \frac{1}{n} \sum_{i=1}^n b^{r_i} \quad (4)$$

where, n is the size of the population, i.e., the number of samples (arithmetic space) or regression residuals (logarithmic space), b is the logarithm base, and r_i is the difference of observed against estimated sediment concentration per sample i measured in logarithmic units.

2.4.2 The Nash-Sutcliffe Efficiency (NSE) Index

The Nash-Sutcliffe efficiency (NSE) (Nash and Sutcliffe 1970) is a time-series convergence index, and a measure of the dispersion (scatter) of observed records based on their divergence from their mean value, as the fraction denominator of Eq. 5 indicates. NSE is the ratio of residual variance to measured data variances, acquiring values in the range $-\infty$ to 1. Negative values indicate poor model performance, i.e., failure to reproduce the observed mean. Contrary, values close to 1 are optimal, evidence of high convergence between observed and simulated series.

$$NSE = 1 - \left[\frac{\sum_{i=1}^N (O_i - P_i)^2}{\sum_{i=1}^N (O_i - \bar{P}_i)^2} \right] \quad (5)$$

where, N is the number of points, O_i the observed values, P_i the simulated values, \bar{P}_i the mean value of the population.

3 Results

3.1 Sediment Rating Curves Development

Alternative methods are introduced in the attempt to minimize the uncertainty of the SRC results. Among them, the hydrological (rising/falling limb of the hydrograph) and seasonal [wet/dry season; monthly (Mao and Carrillo 2017)] stratification of the Q - Q_s pairs with different equations per period/stage, the use of complex (polynomial) formulas (Cordova and Gonzalez 1997; Horowitz 2003), the calibration for different precipitation intensity ranges

(Guzman et al. 2013), etc. However, none is considered universally accepted (Sivakumar and Wallender 2004) and the choice lies with the researcher.

This study utilized four different grouping methods for the $Q-Q_s$ pairs, namely the (i) simple rating curve, (ii) different ratings for the dry and wet season of the year, (iii) hydrographic classification, and (iv) broken line interpolation (Table 2, Figs. 16, 17, 18, 19, 20, 21, 22, 23 and 24). Method (i) employs a single formula to describe the entire dataset. Method (ii) categorizes the $Q-Q_s$ population according to the recording period into dry (June to November) and wet (December to May) season. In method (iii) the grouping is a function of the magnitude of flow, defined by the inflection point (IP) that separates low ($Q \leq \text{IP}$) from high ($Q > \text{IP}$) flows. IP is equal to the mean annual Q value multiplied by the 1.2 constant. However, in the summer, rising stages could still occur when Q is below that threshold, and in the winter, flows exceeding the threshold could belong to the falling stage (Efthimiou et al. 2022). Method (iv) follows a similar approach, i.e., clustering in two discharge classes, however, in this case the IP is retrieved by a trial-and-error process considering the physical characteristics of the surveyed rivers. The objective is to simultaneously minimize the fitting error (if that is the only concern, there is a risk the stratification may end up in a very rough ‘broken line’) and the roughness of the sequential segments of the curve.

The stratification is followed by a regression analysis (least squares fitting), performed on the logarithms of the $Q-Q_s$ pairs. The logarithmic space is selected for (i) presentation reasons, since there the curves ‘become’ straight lines, and (ii) meeting the theoretical hypotheses of normal distribution and homoscedasticity (constant variance) of the Q_s residuals (Ferguson 1986; Cohn et al. 1992; Asselman 2000). The descriptive equations of methods (ii) to (iv) comprise two distinct formulae, i.e., one per segment.

3.2 Simulated Suspended Sediment Discharge

The mean daily Q records were applied on the SRC formulas, developing four simulated (coarse, $> 100 \mu\text{m}$) Q_s series per cross-section. The monthly (Figs. 25, 26, 27, 28, 29, 30, 31, 32 and 33), mean monthly (Fig. 2), and annual (Fig. 3) load was estimated as the average Q_s per timestep. The convergence between observed and simulated data is also displayed.

The transition from logarithmic to arithmetic space inherits a back-transformation bias, i.e., the distribution of the Q_s residuals is not normal (deviation from the theoretical principle mentioned in § 3.1); their mean value is > 0 (Koch and Smillie 1986). The bias is usually negative, leading to underestimated Q_s . According to Ferguson (1986), the underestimation is analogous to the variance of the residuals (additive error terms of the log-linear regression). It occurs because in the arithmetic plot the power function (curve) passes through the arithmetic means of the $Q-Q_s$ pairs, while in the log-log plot (line) through the geometric ones, and the former are systematically higher than the latter. In wash load conditions where the deviation is higher {the mean square error of the log-transformed regression σ^2 (> 0 ; 0 when no dispersion around the regression line occurs) increases, causing the multiplicative error terms to attain higher values} the underestimation grows (Ferguson 1986; Singh and Durgunoglu 1989; Asselman 2000).

Among the several methods proposed for the elimination of the back-transformation bias, e.g., Bradu and Mundlak (1970), Jones (1981), Ferguson (1986), Koch and Smillie (1986), Cohn et al. (1989), Duan (1983), etc., the ‘smearing’ estimator of Duan (1993) was

Table 2 SRC attributes (retrieved from Efthimiou et al. 2020)

Catchment	Station	Period	Q (m ³ s ⁻¹)	Meth-od ^c	Pairs	BCF ^d	a ^e	b ^f	IP	r ²	NSE ⁱ	
Aliakmon	Grevena br.	1962-87	18.25 ^a	i	47	1.71	0.0219	1.264		0.51	0.91	
				ii _a	36	1.64	0.009	1.5129		0.37	0.99	
				ii _b	11	1.69	0.0261	1.2972		0.58		
				iii _a	25	1.88	0.0074	1.5716	21.91 ^g	0.18	0.93	
				iii _b	22	1.48	0.0283	1.1297		0.48		
				iv _a	22	1.48	0.0283	1.1297	22.00 ^h	0.48	0.93	
		iv _b	25	1.88	0.0074	1.5716		0.18				
		Moni Ilarion	1962-82	51.95 ^a	i	93	2.36	0.0029	2.0925		0.68	0.93
					ii _a	63	1.44	0.0001	2.7351		0.80	0.75
					ii _b	30	1.75	0.006	2.1981		0.82	
					iii _a	55	2.43	0.00002	3.0949	62.33 ^g	0.62	-7.85
					iii _b	38	2.86	0.0093	1.7753		0.48	
	iv _a				42	2.90	0.0074	1.8615	66.00 ^h	0.50	-	
	Moni Prodromou	1962-71	72.60 ^a	i	79	1.60	0.0007	2.3722		0.68	10.86	
				ii _a	62	1.37	0.0007	2.3654		0.78	0.78	
				ii _b	17	1.44	0.0002	2.8149		0.85		
				iii _a	40	1.18	0.0003	2.5804	87.12 ^g	0.56	0.89	
				iii _b	39	1.64	0.0007	2.3949		0.52		
				iv _a	35	1.55	0.0003	2.6425	80.00 ^h	0.52	0.75	
		Velventos (Mid)	1962-70	72.68 ^a	i	61	1.41	0.0023	2.1735		0.60	0.73
					ii _a	48	1.30	0.0004	2.5284		0.71	0.19
					ii _b	13	1.01	0.0003	2.8933		0.81	
					iii _a	33	1.50	0.0031	2.1274	87.21 ^g	0.40	0.95
					iii _b	28	1.30	0.0226	1.5645		0.43	
iv _a					16	1.15	0.0033	2.1108	64.00 ^h	0.64	0.74	
Achelous	Avlaki Dam	1950-94	52.40 ^b	i	30	1.45	0.0012	2.1107		0.57	0.70	
				ii _a	25	1.19	0.0007	2.2192		0.78	0.44	
				ii _b	5	1.49	0.0012	2.3104		0.72		
				iii _a	17	1.22	0.00003	2.9418	62.88 ^g	0.66	0.70	
				iii _b	13	1.22	1.514	0.1266		0.006		
				iv _a	12	1.23	1.186	0.1984	60.00 ^h	0.01	0.74	
	Arachthos br.	1962-75	64.62 ^b	i	47	2.95	0.0005	2.3471		0.70	0.69	
				ii _a	34	2.23	0.00001	3.0266		0.88	0.12	
				ii _b	13	1.43	0.0259	1.7617		0.79		

Table 2 (continued)

Catchment	Station	Period	Q (m ³ s ⁻¹)	Meth- od ^c	Pairs	BCF ^d	a ^e	b ^f	IP	r ²	NSE ⁱ	
Plaka br.	1961-79	41.81 ^b	ii _a	25	1.71	0.00003	2.9343	77.54 ^g	0.72	0.17		
			ii _b	22	2.31	0.8174	0.2697	0.01				
			iv _a	27	2.39	0.0679	1.0177	100.00 ^h	0.14	0.18		
			iv _b	20	1.23	0.00002	3.0729	0.65				
			i	122	4.30	0.0065	1.8493	0.38	0.37			
			ii _a	87	1.96	0.00008	2.8494	0.70	0.38			
			ii _b	35	3.45	0.1699	1.2165	0.20				
			iii _a	57	1.52	0.000002	3.739	50.17 ^g	0.59	0.66		
			iii _b	65	6.12	0.1606	0.8759	0.05				
			iv _a	79	5.65	0.2304	0.7547	60.00 ^h	0.04	0.47		
			iv _b	43	1.62	0.00002	3.1966	0.61				
			i	104	6.24	0.0176	1.6936	0.43	-2.51			
			ii _a	72	1.51	0.0006	2.5316	0.81	-0.66			
			ii _b	32	5.09	0.0947	1.4762	0.25				
Tsi- movo br.	1964-01	18.07 ^b	iii _a	58	2.46	0.0002	2.809	21.68 ^g	0.65	0.28		
			iii _b	46	6.55	0.2075	0.7483	0.03				
			iv _a	79	4.99	0.1312	0.9434	40.00 ^h	0.37			
			iv _b	25	1.61	0.0001	3.0202	0.66	0.73			
			i	77	2.30	0.001	2.8174	0.66	0.73			
			ii _a	65	2.34	0.001	2.7911	0.67	0.74			
			ii _b	12	1.78	0.0007	3.1407	0.58				
			iii _a	41	2.56	0.009	2.1162	13.04 ^g	0.21	0.67		
			iii _b	36	1.37	0.003	2.1998	0.41				
			iv _a	63	2.31	0.0007	3.0072	20.00 ^h	0.55	0.42		
			iv _b	14	1.09	0.00009	3.4986	0.77				
			Gogo br.	1965-75	10.87 ^a	ii _a	65	2.34	0.001	2.7911	0.67	0.74
						ii _b	12	1.78	0.0007	3.1407	0.58	
						iii _a	41	2.56	0.009	2.1162	13.04 ^g	0.21
iii _b	36	1.37				0.003	2.1998	0.41				
iv _a	63	2.31				0.0007	3.0072	20.00 ^h	0.55	0.42		
iv _b	14	1.09				0.00009	3.4986	0.77				

^a Mean daily data^b Mean monthly data^c Methods: i Simple rating curve, ii_a Wet season of the year (December-May), ii_b Dry season of the year (June-November), iii_a Rising limb of the runoff hydrograph (Q_{high}> IP), iii_b Falling limb of the runoff hydrograph (Q_{low}< IP), iv_a Broken line interpolation (Q<IP), iv_b Broken line interpolation (Q>IP)^d Bias correction factor^e Rating coefficient^f Rating exponent^g Inflection point: Q=1.2×Q_{average}^h Inflection point: trial and error procedureⁱ Nash-Sutcliffe efficiency index (observed against simulated mean monthly values)

ultimately selected due to its widespread use. However, there is no consensus on which BCF is prevalent.

The unbiased estimator of the true load is acquired by applying the BCF (multiplying it directly with the rating coefficient) to the simulated Q_s time series. This causes the curve to shift upwards, towards higher loads (Figs. 16, 17, 18, 19, 20, 21, 22, 23 and 24).

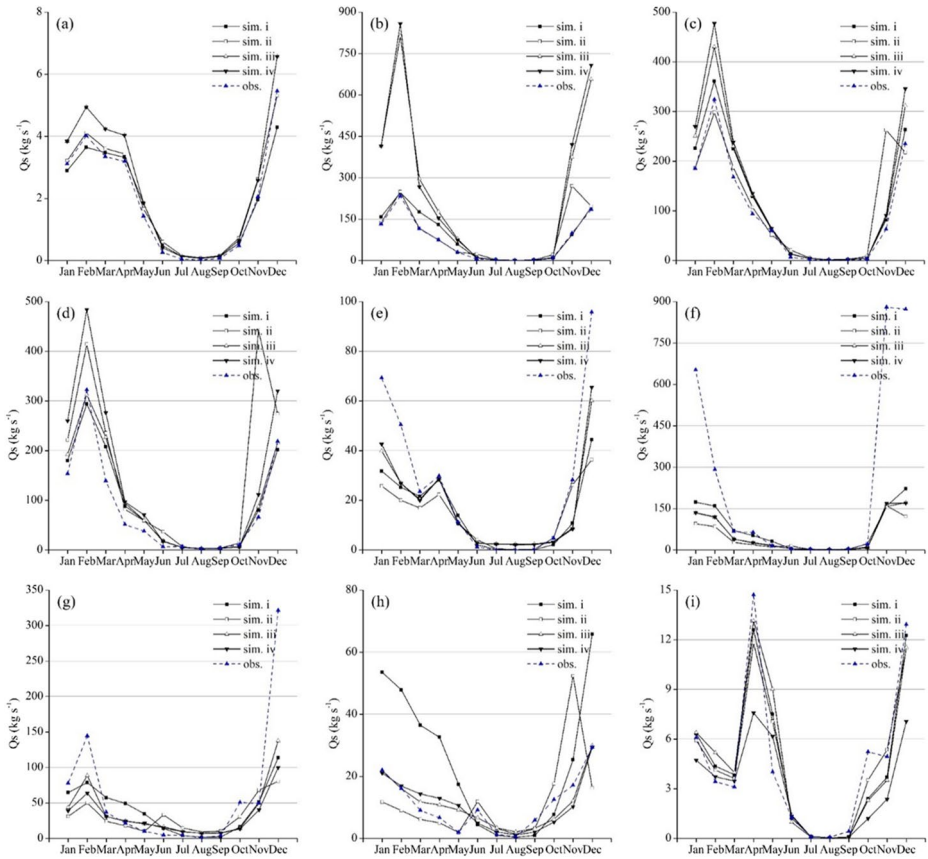


Fig. 2 Mean monthly simulated suspended sediment discharge (Q_s , kg s^{-1}) and convergence with field measurements at the station; river (a) Grevena bridge, Aliakmon, (b) Moni Ilarion, Aliakmon, (c) Moni Prodromou, Aliakmon, (d) Velventos, Aliakmon, (e) Avlaki dam, upper Acheloos, (f) Arta bridge, Arachthos, (g) Plaka bridge, Arachthos, (h) Tsimovo bridge, Arachthos, (i) Gogo bridge, Arachthos

4 Discussion

4.1 Datasets Variability

4.1.1 Causality Drivers

Suspended sediment discharge (Q_s) largely depends on the watershed's (riverbed; banks included) sediment supply, the composite detachment-transport-deposition mechanism that regulates its routing towards the fluvial network, the network's and tributary inflows' pattern that governs floodwater travel rate and distance, and the storage-mobilization-depletion cycle (Williams 1989). The latter display strong spatial and temporal heterogeneity, especially in alpine basins of diverse morphology (Lenzi et al. 2003; Mao et al. 2009). Soil loss is a multifactorial process, conditioned upon the complexity of the associated variables and the heterogeneity of their interrelations. The impact of an individual variable on the

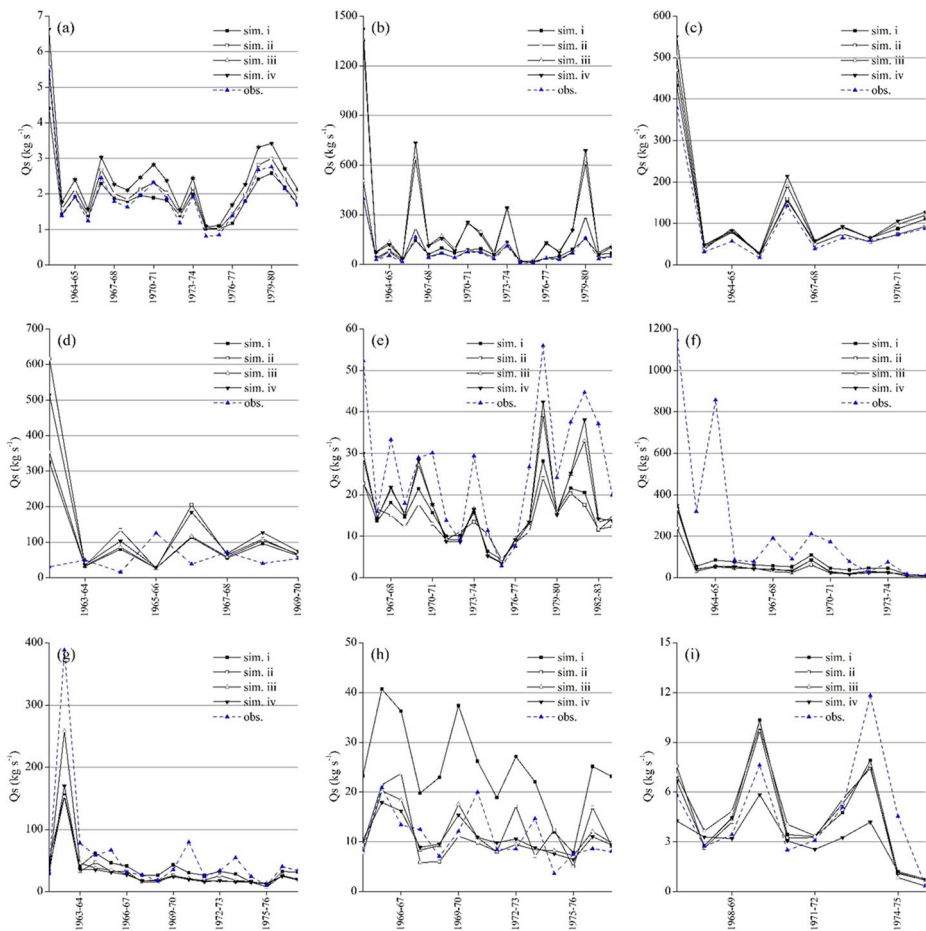


Fig. 3 Annual simulated suspended sediment discharge (Q_s , kg s^{-1}) and convergence with field measurements at the station; river (a) Grevena bridge, Aliakmon, (b) Moni Ilarion, Aliakmon, (c) Moni Prodro-mou, Aliakmon, (d) Velventos, Aliakmon, (e) Avlaki dam, upper Acheloos, (f) Arta bridge, Arachthos, (g) Plaka bridge, Arachthos, (h) Tsimovo bridge, Arachthos, (i) Gogo bridge, Arachthos

magnitude and frequency of soil displacement, though, is neither linear nor explicit, while it is often difficult to identify whether these variables act complementary or contradictory towards sediment production (or soil protection for that matter). These non-deterministic interactions need to be deciphered, without omitting the spatial component of all causality agents. Overall, physical basins, and especially mountainous landscapes, are typical non-linear, -stationary systems that result in non-Gaussian sediment load/hydrometric variables' distributions (Lenzi et al. 2003; Mao et al. 2009).

Rainfall (depth; intensity) displays distinct seasonal variation (as Q and water temperature⁴), evolving in clear cycles⁵ (intra-annual, annual), typical of the Mediterranean climate. Its spatial distribution in Greece is defined by the mountain range of Pindos that demarcates western from eastern Greece in terms of water abundance (see § 2.1). The parameter manifests in winter depths of high erosivity (Panagos et al. 2016) and intense summer thunderstorms (Kottek et al. 2006). These infrequent, transient events (Poesen and Hooke 1997) largely govern sediment rates (Martinez-Mena et al. 2001). A striking example is the formation of torrents⁶. Apart from the apparent risks entailed by the intensity of the dry season outbursts, rainfall (runoff) increases its erosive potential when falling on (flowing over) unprotected surfaces, especially from October to January, when the highest rainfall erosivity rates are met (Panagos et al. 2016). Mismanagement results to soil stripped of vegetation due to overgrazing, forest fires, and fuelwood gathering (Woodward 1995), and bare farmlands due to ‘unregulated’ tillage, cultivation, or harvesting. Fallow (continuous, or part of a crop rotation schedule), ploughing (in September, October), sowing (roughly from November–April), cultivation of vulnerable crop types or ‘unsynchronized’ phenological phases (the canopy is not fully developed during the early growth stages) (Schmidt et al. 2018; Baiamonte et al. 2019), random distribution of winter (non-irrigated; soil is assumed bare from June–November) and summer (permanently irrigated; soil is assumed bare from December–May) crops without considering the spatiotemporal patterns of rainfall, and bad post-harvesting ‘habits’⁷ leave the soil exposed to the abrading forces of rainfall and runoff. Vulnerability is increased by the abandonment of traditional conservation techniques. For example, the deterioration of terraces leads to longer slopes; greater floodwater/sediment volume and travel distance (Koulouri and Giourga 2007). Besides, deep ploughing and intensive cultivation destroy soil structure (Faust and Schmidt 2009), further exacerbating soil’s inability to sustain vegetation. Since most of the annual soil in agricultural lands is lost during few severe events (Nadal-Romero et al. 2012; Rodrigo-Comino et al. 2017) the joint rainfall-biomass density coupling becomes critical for the identification of the hazardous region-period combinations.

Other inherent characteristics of the Mediterranean landscape, namely the diverse topography (Polykretis et al. 2020), the erodible bedrock (flysch, alluvial formations, etc.) (Kosmas et al. 2001), the active tectonic processes (Bailey et al. 1993), the pedological properties, e.g., shallow profiles, low Organic Matter Content (OMC), etc. (Poesen and Hooke 1997; Canton et al. 2011) classify Mediterranean soils as highly susceptible to erosion (Cerdeira et al. 2010).

Finally, the watershed scale exerts notable influence on the accuracy of Q_s assessment (Richards and Holloway 1987), with the quality of estimates being inversely related to it (Phillips et al. 1999) – according to Walling and Webb (1988) the estimation error decreases as the basin size increases. Boyce (1975) interpreted the inverse relationship of net to gross

⁴ Water temperature affects viscosity and by extension sediment transport and soil moisture (Ramalingam and Chandra 2019).

⁵ The hydrometric variables’ seasonality is controlled by the watershed’s climate pattern, e.g., rainfall is regulated in cycles. Conversely, the temporal resolution of SSC is controlled by flow dynamics and sediment storage, regulated in intra-annual; annual (multiannual) scales. The multiannual response denotes the importance of the sediment storage/depletion cycle (Juez and Nadal-Romero 2020).

⁶ Ephemeral intermittent-flow streams responsible for the detachment and transport of severe amounts of sediment.

⁷ In Greece, the proportion of soils left bare after the harvest is approximately 57% (EUROSTAT 2014).

erosion as a function of slope steepness. This fraction (transported to on-site mean annual soil loss) is always < 1 and is reduced as the basin scale increases. Specifically, at the topographically diverse parts of the watershed, strong inclinations are responsible for the prevalence of net erosion (high detachment rates) over deposition. As watershed scale increases, mean slope decreases, causing sediment production rate per unit area to decrease accordingly. Furthermore, at larger scales, the higher number of sinks, depressions, valleys, etc., favours deposition, leading to lower net erosion rates (there and throughout) (van Rompaey et al. 2001).

4.1.2 Temporal Fluctuation

Discharge (Q) and suspended sediment discharge (Q_s) display inter- (monthly, seasonal) (Fig. 4) and intra-annual temporal variability (Fig. 5).

At the monthly scale (Fig. 12) the Q_s outliers recorded in the summer and early fall are ascribed to the outburst of intense storms falling onto bare soil (Steegeen et al. 2000; Lecce et al. 2006). During the winter and early spring, the rainfall and snowmelt patterns lead to increased streamflow, and, by extension, sediment transport. Overall, the intra-annual patterns of Q (and sediment storage; see § 1) are strongly correlated with the monthly dynamics of Q_s .

At the mean monthly scale (Fig. 4), the variables' fluctuation is depicted by inverse bell shape curves. The highest values (left/right tail) are acquired in the winter and the lowest in the summer, a common trend to all stations. May is the turning point when precipitation decreases, and the soil is adequately protected by fully grown canopies at the end of the growing season. In the warm period, from June to September, the minimal streamflow (and soil loss, due to the coupling of low intensity non-erosive storms with sufficient biomass density) is reflected in the routed sediment volume. The lowest Q , Q_s values are met to all stations in August (Figs. 4 and 6). Among them, Grevena bridge yields the minimum records at $1.62 \text{ m}^3 \text{ s}^{-1}$, and 0.02 kg s^{-1} , respectively. The maximum Q is recorded in March at Moni

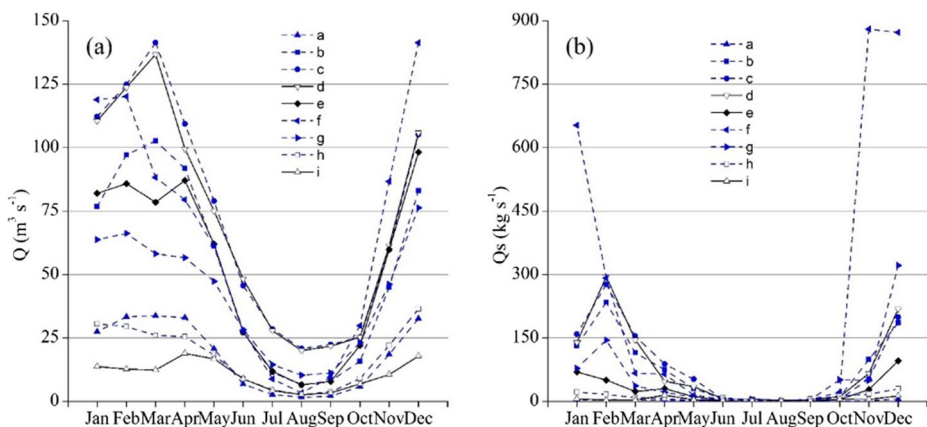


Fig. 4 Mean monthly (a) discharge (Q , $\text{m}^3 \text{ s}^{-1}$) and (b) suspended sediment discharge (Q_s , kg s^{-1}) measurements inter-annual variability at the station; river (a) Grevena bridge, Aliakmon, (b) Moni Ilarion, Aliakmon, (c) Moni Prodomou, Aliakmon, (d) Velventos, Aliakmon, (e) Avlaki dam, upper Acheloos, (f) Arta bridge, Arachthos, (g) Plaka bridge, Arachthos, (h) Tsimovo bridge, Arachthos, (i) Gogo bridge, Arachthos

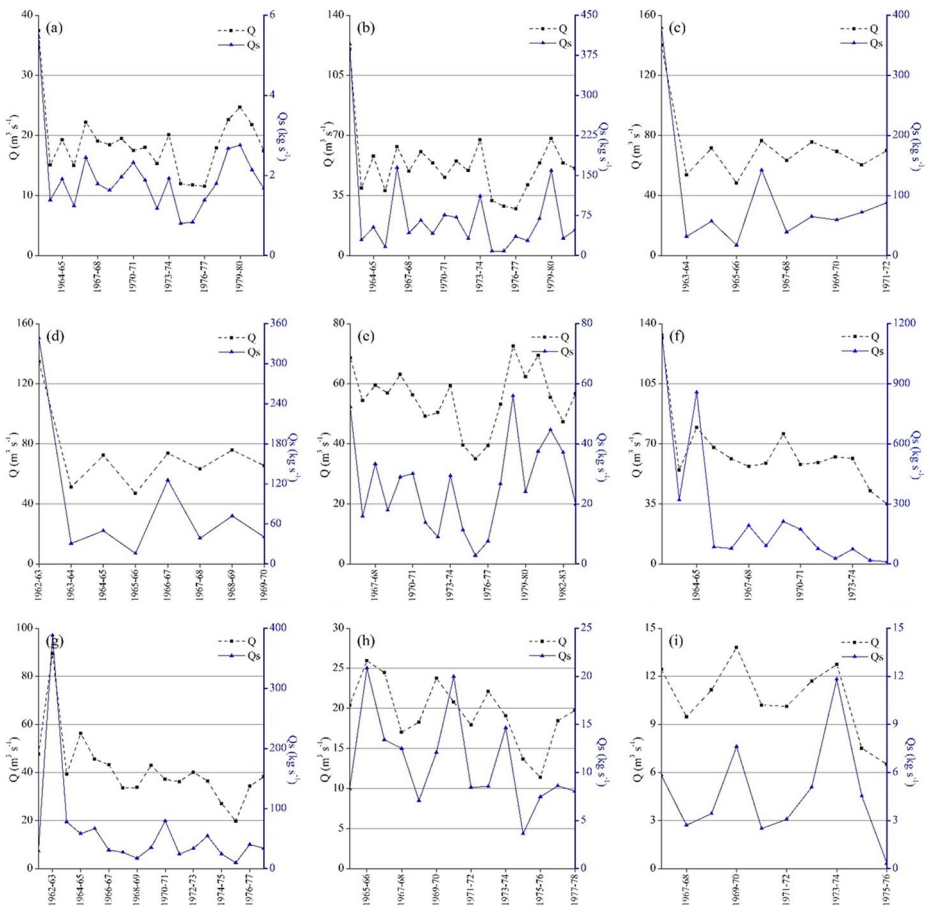


Fig. 5 Annual discharge (Q , $\text{m}^3 \text{s}^{-1}$) and suspended sediment discharge (Q_s , kg s^{-1}) measurements intra-annual variability at the station; river (a) Grevena bridge, Aliakmon, (b) Moni Ilarion, Aliakmon, (c) Moni Prodromou, Aliakmon, (d) Velventos, Aliakmon, (e) Avlaki dam, upper Acheloos, (f) Arta bridge, Arachthos, (g) Plaka bridge, Arachthos, (h) Tsimovo bridge, Arachthos, (i) Gogo bridge, Arachthos

Prodromou ($141.39 \text{ m}^3 \text{ s}^{-1}$), and the maximum Q_s in November at Arta bridge (880.10 kg s^{-1}). The individual (per station) Q , Q_s patterns are displayed in Figs. 13, 14 respectively.

At the annual scale (Fig. 5) the Q and Q_s time series display strong variability, however, there is a satisfactory convergence of their trend in most stations. The lowest mean annual Q value ($18.10 \text{ m}^3 \text{ s}^{-1}$) is calculated at Gogo bridge and the highest at Velventos ($72.88 \text{ m}^3 \text{ s}^{-1}$). The respective Q_s values are retrieved at Grevena bridge (1.96 kg s^{-1}) and Arta bridge (239.75 kg s^{-1}) (Figs. 5 and 6).

The graphical investigation of Fig. 12 reveals two evident characteristics of the Q , Q_s time series, common to all stations, i.e., strong seasonal diversification and notable deviations from the mean state. The inter-quantile range (equal to the boxplot length) and overall data range (equal to the distance between the edge of the two whiskers) illustrated in Figs. 7 and 8 verify such variability. According to Markonis et al. (2017) both are a direct impact of the Mediterranean climate and the seasonality of rainfall. These fluctuations further affect

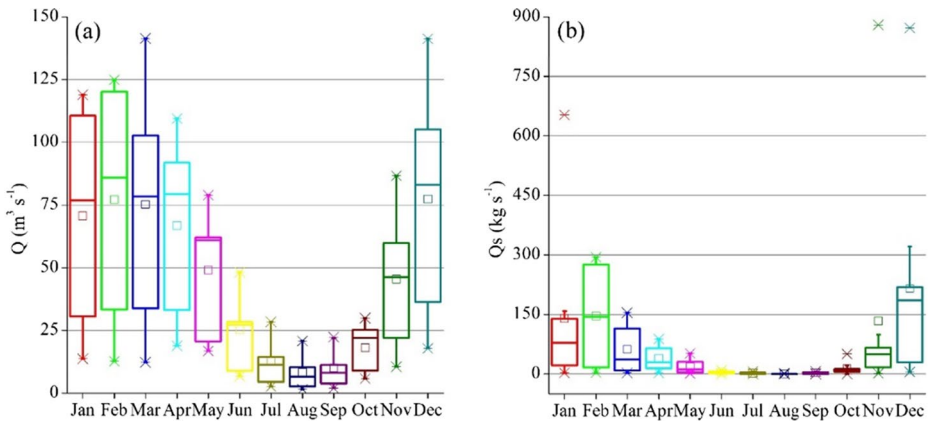


Fig. 6 Mean monthly (a) discharge (Q , $\text{m}^3 \text{s}^{-1}$) and (b) suspended sediment discharge (Q_s , kg s^{-1}) measurements value range

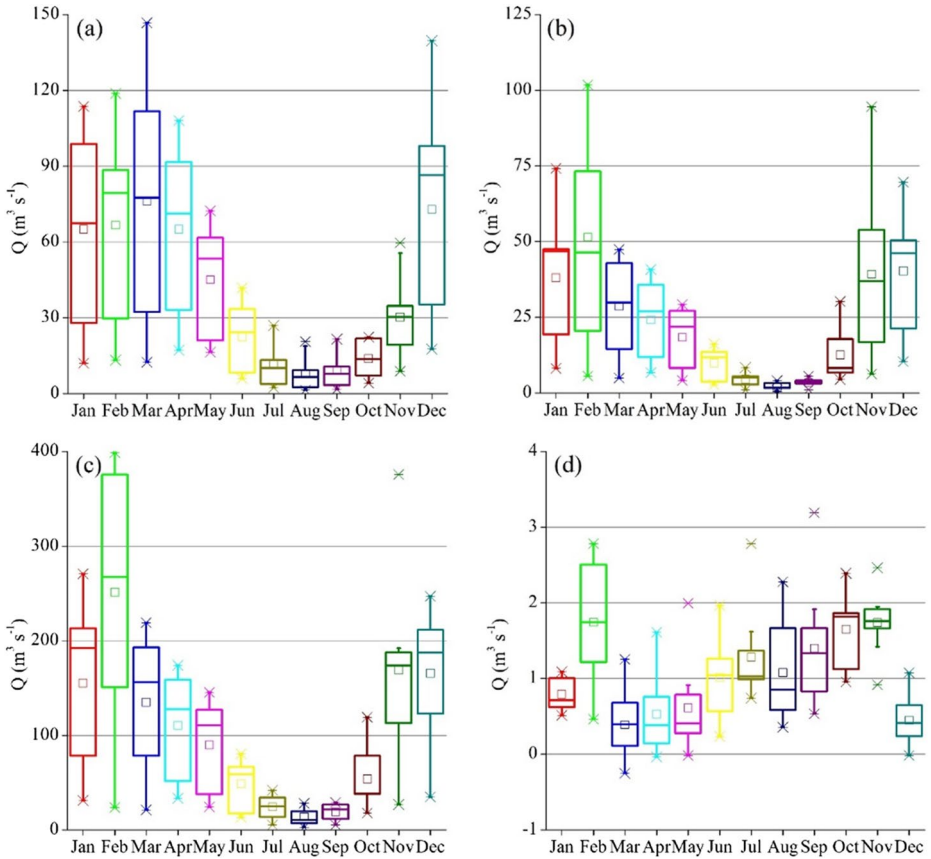


Fig. 7 Monthly statistics of discharge (Q , $\text{m}^3 \text{s}^{-1}$) measurements (a) median, (b) standard deviation, (c) maximum, (d) skewness

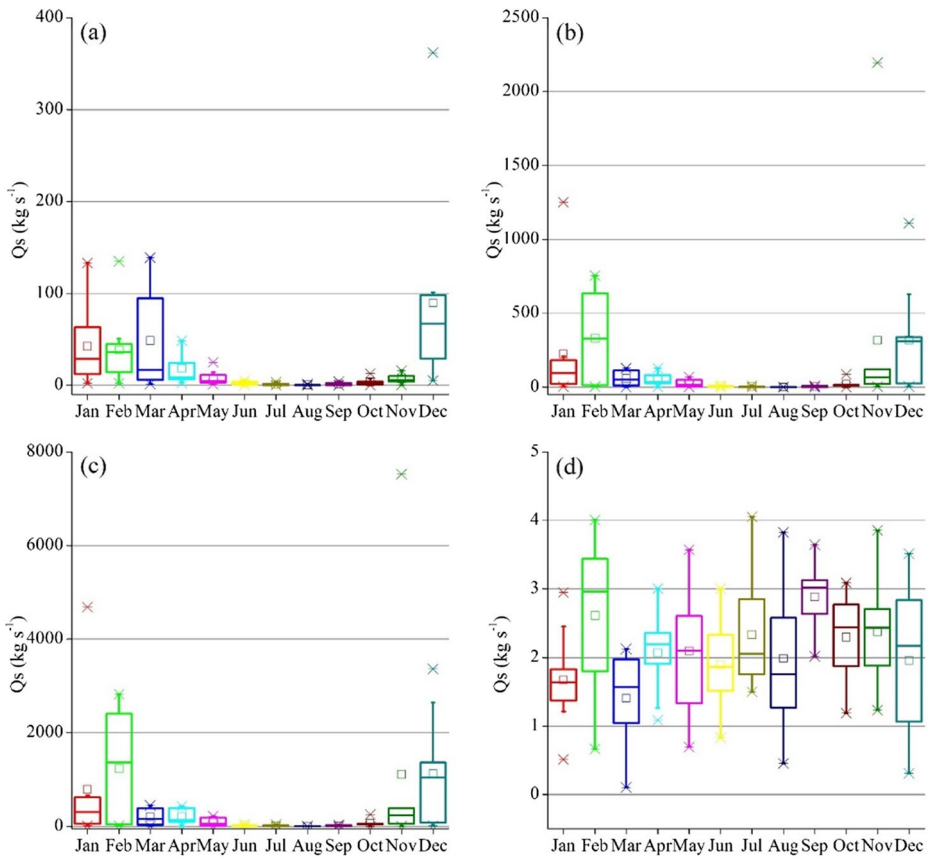


Fig. 8 Monthly statistics of suspended sediment discharge (Q_s , kg s^{-1}) measurements (a) median, (b) standard deviation, (c) maximum, (d) skewness

sediment load variability (standard deviation) and maxima (Fig. 8). However, the skewness of the time series of both variables (Figs. 7 and 8) does not depend on seasonality, yielding positive values throughout the year. This indicates that extreme deviations from the mean state can occur in various months (Efthimiou et al. 2022).

4.2 Sediment Rating Curves Deciphering

The simple rating curve (method i) uses a single equation to describe the entire range of measured Q (base flow, flood events). At the Grevena bridge station (Fig. 16(a)) the method underestimated the high Q_s records and overestimated the low ones, i.e., the application of high Q values on its formula yielded lower simulated Q_s against the observed ones, and vice versa. The former are depicted by the points above the line (wash load, few events), and the latter by those below it (base flow). Comparatively, the underprediction (wash load conditions, where most of the annual sediment load is delivered) is notably greater and more critical for the total load estimation than the overprediction (Horowitz 2003; Cox et al. 2008). This behavior is ascribed to the (i) inadequacy of the regression model to describe

the data population (Freund et al. 2006) – in other words, the limitation of a single-segment line fit to incorporate the factors known to affect sediment transport – and (ii) the effect of the Q - Q_s sampling program (the majority of records taken during low flows) on the slope of the least squares curve. The coefficient of determination (r^2) – the level of explanation of the variance of the data concentration – is rather low (51%), indicating a poor correlation between Q (independent variable) and suspended Q_s .

The different ratings for the dry and wet season of the year (method ii) clusters the Q - Q_s pairs according to their recording period. Aside from Q and Q_s , the method considers (indirectly) several temporally variable parameters, such as water temperature, storm type, vegetation cover, the erosion process (Mimikou 1982; Koutsoyiannis and Tarla 1987). At the Grevena bridge station (Fig. 16(b)), of the 47 pair measurements 11 were apportioned to the dry season (June to November) and 36 to the wet one (December to May). For every Q value, the dry season segment yields higher Q_s than the wet season one. This is ascribed to the (i) greater erosive potential of a dry season precipitation event (that has conveyed equal volume of Q), and (ii) watershed's higher sediment availability, due to physical, atmospheric, etc., conditions, e.g., high temperatures that lead to increased evapotranspiration, low soil moisture, and eventually dry and fragmented soil. Additionally, the wet season yields the highest mean and maximum Q [in this case $32.26 \text{ m}^3 \text{ s}^{-1}$ and $140.71 \text{ m}^3 \text{ s}^{-1}$ (13/02/1980), respectively], while the dry season has the lowest minimum Q ($1.29 \text{ m}^3 \text{ s}^{-1}$). The Q patterns are driven by the seasonality of rainfall and snowmelt, with Q_s following these cycles. Furthermore, the exponent of the wet season segment is relatively higher than that of the dry season (1.51 instead of 1.30), denoting more erosive power and efficient transport capacity of the flow, and of runoff (in terms of supply rate and degree) (see § 2.3). The r^2 index is rather low in both periods (wet: 37%, dry: 58%), with the Q - Q_s pairs displaying greater scatter in the first cluster.

The hydrographic classification (method iii) stratifies the Q - Q_s pairs according to the magnitude of flow. At the Grevena bridge station (Fig. 16(c)), the IP, i.e., the threshold between low and high flows, is calculated as $21.91 \text{ m}^3 \text{ s}^{-1}$, given the average daily Q ($18.25 \text{ m}^3 \text{ s}^{-1}$) for the period 1962–1988 (Table 2). Of the 47 pair measurements 25 were grouped to the high flows cluster ($Q > \text{IP}$, rising limb of the hydrograph) and 22 to the low flows one ($Q \leq \text{IP}$, falling limb of the hydrograph). For every Q value, the rising limb yields higher Q_s than the falling one. Furthermore, the slope of the segment above the IP is steeper, denoting that Q_s is increasing faster in this value range. This implies the presence of different sources of sediments, e.g., bank erosion, washed away deposits of bed material piled-up at low flow periods, riverbed deterioration, upland supply, the 'production' of which occurs during intense floods and Q rates that far exceed the IP. The r^2 index of both clusters is low, especially that of the rising limb (18%).

The broken line interpolation (method iv) also stratifies the Q - Q_s pairs according to the magnitude of flow yet following a different approach (see § 3.1). At the Grevena bridge station (Fig. 16(d)), a single IP is calculated as $22.00 \text{ m}^3 \text{ s}^{-1}$, leading to the formation of two discharge classes. It so happens that the IP in methods (iii) and (iv) is almost identical ($21.91 \text{ m}^3 \text{ s}^{-1} \approx 22.00 \text{ m}^3 \text{ s}^{-1}$), hence they both behave similarly, i.e., (a) from the 47 pair measurements 25 were grouped to the high Q cluster and 22 to the low Q one, (b) the respective segments are described by the same mathematical formulas, (c) the slope of the segment above the IP is subject to the same causes and limitations as the one of method (iii), (d) the r^2 indices are equally low. The two-segment line was selected based on the physical

characteristics of the watercourse (and the study area in general). In gravel bed rivers the riverbed surface forms an ‘armor’ layer, which is coarser than both the substrate and the suspended sediments. Past a certain Q value, the layer starts to deteriorate, or gets completely washed out. During the flood event, the exceedance of this threshold causes the exposing and mobilization of a larger range of particle sizes and the notable increase of the transport rate. Under such conditions, Q_s is further enhanced by other processes/sources of sediment, such as bank erosion. Conversely, below this threshold no exchange occurs between the suspended and the ‘shielded’ material. The fact that the IP is higher than the mean daily Q value ($18.25 \text{ m}^3 \text{ s}^{-1}$) implies that the armor layer breaks up less frequently, and extreme floods contribute more to the long-term Q_s than ordinary runoff events.

The interpretation of the curve form and placement at the other sites is analogous to that of Grevena bridge. In brief:

Moni Ilarion, Aliakmon.

The average daily Q for the period 1962-82 is $51.95 \text{ m}^3 \text{ s}^{-1}$, the IP of method (iii) ($1.2 \times Q_{\text{avg}}$) that demarcates low from high flows is $62.33 \text{ m}^3 \text{ s}^{-1}$, and the threshold of method (iv) is $66.00 \text{ m}^3 \text{ s}^{-1}$ (Table 2).

Moni Prodromou, Aliakmon.

The average daily Q for the period 1962-71 is $72.60 \text{ m}^3 \text{ s}^{-1}$, the IP of method (iii) ($1.2 \times Q_{\text{avg}}$) that demarcates low from high flows is $87.12 \text{ m}^3 \text{ s}^{-1}$, and the threshold of method (iv) is $80.00 \text{ m}^3 \text{ s}^{-1}$ (Table 2).

Velventos, Aliakmon.

The average daily Q for the period 1962-70 is $72.68 \text{ m}^3 \text{ s}^{-1}$, the IP of method (iii) ($1.2 \times Q_{\text{avg}}$) that demarcates low from high flows is $87.21 \text{ m}^3 \text{ s}^{-1}$, and the threshold of method (iv) is $64.00 \text{ m}^3 \text{ s}^{-1}$ (Table 2).

Avlaki dam, upper Acheloos.

The average daily Q for the period 1950-94 is $52.40 \text{ m}^3 \text{ s}^{-1}$, the IP of method (iii) ($1.2 \times Q_{\text{avg}}$) that demarcates low from high flows is $62.88 \text{ m}^3 \text{ s}^{-1}$, and the threshold of method (iv) is $60.00 \text{ m}^3 \text{ s}^{-1}$ (Table 2).

Arta bridge, Arachthos.

The average daily Q for the period 1962-75 is $64.62 \text{ m}^3 \text{ s}^{-1}$, the IP of method (iii) ($1.2 \times Q_{\text{avg}}$) that demarcates low from high flows is $77.54 \text{ m}^3 \text{ s}^{-1}$, and the threshold of method (iv) is $100.00 \text{ m}^3 \text{ s}^{-1}$ (Table 2).

Plaka bridge, Arachthos.

The average daily Q for the period 1961-79 is $41.81 \text{ m}^3 \text{ s}^{-1}$, the IP of method (iii) ($1.2 \times Q_{\text{avg}}$) that demarcates low from high flows is $50.17 \text{ m}^3 \text{ s}^{-1}$, and the threshold of method (iv) is $60.00 \text{ m}^3 \text{ s}^{-1}$ (Table 2).

Tsimovo bridge, Arachthos.

The average daily Q for the period 1964-01 is $18.07 \text{ m}^3 \text{ s}^{-1}$, the IP of method (iii) ($1.2 \times Q_{\text{avg}}$) that demarcates low from high flows is $21.68 \text{ m}^3 \text{ s}^{-1}$, and the threshold of method (iv) is $40.00 \text{ m}^3 \text{ s}^{-1}$ (Table 2).

Gogo bridge, Arachthos.

The average daily Q for the period 1965-75 is $10.87 \text{ m}^3 \text{ s}^{-1}$, the IP of method (iii) ($1.2 \times Q_{\text{avg}}$) that demarcates low from high flows is $13.04 \text{ m}^3 \text{ s}^{-1}$, and the threshold of method (iv) is $20.00 \text{ m}^3 \text{ s}^{-1}$ (Table 2).

In some cases, e.g., Moni Ilarion; method iia, iib, Velventos; method iia, iib, etc., r^2 is sufficiently high, acquiring its maximum value at Arta bridge (88%, method iia). According to Koutsoyiannis and Tarla (1987) this is because Q ‘embodies’ both the hydraulic characteristic of a cross section and the hydrological attributes of the watershed. Arguably, the relationship may be largely spurious (Benson 1965), considering that Q is, at the same time, the independent variable (instantaneous point measurement) and part of the depended variable (product of Q with mean SSC). Hence the goodness of fit might be rather deceptive (McBean and Al-Nassri 1988).

4.3 Validation of Simulated Suspended Sediment Discharge

The level of convergence between monthly observed and modelled timeseries (Figs. 25, 26, 27, 28, 29, 30, 31, 32 and 33) was evaluated utilizing the NSE index. In general, all methods display weakness in simulating Q_s extremes to all stations. Surprisingly, the negative deviations (underprediction) remain even after the application of the BCF. Apparently, the correction forces the curve to shift towards higher loads (see § 3.2), leading to a relatively better fit at high flows. Yet, the low and medium Q_s get overestimated. The poor fit is attributed to (i) the rather high BCF values, resulting from the obvious scatter (high standard deviation) of the error terms’ log-linear regression per sample/population, (ii) the ability level of BCF to provide reliable Q_s records (Ashmore 1986; Koch and Smillie 1986), and (iii) the fact that bias is not the dominant cause of inaccuracy (Walling and Webb 1988), against more significant sources of error, not reflected in the BCF, such as the population scatter, the seasonal fluctuations of the rating relationship, hysteretic and exhaustion effects, etc. (Walling 1977). Conversely, the total sediment volume is assessed quite satisfactory. Indicatively, at Grevena bridge (Fig. 25) method (i) continuously underestimated the observed Q_s , method (iii) and (iv) performed similarly (irregular case where the respective low; high flows segments are described by the same equations, given the almost identical IP value), continuously overpredicting the measured data, while method (ii) performed exceptionally well, successfully simulating all outliers. Overall, at such analysis, there is no distinct trend of over- or under-prediction by any method. The NSE values indicate that method (i) performs best at Moni Ilarion (0.93), Moni Prodromou (0.98), and (comparatively) Arta bridge (0.19),

method (ii) is prevalent at Grevena bridge (0.99) and Gogo bridge (0.74), method (iii) suits Velventos (0.95) and Plaka bridge (0.66), and method (iv) better fits Avlaki dam (0.74) and Tsimovo bridge (0.37).

The correlation of the monthly observed and modelled Q_s was additionally assessed employing a least squares fitting (Figs. 34, 35, 36, 37, 38, 39, 40, 41 and 42). The observed data were placed on the y-axis and the simulated values on the x-axis (Pineiro et al. 2008). Each plot depicts the $y=x$ line (45 degrees or slope equal to 1) with black colour, the trend-line ($y=a+b x$) with red colour and the regression formulas (a is the intercept, b the slope, r^2 the coefficient of determination). Indicatively, at Grevena bridge (Fig. 34) the r^2 values are extremely high for all methods, denoting minimum variance of the data pairs. Slope values > 1 (Fig. 36(a)/ method (i), 36(b)/ method (ii)) indicate underestimation and < 1 (Fig. 36(c)/ method (iii), 36(d)/ method (iv)) overestimation. Furthermore, at low flows the scatter is low, and most pairs are pinned close to the regression line. As Q increases, the dispersion widens, and the underprediction grows proportionally. This pattern, however, is not consistent. Methods (iii) and (iv), despite their overestimating trend, keep all pairs close to regression line throughout the Q range. Hence, they are more reliable to predict the variable's actual values, even at high Q where greater uncertainty occurs. The interpretation of the curve form and placement at the other sites is analogous to that of Grevena bridge.

At the mean monthly scale (Fig. 2), inverse bell curves depict the datasets fluctuation. The highest Q_s values are yielded to all stations by every method in the winter and the lowest in the summer. The minimal Q_s from June to October is ascribed to the warm period's low flow values (see § 4.1.2). All methods deliver the lowest Q_s to all stations in August. Positive deviations denote that the simulated Q_s is higher than the observed one, and vice versa. Indicatively, at Grevena bridge, methods (iii) and (iv) continuously overpredicted Q_s displaying positive divergence from the measured records, method (ii) followed the same trend but with smaller deviations, and method (i) was inconsistent with positive deviations from March to October and underprediction in the remaining months. Overall, all simulated values are considered similar, and in accordance with the observed ones. The interpretation of the curve form and placement at the other sites is analogous to that of Grevena bridge.

Although the observed Q_s (Fig. 3) displays strong intra-annual variability, there is satisfactory convergence between measured and modelled time series in most stations. Indicatively, at Grevena bridge, as in the case of the mean monthly time step, methods (iii) and (iv) continuously overpredicted Q_s , method (ii) also displayed constant positive divergence, yet it was comparatively more accurate (smaller deviations), and method (i) was anew inconsistent (no specific trend was detected).

4.4 Advantages of SRCs and Reasons of Inaccuracy in Sediment Load Estimates

SRCs can produce synthetic Q_s records of satisfactory validity at cross-sections with limited inputs (Efthimiou 2019; Efthimiou et al. 2022). The method merits a rather simple development of a continuous series of detailed (analogous to the resolution of Q) analysis of high interpolating (filling gaps of disrupted historical series), extrapolating (extending short and/or outdated series) and reproducibility potential without the requirement⁸ of a regular sam-

⁸ Required when suspended sediment load is quantified using an interpolation procedure, which assumes that daily (or weekly) sediment discharge (or concentration) can be described by instant field measurements.

pling program. The reduced sampling intensity – typical characteristic of an extrapolation⁹ procedure – allows for a straightforward cost-effective application, particularly in the case of poor financial and labor resources (Walling 1977).

However, several researchers have identified the notably greater error (80–900%) involved in sediment load estimates by SRC against field observations (Dickinson 1981; Ferguson 1986; Walling and Webb 1988; Asselman 2000; Horowitz 2003). A major reason of inaccuracy is the limitations of the Q , Q_s sampling program (Douglas 1971; Horowitz 2003). In this study, elevated cost and the technical difficulties entailed, forced the Greek PPC to omit bed load sampling and the measuring of other critical parameters, i.e., suspended load granulometry, per depth concentration distribution, etc. Furthermore, most Q - Q_s pairs were taken in low and normal flow conditions (on the rising and falling limb of the runoff hydrograph, and definitely not around its peaks), even though in Mediterranean watersheds the majority of the annual wash load volume is delivered by few flood events. In other words, the program was established on hydrological criteria rather than a systematic calendar-based approach. This means that the records were not representative of a random sample of the population (Ferguson 1986). The temporal infrequency and the long non-recording intervals hindered the program's capability to fully describe sediment transport on the surveyed rivers. Similarly, the Q dataset failed to represent the entire range of possible flows, since the mean daily Q data available cannot describe flood conditions that require finer analysis measurements. Finally, the operation of the Delft bottle induced errors in the sampling process, providing only a rough estimate of the sand transport. These are quite important, since they can rise up to 50% for single samples, even after the implementation of correction measures. Specifically, (i) the intake velocity deviates from that of the local flow, (ii) the instrument can only collect a fragment of the total sediment volume, namely the coarse ($>100\ \mu\text{m}$) suspended particles that approximate a capacity load (not supply-controlled bed material load), while the non-capacity loads consisting of finer than $100\ \mu\text{m}$ particles such as the suspended silt ($63\text{--}2\ \mu\text{m}$) and clay ($<2\ \mu\text{m}$) fractions are disregarded (Dijkman 1978, 1981), (iii) during the emerging and submerging of the bottle superfluous particles enter the nozzle, and (iv) a small part of the sample is lost during the removal of the sand-catch.

The quality of estimates is equally affected by the limitations of the SRC, namely the stationarity of the rating parameters, and errors ascribed to other intrinsic determinants like the population scatter, the statistical bias, hysteretic and exhaustion effects. To further elaborate, the non-temporal character of the a and b coefficients implies a permanent relationship between Q and Q_s , which was also adopted in this study to justify the seamless use of the rating formulas throughout the application period. However, this hypothesis does not apply in flood events, and predominately to intra-annual studies. During floods, Q and Q_s fluctuate intensely (Rieger et al. 1988; Walling and Webb 1988), while other sources of sediment, e.g., bank erosion, scouring, etc., must be considered. Hence, in such conditions, the predictability of the curves is rather poor (Blanco et al. 2010). This nonlinearity presents challenges in developing universally reliable models for sediment management (Wright and Parker 2004). Moreover, the hypothesis is violated in natural watersheds, where changes in precipitation (due to seasonal patterns, climate crisis, etc.), land cover (due to urbanization,

⁹ A regression analysis delivers the rating relationship (usually a power function) between Q_s and the magnitude of flow Q (independent variable). Extrapolation is achieved by implementing the Q records to the respective mathematical formula.

wildfires, construction sites, etc.), landscape morphology (due to landslides, earthquakes, etc.), channel morphology (the aggradation/degradation cycle), and flow fluctuation, occur over longer periods of time (Kuhnle et al. 1996; Presteggaard 1988; Yang et al. 2007).

Hysteresis is the lack of temporal homogeneity between Q_s for the same Q on the rising and falling limb of a hydrograph (Walling 1977). The greater concentration, i.e., by two or more orders of magnitude (Walling 1977), is met on the rising limb (Gurnell 1987; Kronvang et al. 1997). Specifically, gravity causes a downward transport and storage of suspended sediments at low Q . As Q rises, and especially during flood events, the turbulence of the flow forces an upward transport. These observations, though, may not be proportional to the paired flow rate records. The phenomenon could also indicate different runoff and erosion types (Seeger et al. 2004), and sediment delivery and source area (Klein 1984; Williams 1989; DiCenzo and Luk 1997). Apparently, the knowledge of sediment sources within a drainage canal, e.g., when its morphology is altered (Juez et al. 2018), is essential for the accurate calculation of the sediment budget. In this study, however, the lack of data prevented such analysis. Overall, the hysteresis phenomenon is difficult to decipher using SRC, even when different segments/data stratification per limb is employed.

The scatter of the Q - Q_s population, that largely defines the slope of the trendline, is associated with the features of the sampling program (recording frequency, flow; SSC conditions, etc.), the rating curve plot, the seasonality of the rating relationships, and the lag between SSC and Q response (Tanaka et al. 1983; Walling and Webb 1988; Roberts 1997; Gao et al. 2007). According to Walling (1977), the dispersion of the Q - Q_s pairs can be interpreted by stream hydraulics, since in natural watercourses suspended sediment load is actually a non-capacity load. Such dispersion could also be ascribed to the hysteresis effect, of short (within events) or longer (between events) duration.

The back-transformation of the Q , Q_s logarithms to arithmetic values entails a statistical bias, which is an appreciable cause of inaccuracy leading to underpredictions. The application of the BCF reduces to a large extent the deviation between observed and modelled Q_s (Ferguson 1986; Hansen and Bray 1987), yet it does not zero it out. Overall, concerns are raised about the merits of the BCF application on bias removal (see § 4.3), the responsibility extend of bias regarding sediment load estimation errors (see § 4.3) and the problems arising in the attempt to analyze long-term Q_s trends due to the interannual variability of load estimates (Walling and Webb 1988).

Size range and other intrinsic characteristics of the watersheds, e.g., the hydrological regime, affect the relative accuracy of the estimates between them. For example, the SRC does not perform well in small basins (Walling and Webb 1988). Furthermore, in this study, the Aliakmon river mainstem is modified, and the flow is regulated by a cascade of five dams. In such way, suspended routing and deposition within the watercourse is tampered, extending to the SRC development (Q - Q_s pairs) and application (Q implementation). Besides, SRCs are often specific to individual rivers or even locations within a river system. Variability in watershed characteristics such as geology, vegetation, land use, and slope can all influence sediment transport, making it difficult to transfer the curves from one site to another without the need for recalibration. This limits their broader applicability, requiring continuous monitoring and adjustments for changing conditions at each location (Horowitz 2003).

Other sources of inaccuracy are the erroneous Q measurements (Achite and Ouillon 2007; Crowder et al. 2007), the incorrect application of Q to the rating formulas (Colby 1956; Gregory and Walling 1973), and the use of mean daily Q to describe the flow range implemented

to a SCR (this could result in notable underprediction of the daily load, especially in the case of floods). The lack of high-resolution data can also hinder efforts to accurately model the effects of land use changes or climate variability on sediment dynamics (Ferguson 1986).

4.5 Implications for River Management

SRCs are an essential tool in river management. The valid quantification of a natural watercourse's sedimentary budget under different flow conditions is critical to policy makers and stakeholders for the implementation of efficient management strategies, including sediment transfer control, water quality restoration, improved reservoir operations, and effective flood mitigation.

- **Predicting sediment transport:** Excessive sedimentation can lead to reduced (active and/or flood) water storage capacity of reservoirs over time, equipment damage, and pressure exertion on the base of the dam (Schleiss et al. 2016). Understanding sediment dynamics enables the compilation of dredging schedules and sediment traps, and other solutions that optimize their performance and longevity, such as dead volume storage design, regulation planning (return period; exceedance risk), revision of operations (water storage; release time) (Molino et al. 2023).
- **Informing infrastructure design:** With knowledge of sediment loads, managers can design and operate other hydraulic structures like levees and flood channels more effectively. For example, levees can be constructed to withstand erosional forces caused by high sediment flows. This is crucial in regions prone to high sediment loads, where river infrastructure may deteriorate more rapidly without proper consideration of sediment dynamics (Brandt 2000).
- **Flood risk management:** By predicting sediment deposition and erosion, rating curves help improve flood modelling, preventing riverbed aggradation and enhancing flood prevention efforts (Horowitz 2003). When coupled with hydrologic models, they improve the ability to forecast the impacts of floods on downstream infrastructure and communities.
- **Water quality and ecosystem health:** Suspended sediment can carry pollutants, nutrients, and organic matter. High sediment loads may reduce water quality, impair aquatic habitats, and harm fish populations by smothering spawning grounds. Moreover, drinking water quality declines requiring increased treatment costs, and recreational activities are restricted. SRCs help identify critical periods when sediment loads are likely to spike, allowing for better timing of interventions aimed at preserving ecosystem health (Collins & Walling, 2007).
- **Long-term monitoring and adaptive management:** SRCs support continuous monitoring of sediment dynamics, which is crucial for adapting management strategies to changing environmental conditions, such as climate variability or land use changes.

4.6 Future Research

By focusing on improved data collection, integration with advanced modelling, and leveraging Artificial Intelligence (AI), SRCs can better predict sediment transport and enhance river management under changing environmental conditions.

Indicative suggestions include:

- **Improved data collection techniques:** Traditional SRCs rely on periodic sampling, which may miss short-term or extreme events. Advances in real-time monitoring and remote sensing technologies (Zahiri et al. 2020), such as acoustic or optical sensors, can help collect continuous sediment and flow data, improving the accuracy of sediment load predictions, particularly during storms or floods (Gray and Gartner 2009).
- **Event-based calibration:** Given that sediment transport often spikes during extreme weather events, there is a need to focus on event-based sampling (Gupta et al. 2019) to capture these anomalies more effectively. This will help develop more robust SRCs that account for variability during high-flow conditions, which traditional methods often underestimate (Asselman 2000).
- **Integration with predictive models:** The future of sediment management lies in the integration of SRCs with hydrological, geomorphological, and land-use models. These models can consider the effects of erosion, land cover changes, and climate variability, offering a more comprehensive understanding of sediment dynamics over longer time periods (Syvitski et al. 2005).
- **Machine learning and AI:** Incorporating machine learning algorithms (Kumar et al. 2019) could help improve the predictive power of sediment rating curves. By analysing large datasets and identifying patterns, AI tools could refine predictions by adapting to changing environmental conditions and complex non-linear relationships between discharge and sediment load.
- **Adaptation to the climate crisis:** As the climate crisis intensifies rainfall patterns and alters river dynamics, sediment rating curves will need to be updated more frequently. Adaptive management strategies that continuously revise and recalibrate rating curves using new data are essential for addressing the increased variability in sediment transport.
- **Holistic, system-wide approaches:** SRCs should be part of a broader, integrated river management approach. Combining sediment data with water quality, ecological health, and socioeconomic factors will support sustainable decision-making. This requires collaboration between hydrologists, ecologists, and policymakers.

5 Conclusions

The study provided insight on the most appropriate SRC development method for the estimation of coarse suspended sediment load at the outlet of nine Mediterranean sub-watersheds. The results were site/station dependent, i.e., no methodology emerged as universally accepted. The NSE values indicate that the simple rating curve performs best at the cross-sections Moni Ilarion, Moni Prodromou, and Arta bridge, the different ratings for the dry and wet season of the year at Grevena bridge and Gogo bridge, the hydrographic classification at Velventos and Plaka bridge, and the broken line interpolation at Avlaki dam and Tsimovo bridge. In this regard, the study advocates the use of multiple SRC methods followed by the quantification of the derivative uncertainty. The results are encouraging enough to valorize SRC as reliable alternative for the assessment of suspended sediment load in data-scarce rivers.

Appendix

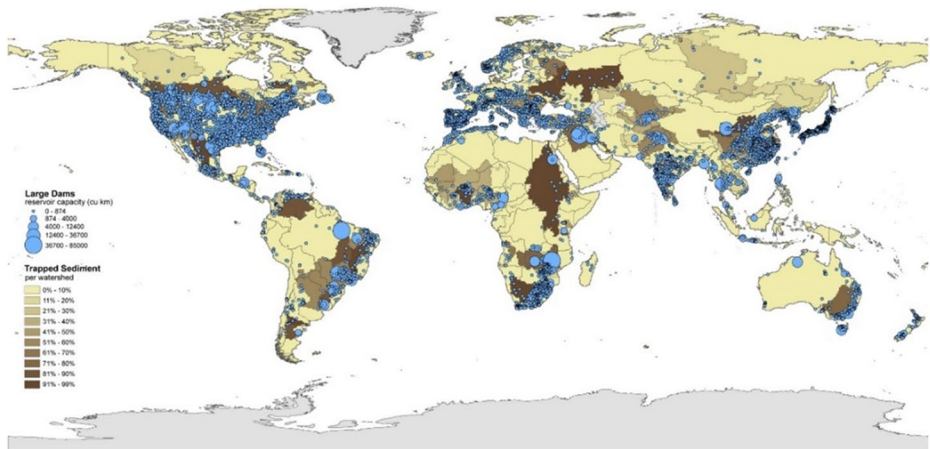


Fig. 9 Map of the global distribution of large dams and their reservoirs, overlaid with the percentage of sediment trapped within watersheds by dams. Data supplied by the Global Reservoir and Dam (GRaND) Database. <https://landscapebangalore.wordpress.com/2014/08/14/dams-sediments-erosion-from-free-association-design/>. Accessed 9 February 2024

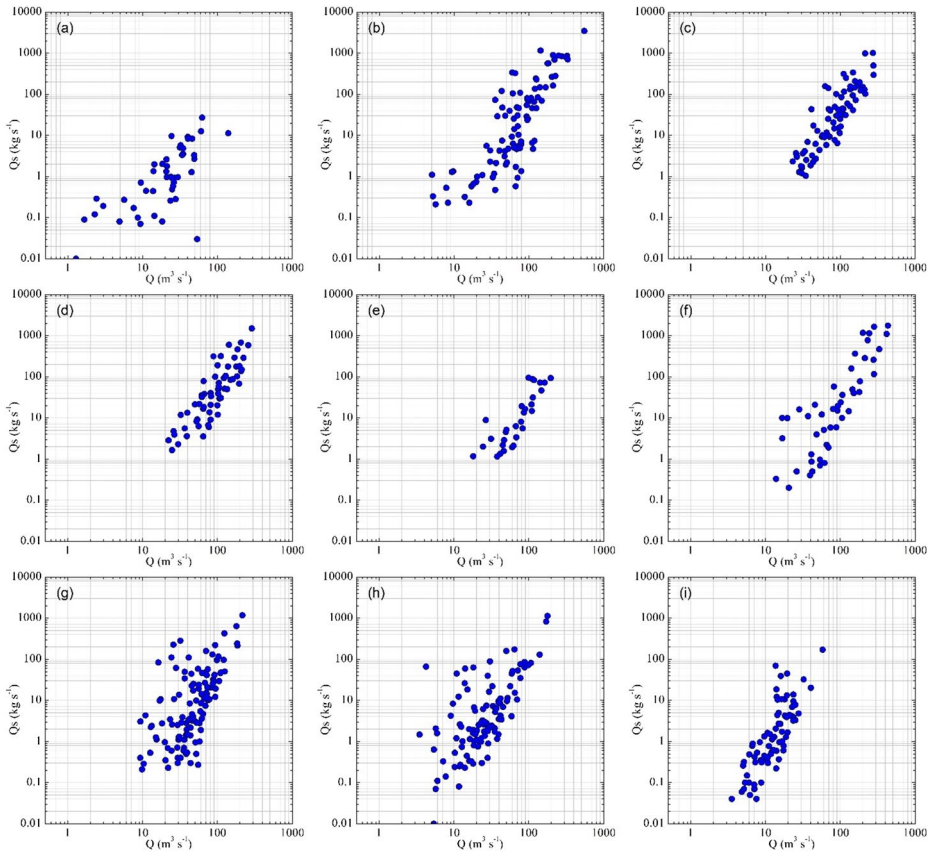


Fig. 10 Simultaneous discharge (Q) - suspended sediment discharge (Q_s) measurements (Q - Q_s pairs) at the station; river (a) Grevena bridge, Aliakmon, (b) Moni Ilarion, Aliakmon, (c) Moni Prodromou, Aliakmon, (d) Velventos, Aliakmon, (e) Avlaki dam, upper Acheloos, (f) Arta bridge, Arachthos, (g) Plaka bridge, Arachthos, (h) Tsimovo bridge, Arachthos, (i) Gogo bridge, Arachthos

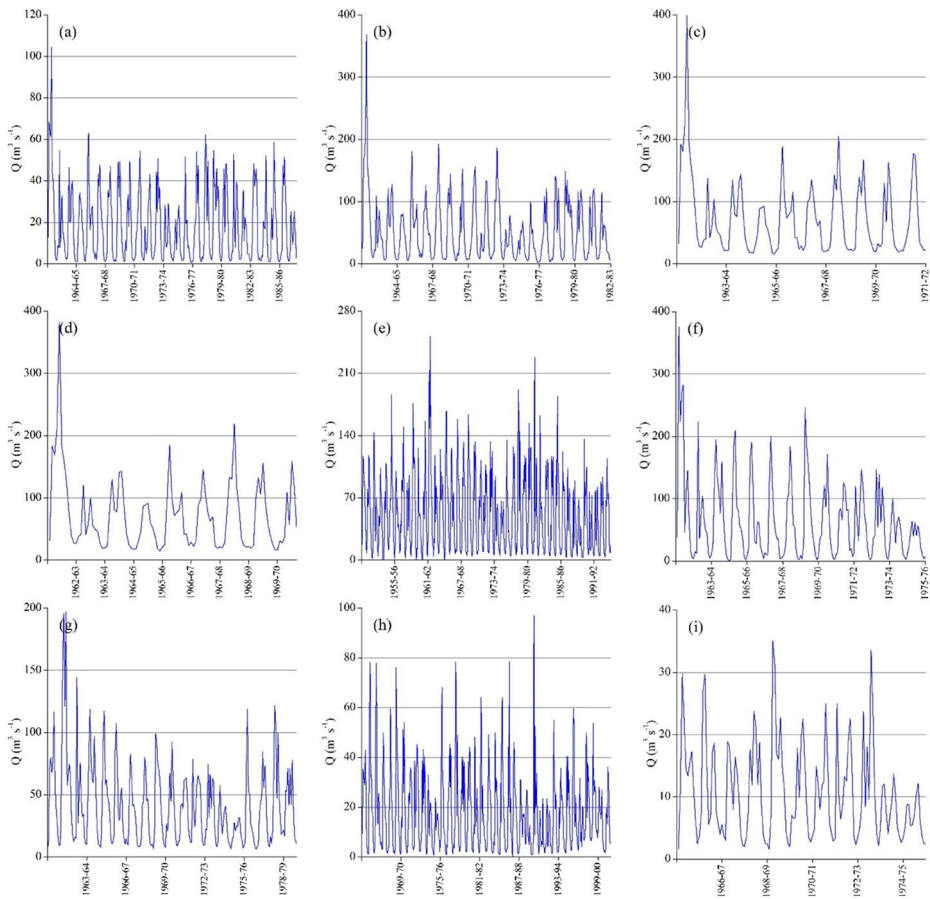


Fig. 11 Monthly discharge (Q , $\text{m}^3 \text{s}^{-1}$) measurements at the station; river (a) Grevena bridge, Aliakmon, (b) Moni Ilarion, Aliakmon, (c) Moni Prodomou, Aliakmon, (d) Velventos, Aliakmon, (e) Avlaki dam, upper Acheloos, (f) Arta bridge, Arachthos, (g) Plaka bridge, Arachthos, (h) Tsimovo bridge, Arachthos, (i) Gogo bridge, Arachthos

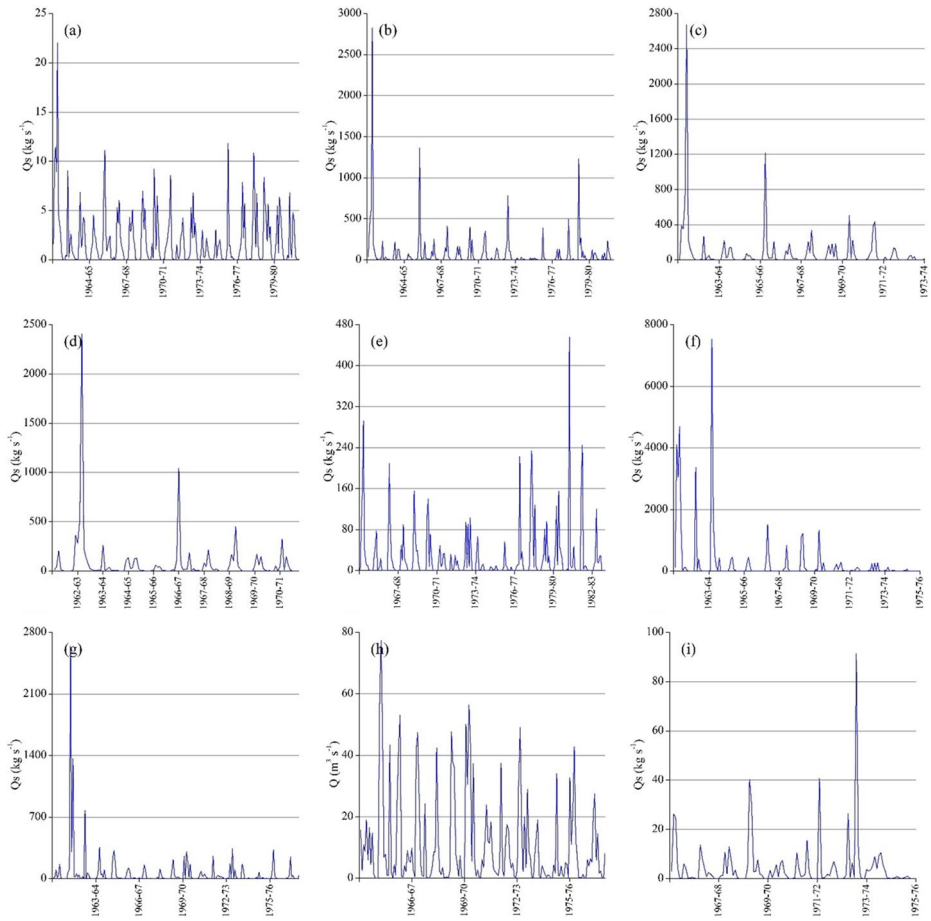


Fig. 12 Monthly suspended sediment discharge (Q_s , kg s^{-1}) measurements at the station; river (a) Grevena bridge, Aliakmon, (b) Moni Ilarion, Aliakmon, (c) Moni Prodromou, Aliakmon, (d) Velventos, Aliakmon, (e) Avlaki dam, upper Acheloos, (f) Arta bridge, Arachthos, (g) Plaka bridge, Arachthos, (h) Tsimovo bridge, Arachthos, (i) Gogo bridge, Arachthos

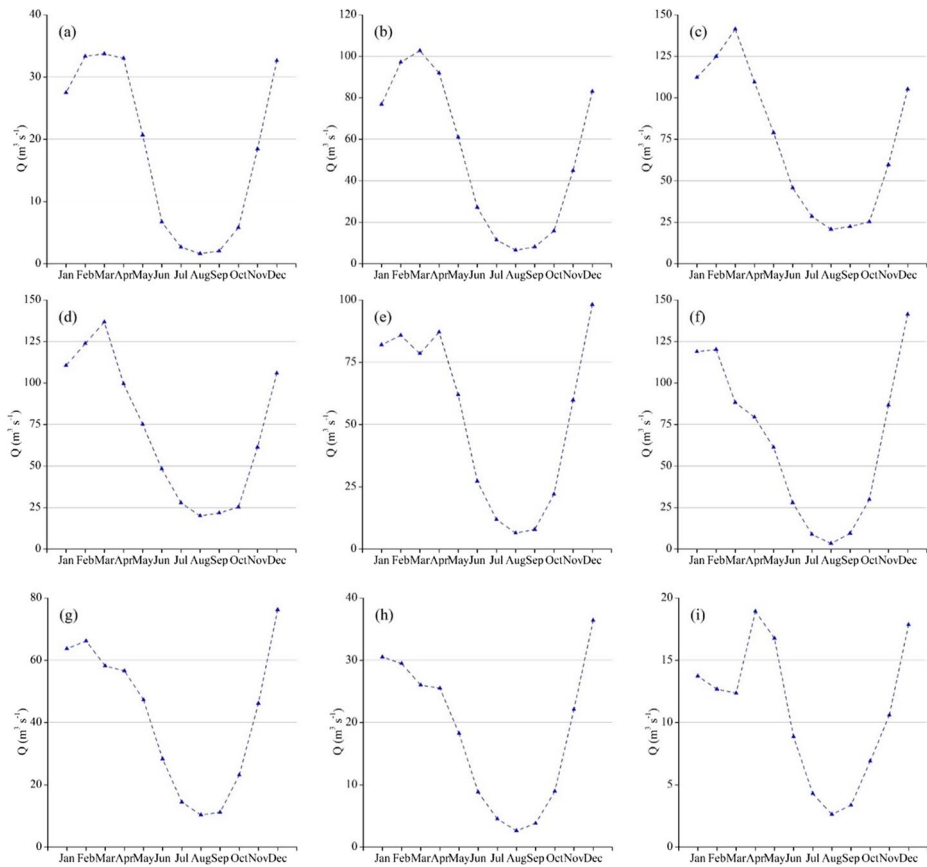


Fig. 13 Mean monthly discharge (Q , $\text{m}^3 \text{s}^{-1}$) records at the station; river (a) Grevena bridge, Aliakmon, (b) Moni Ilarion, Aliakmon, (c) Moni Prodromou, Aliakmon, (d) Velventos, Aliakmon, (e) Avlaki dam, upper Acheloos, (f) Arta bridge, Arachthos, (g) Plaka bridge, Arachthos, (h) Tsimovo bridge, Arachthos, (i) Gogo bridge, Arachthos

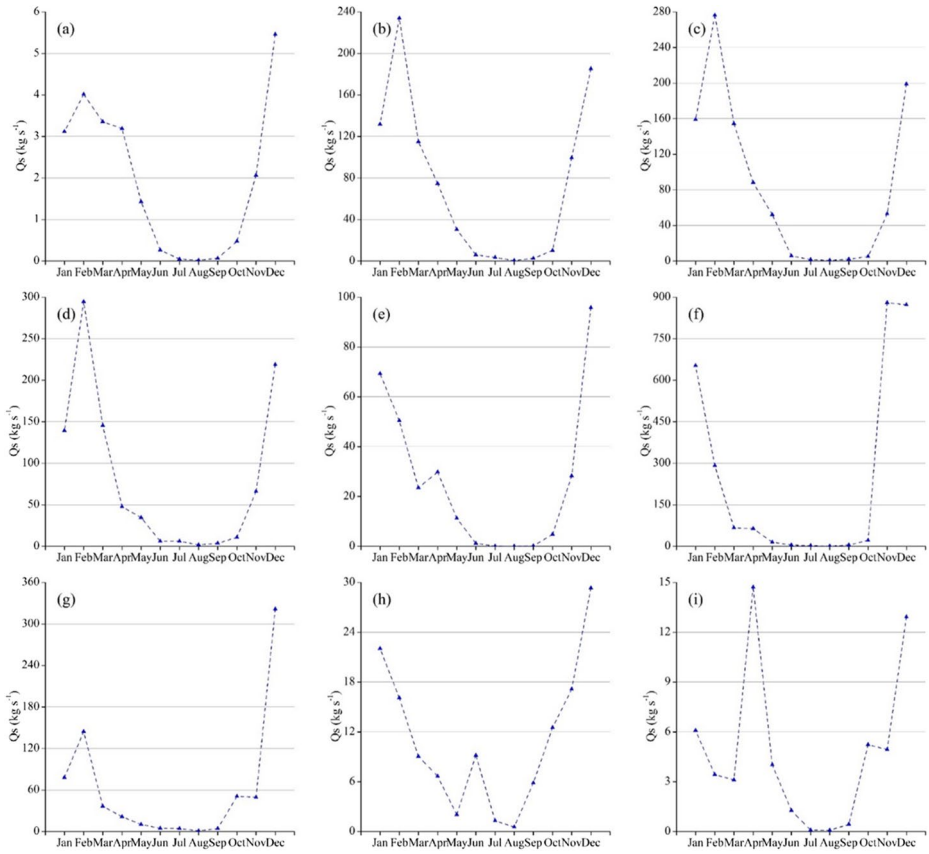


Fig. 14 Mean monthly suspended sediment discharge (Q_s , kg s^{-1}) records at the station; river (a) Grevena bridge, Aliakmon, (b) Moni Ilarion, Aliakmon, (c) Moni Prodromou, Aliakmon, (d) Velventos, Aliakmon, (e) Avlaki dam, upper Acheloos, (f) Arta bridge, Arachthos, (g) Plaka bridge, Arachthos, (h) Tsimovo bridge, Arachthos, (i) Gogo bridge, Arachthos

Fig. 15 The Delft bottle sampler



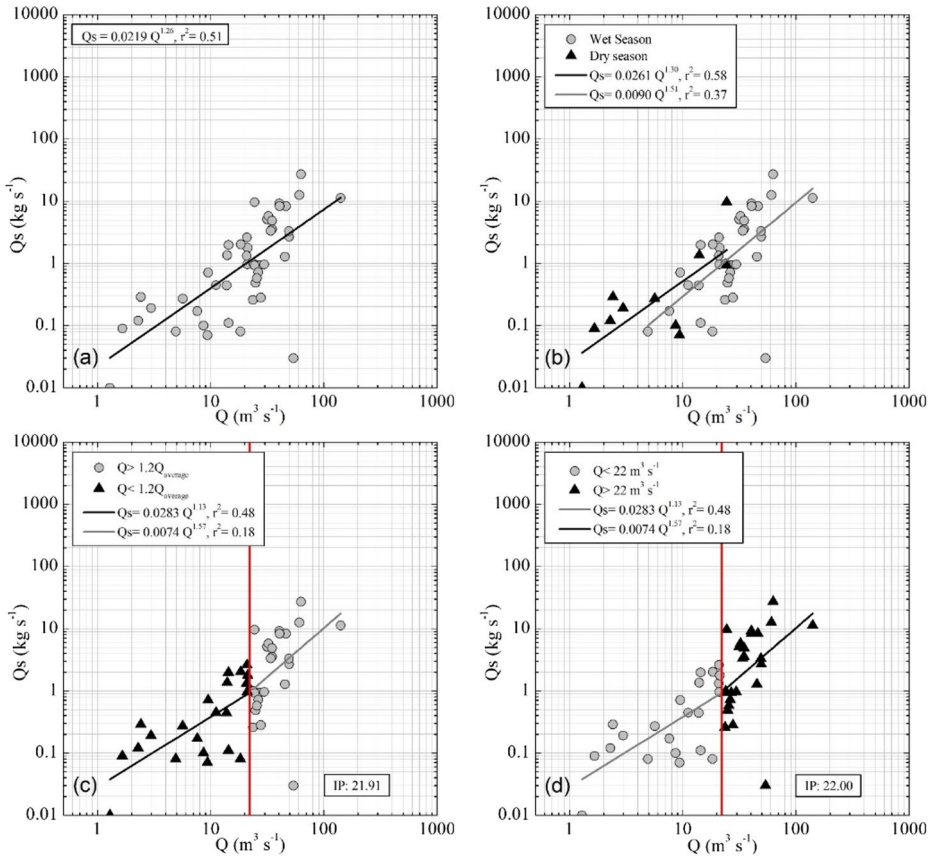


Fig. 16 Forms of different SRC methods, Aliakmon River, Grevena bridge station: (a) simple rating curve, (b) different ratings for the dry and wet season of the year, (c) hydrographic classification, (d) broken line interpolation

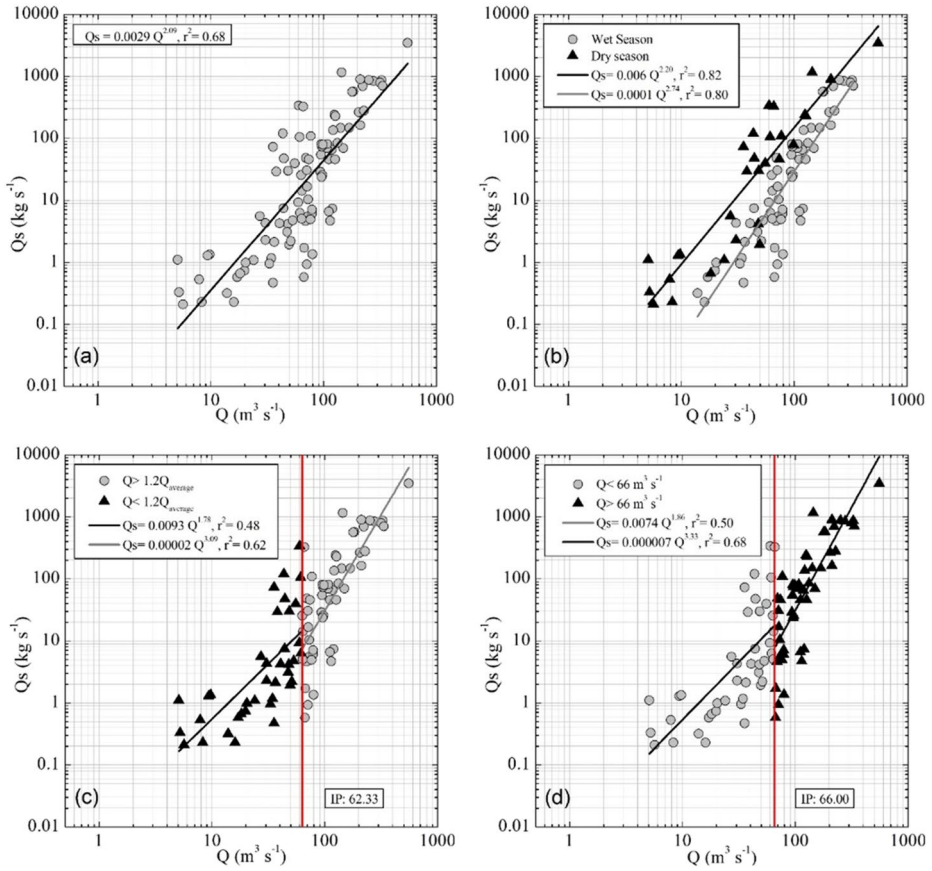


Fig. 17 Forms of different SRC methods, Aliakmon River, Moni Ilarion station: (a) simple rating curve, (b) different ratings for the dry and wet season of the year, (c) hydrographic classification, (d) broken line interpolation

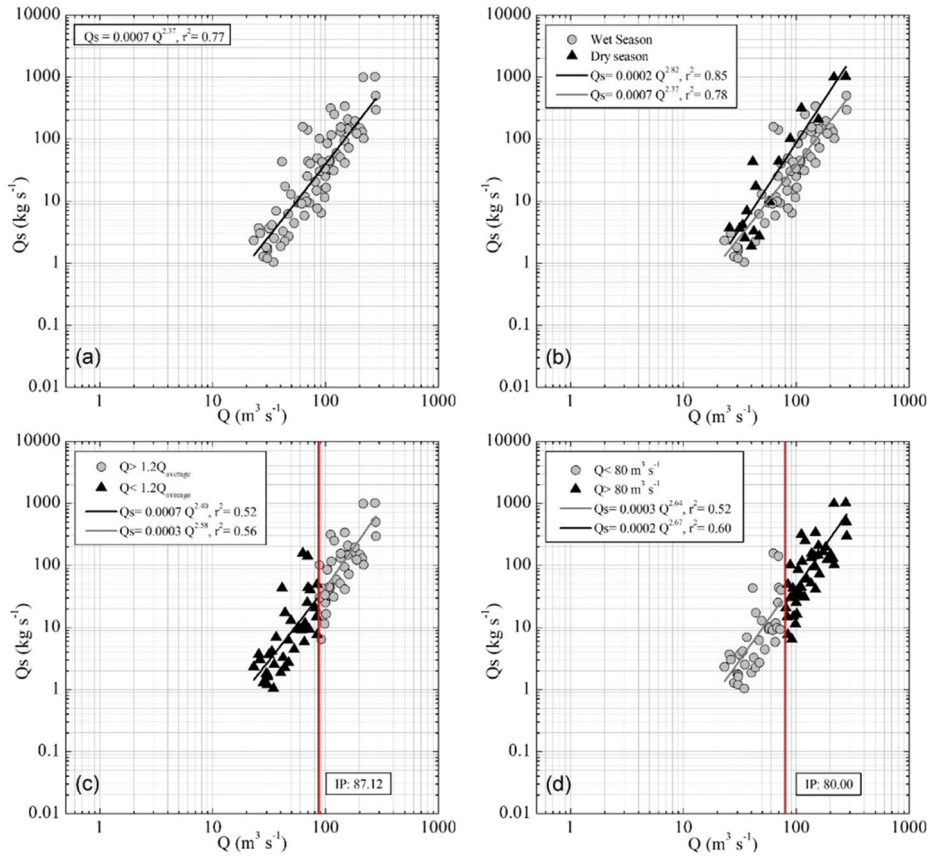


Fig. 18 Forms of different SRC methods, Aliakmon River, Moni Prodromou station: (a) simple rating curve, (b) different ratings for the dry and wet season of the year, (c) hydrographic classification, (d) broken line interpolation

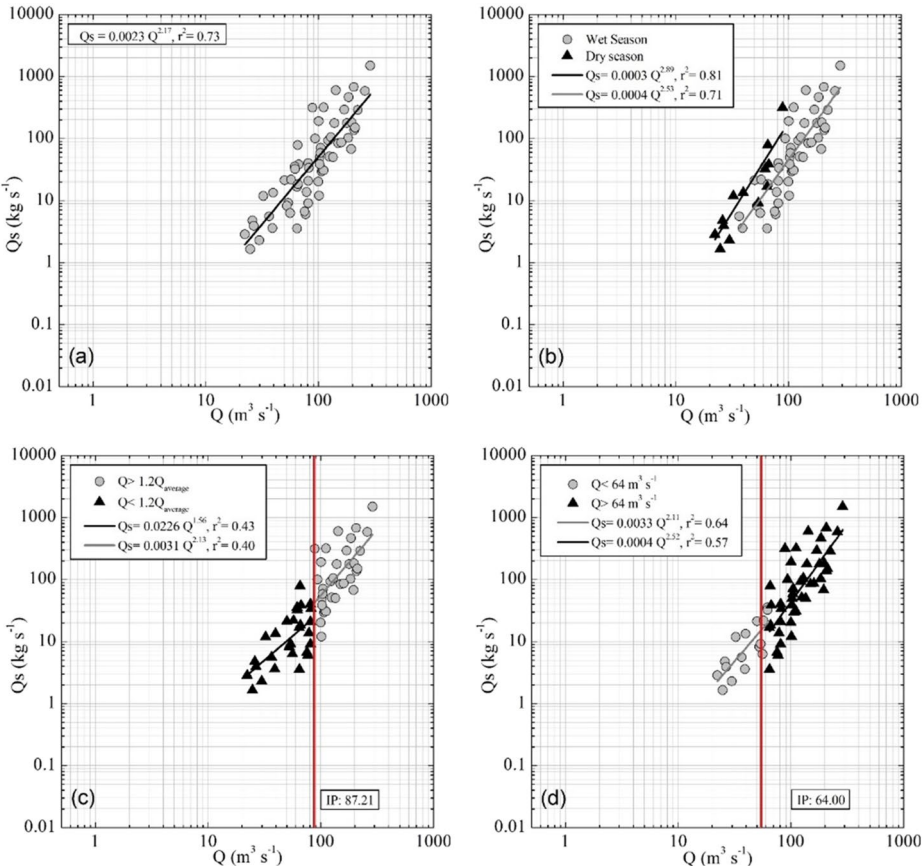


Fig. 19 Forms of different SRC methods, Aliakmon River, Velventos station: (a) simple rating curve, (b) different ratings for the dry and wet season of the year, (c) hydrographic classification, (d) broken line interpolation

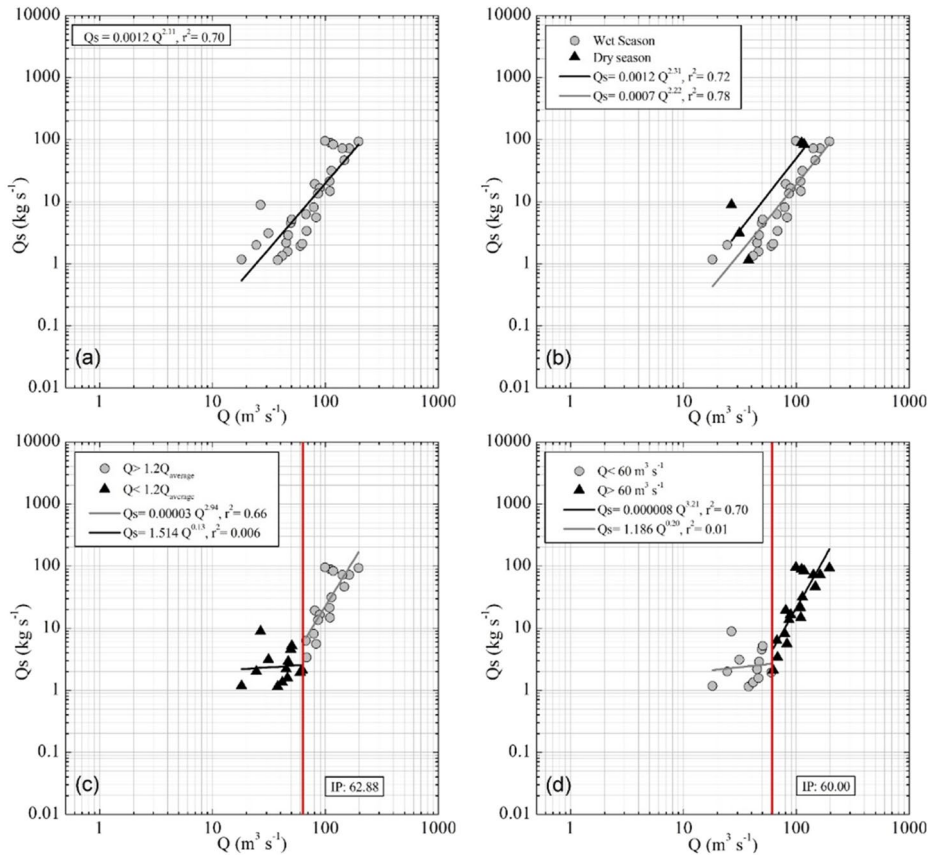


Fig. 20 Forms of different SRC methods, upper Acheloos River, Avlaki dam station: (a) simple rating curve, (b) different ratings for the dry and wet season of the year, (c) hydrographic classification, (d) broken line interpolation

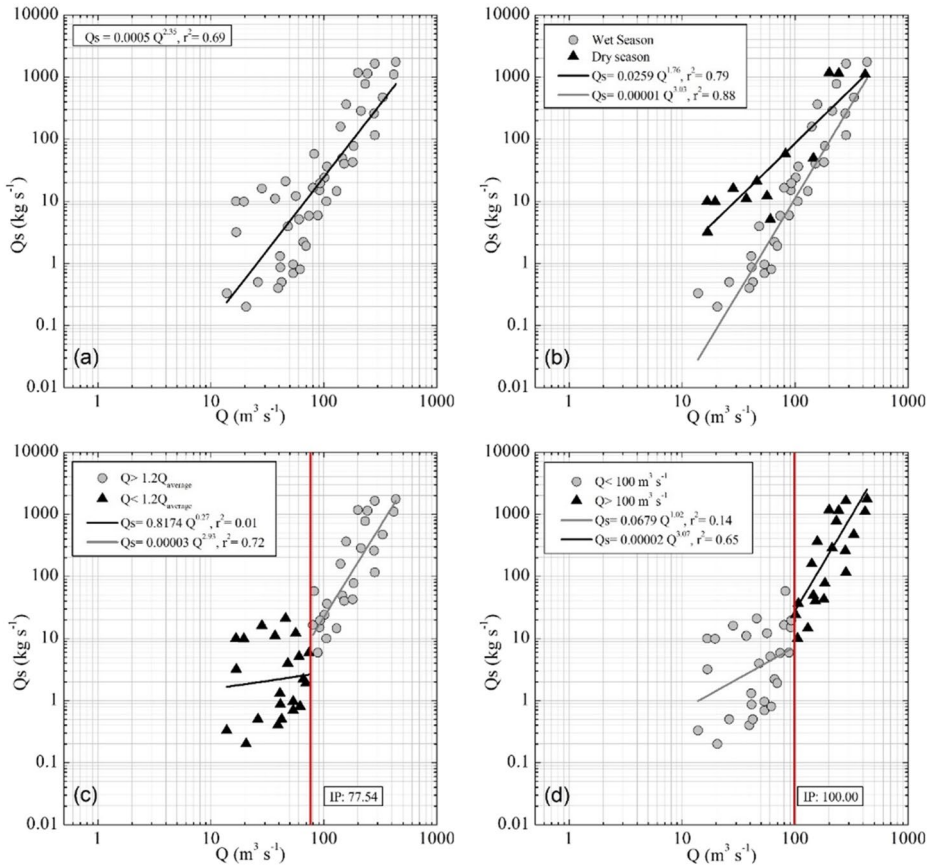


Fig. 21 Forms of different SRC methods, Arachthos River, Arta bridge station: (a) simple rating curve, (b) different ratings for the dry and wet season of the year, (c) hydrographic classification, (d) broken line interpolation

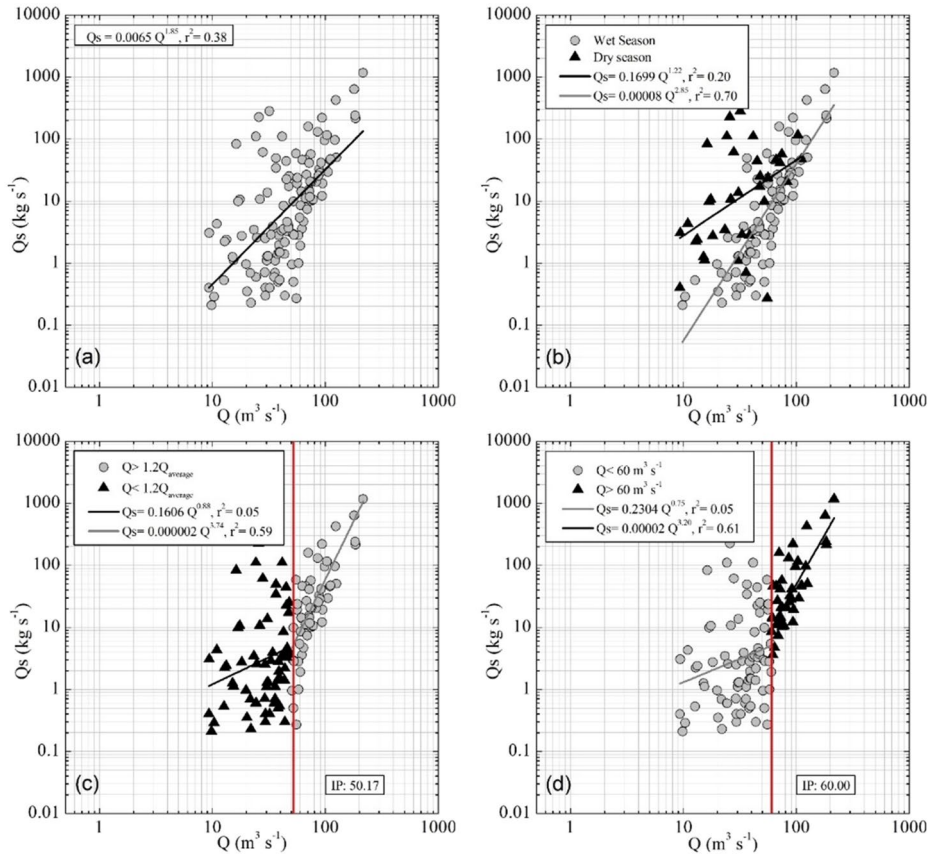


Fig. 22 Forms of different SRC methods, Arachthos River, Plaka bridge station: (a) simple rating curve, (b) different ratings for the dry and wet season of the year, (c) hydrographic classification, (d) broken line interpolation

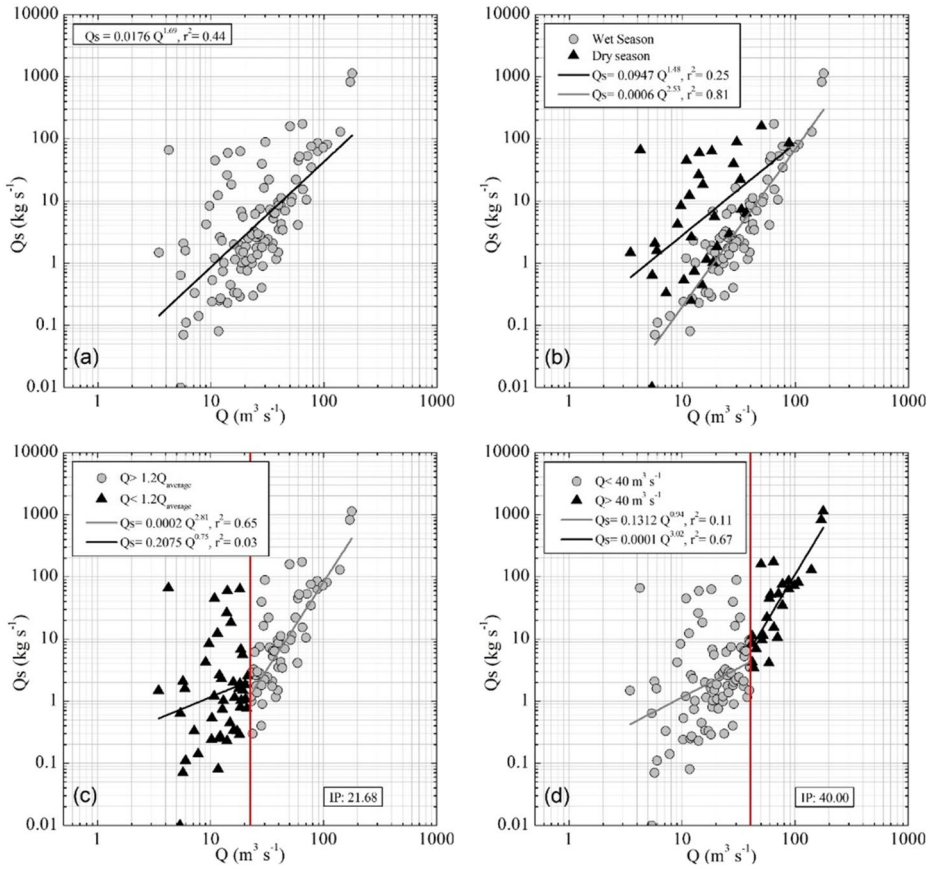


Fig. 23 Forms of different SRC methods, Arachthos River, Tsimovo bridge station: (a) simple rating curve, (b) different ratings for the dry and wet season of the year, (c) hydrographic classification, (d) broken line interpolation

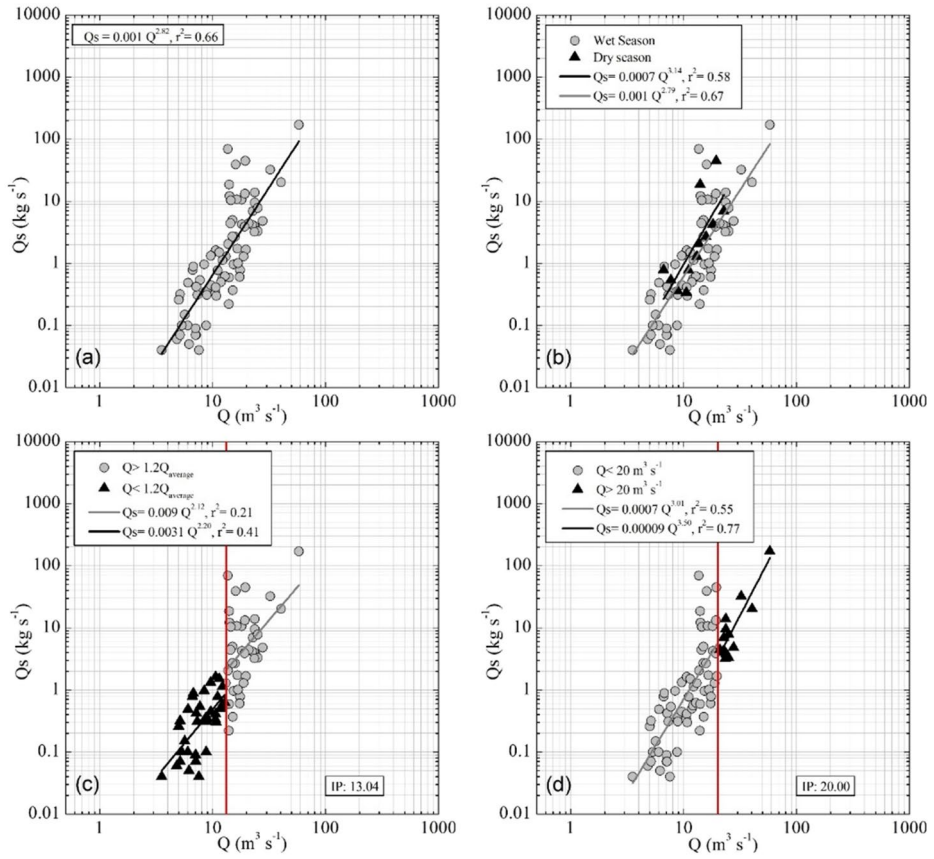


Fig. 24 Forms of different SRC methods, Arachthos River, Gogo bridge station: (a) simple rating curve, (b) different ratings for the dry and wet season of the year, (c) hydrographic classification, (d) broken line interpolation

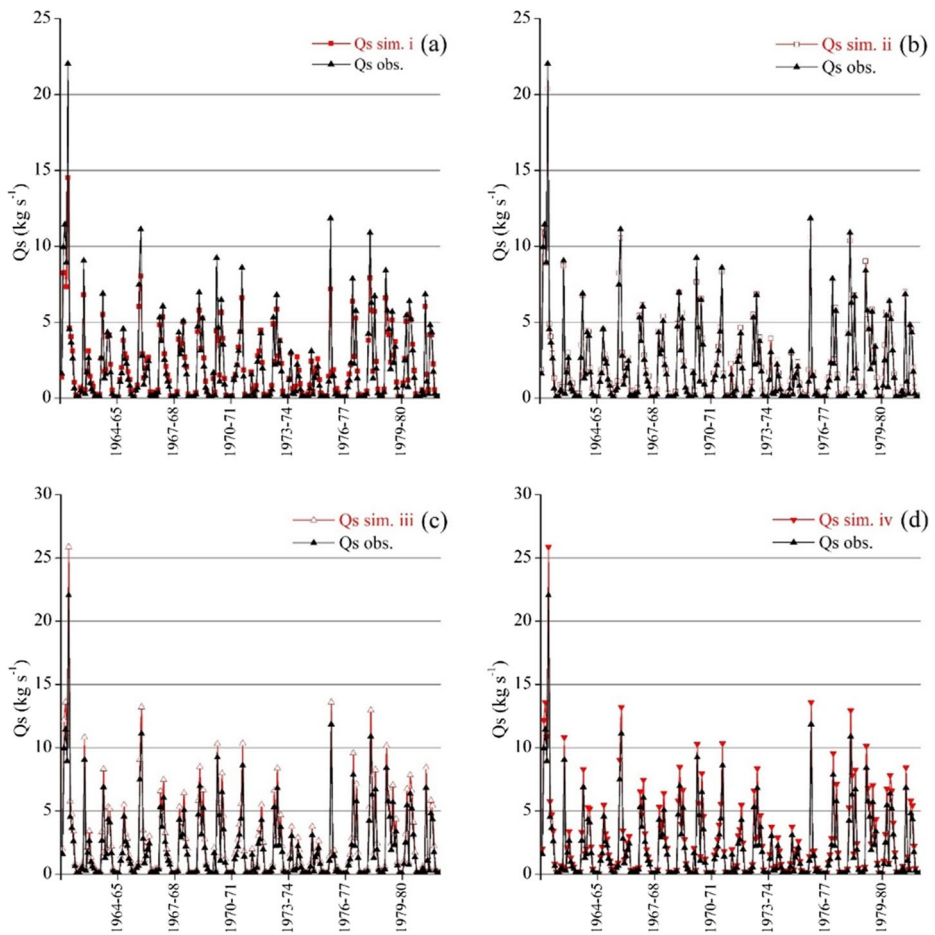


Fig. 25 Monthly simulated suspended sediment discharge (Q_s , kg s^{-1}) and convergence with field measurements, Aliakmon River, Grevena bridge station: (a) simple rating curve, (b) different ratings for the dry and wet season of the year, (c) hydrographic classification, (d) broken line interpolation

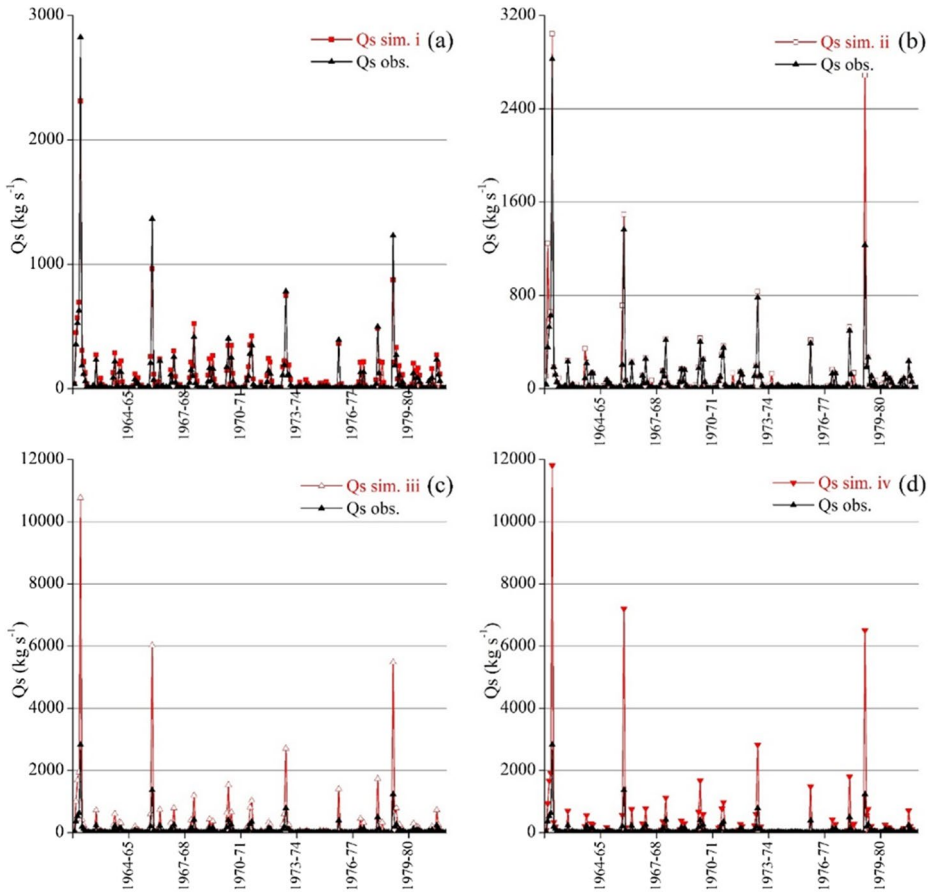


Fig. 26 Monthly simulated suspended sediment discharge (Q_s , kg s^{-1}) and convergence with field measurements, Aliakmon River, Moni Ilarion station: (a) simple rating curve, (b) different ratings for the dry and wet season of the year, (c) hydrographic classification, (d) broken line interpolation

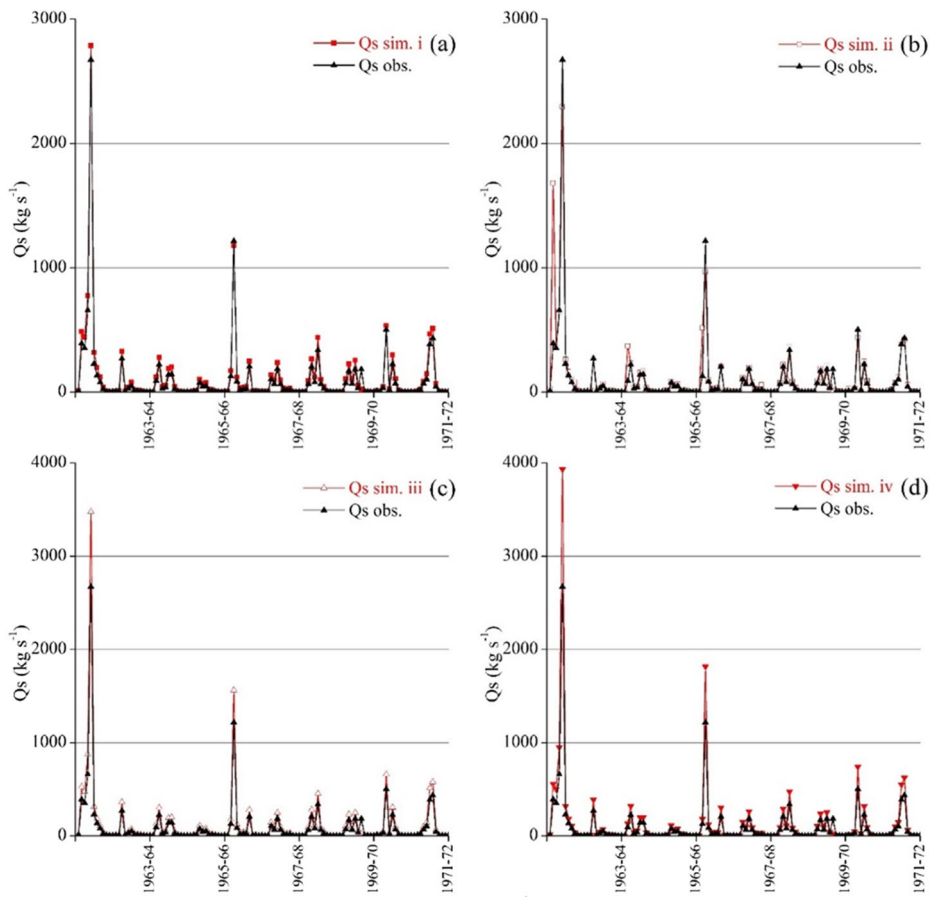


Fig. 27 Monthly simulated suspended sediment discharge (Q_s , kg s^{-1}) and convergence with field measurements, Aliakmon River, Moni Prodrromou station: (a) simple rating curve, (b) different ratings for the dry and wet season of the year, (c) hydrographic classification, (d) broken line interpolation

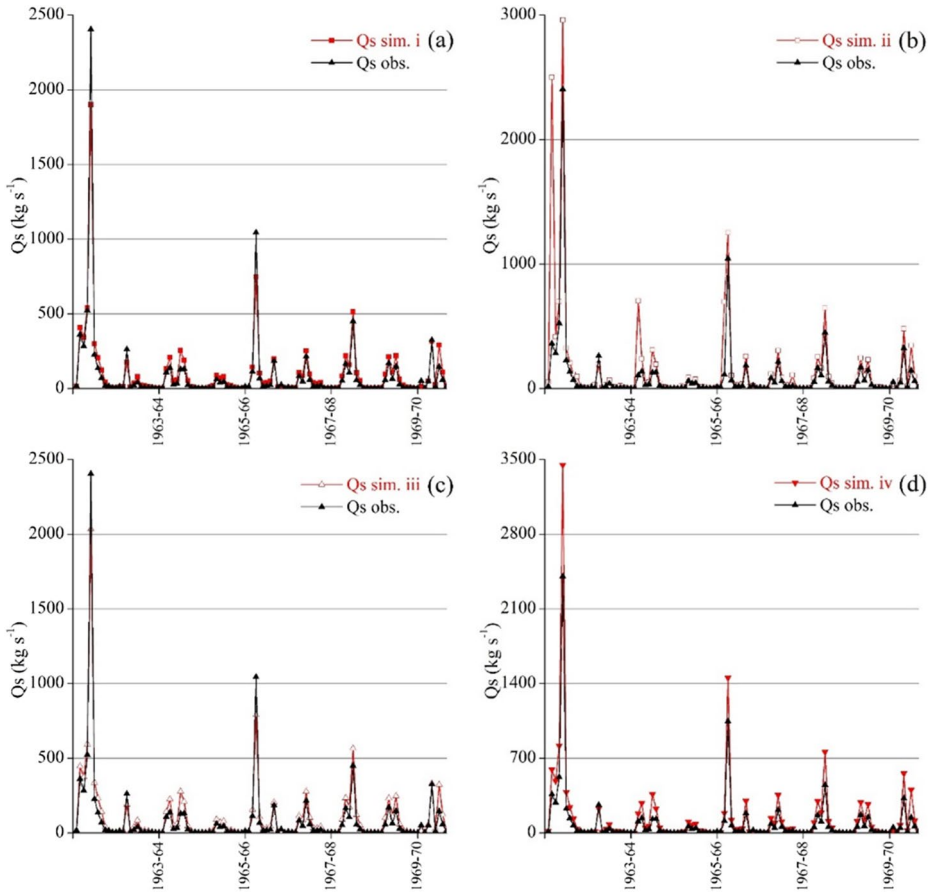


Fig. 28 Monthly simulated suspended sediment discharge (Q_s , kg s^{-1}) and convergence with field measurements, Velventos station: (a) simple rating curve, (b) different ratings for the dry and wet season of the year, (c) hydrographic classification, (d) broken line interpolation

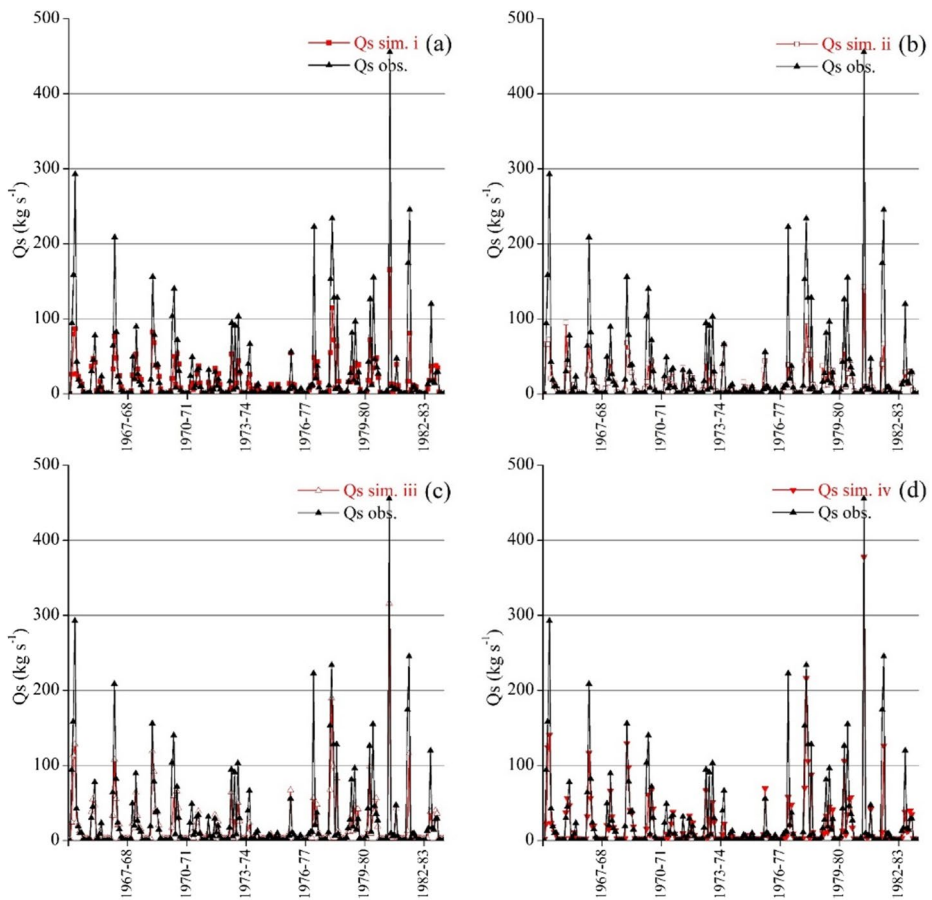


Fig. 29 Monthly simulated suspended sediment discharge (Q_s , kg s^{-1}) and convergence with field measurements, upper Acheloos River, Avlaki dam station: (a) simple rating curve, (b) different ratings for the dry and wet season of the year, (c) hydrographic classification, (d) broken line interpolation

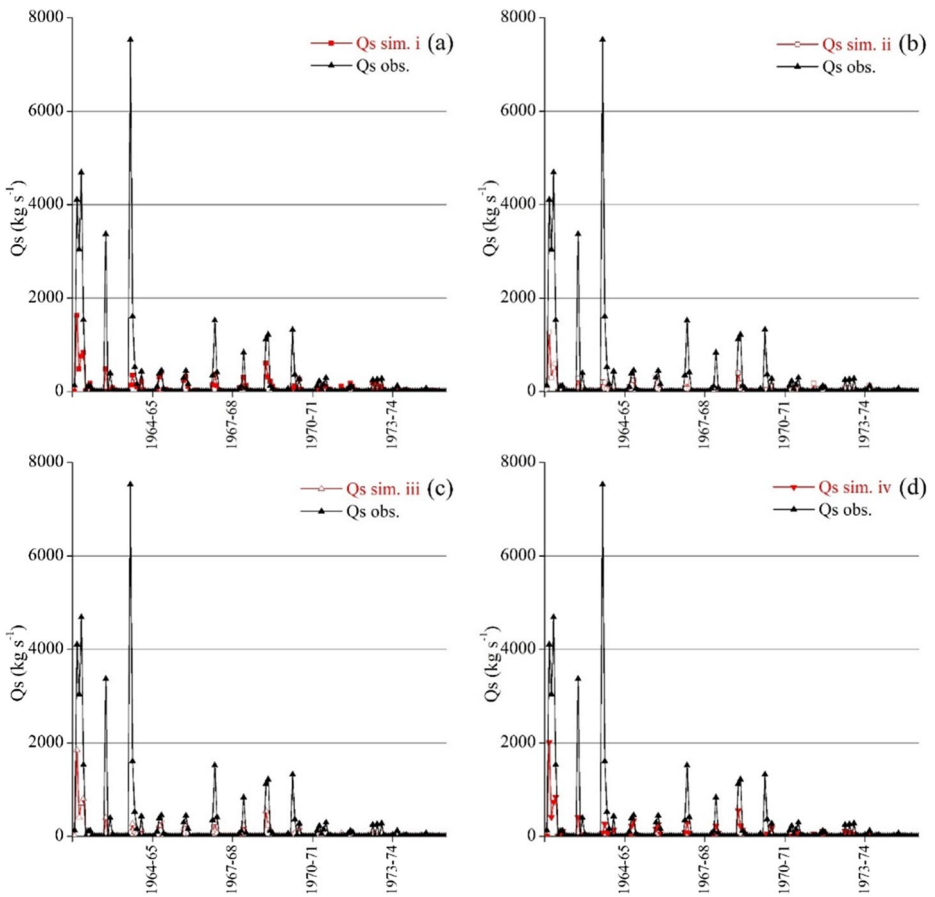


Fig. 30 Monthly simulated suspended sediment discharge (Q_s , kg s^{-1}) and convergence with field measurements, Arachthos River, Arta bridge station: (a) simple rating curve, (b) different ratings for the dry and wet season of the year, (c) hydrographic classification, (d) broken line interpolation

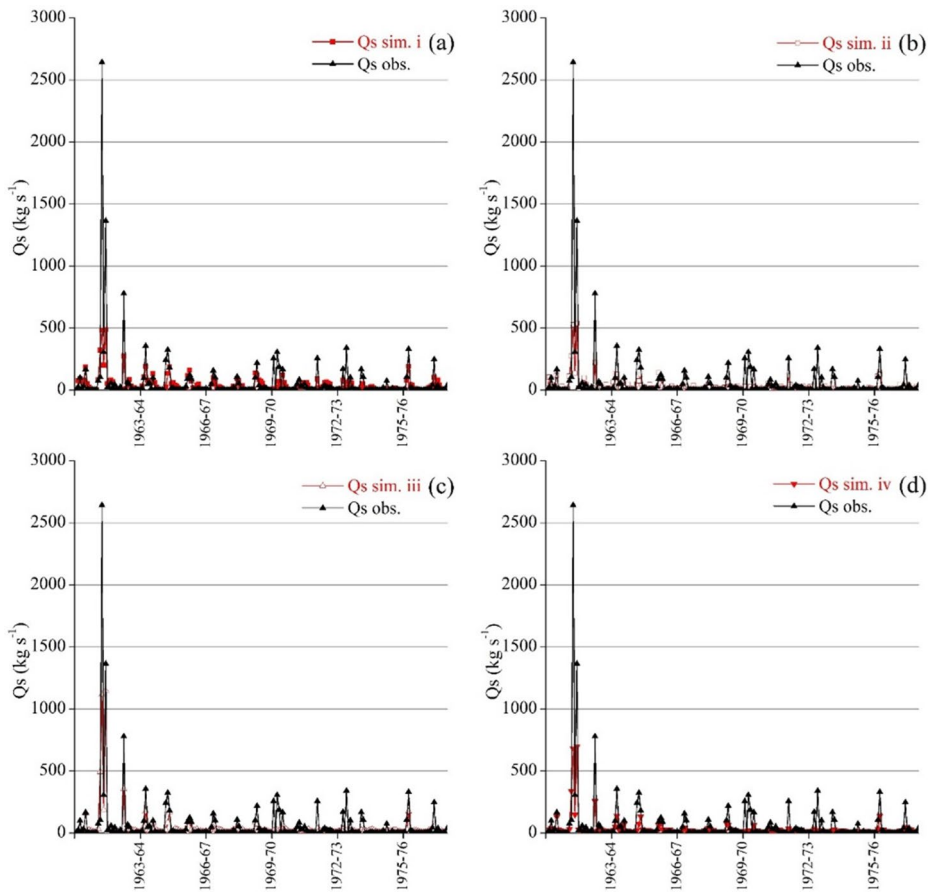


Fig. 31 Monthly simulated suspended sediment discharge (Q_s , kg s^{-1}) and convergence with field measurements, Arachthos River, Plaka bridge station: (a) simple rating curve, (b) different ratings for the dry and wet season of the year, (c) hydrographic classification, (d) broken line interpolation

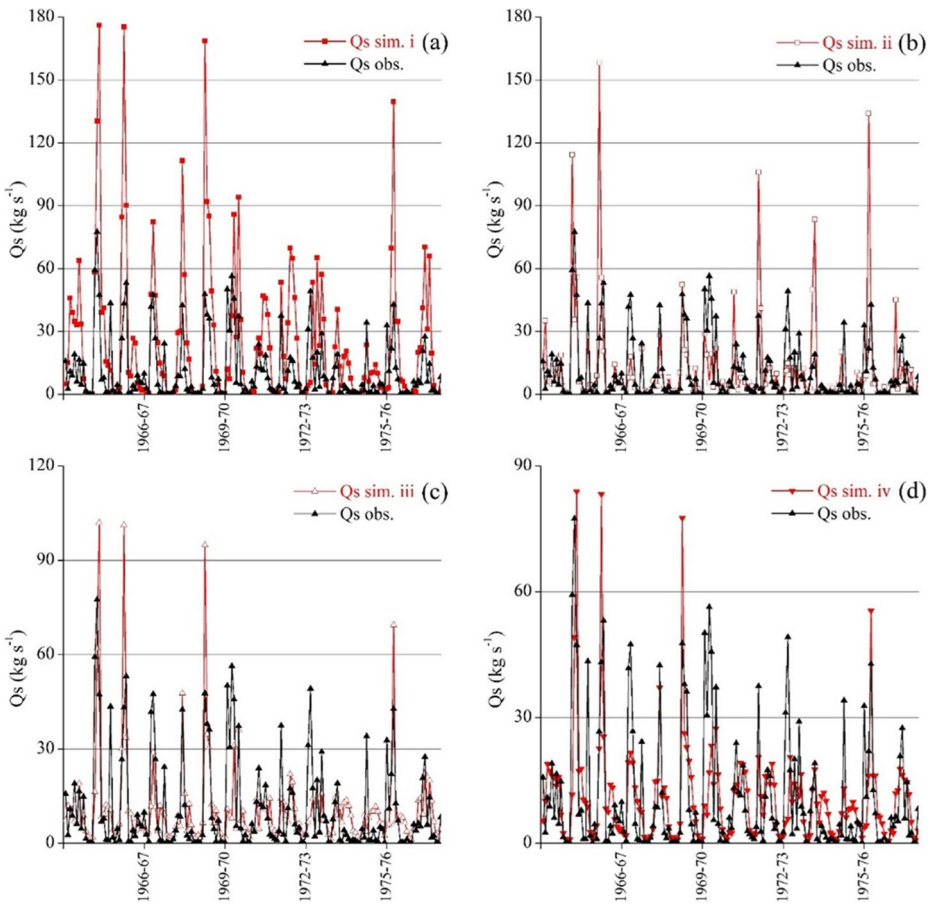


Fig. 32 Monthly simulated suspended sediment discharge (Q_s , kg s^{-1}) and convergence with field measurements, Arachthos River, Tsimovo bridge station: (a) simple rating curve, (b) different ratings for the dry and wet season of the year, (c) hydrographic classification, (d) broken line interpolation

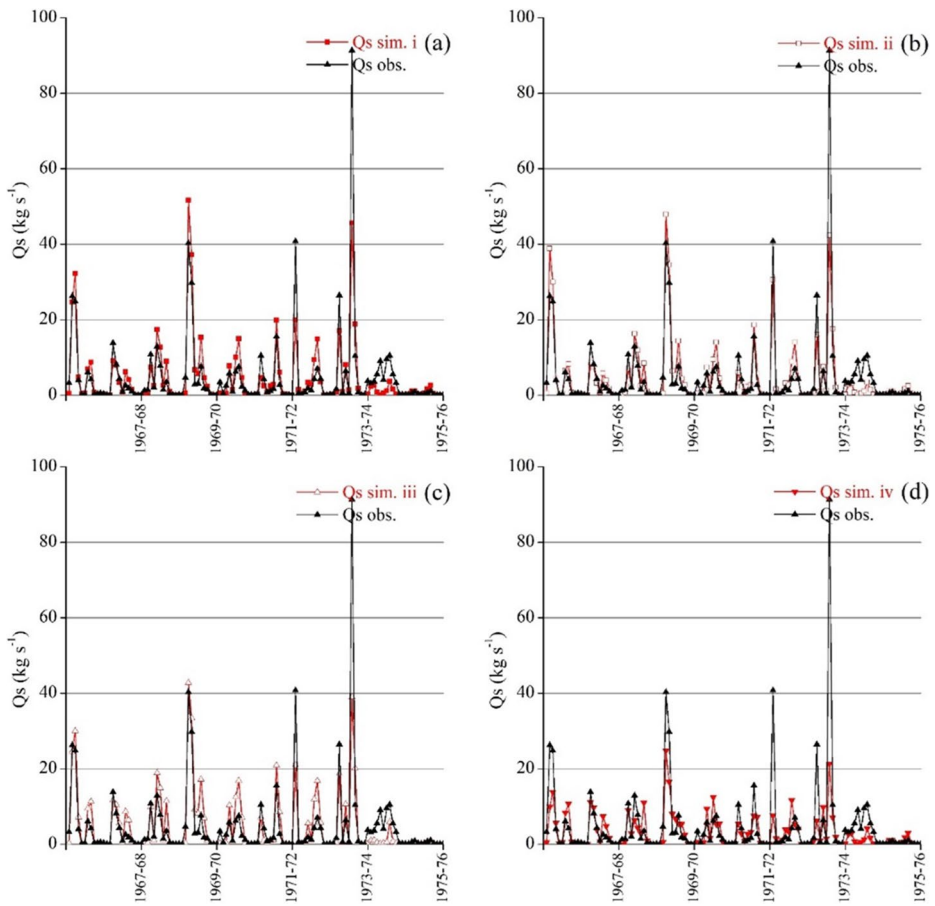


Fig. 33 Monthly simulated suspended sediment discharge (Q_s , kg s^{-1}) and convergence with field measurements, Arachthos River, Gogo bridge station: (a) simple rating curve, (b) different ratings for the dry and wet season of the year, (c) hydrographic classification, (d) broken line interpolation

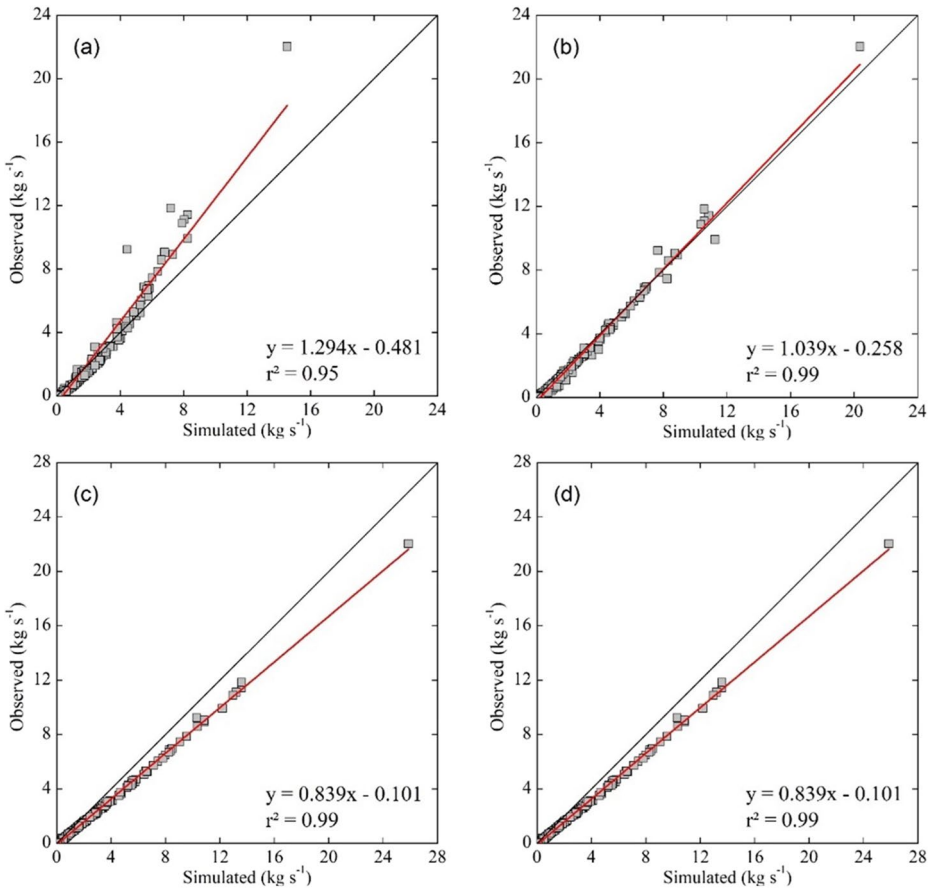


Fig. 34 Correlation of different SRC methods with monthly field measurements, Aliakmon River, Grevena bridge station: (a) simple rating curve, (b) different ratings for the dry and wet season of the year, (c) hydrographic classification, (d) broken line interpolation

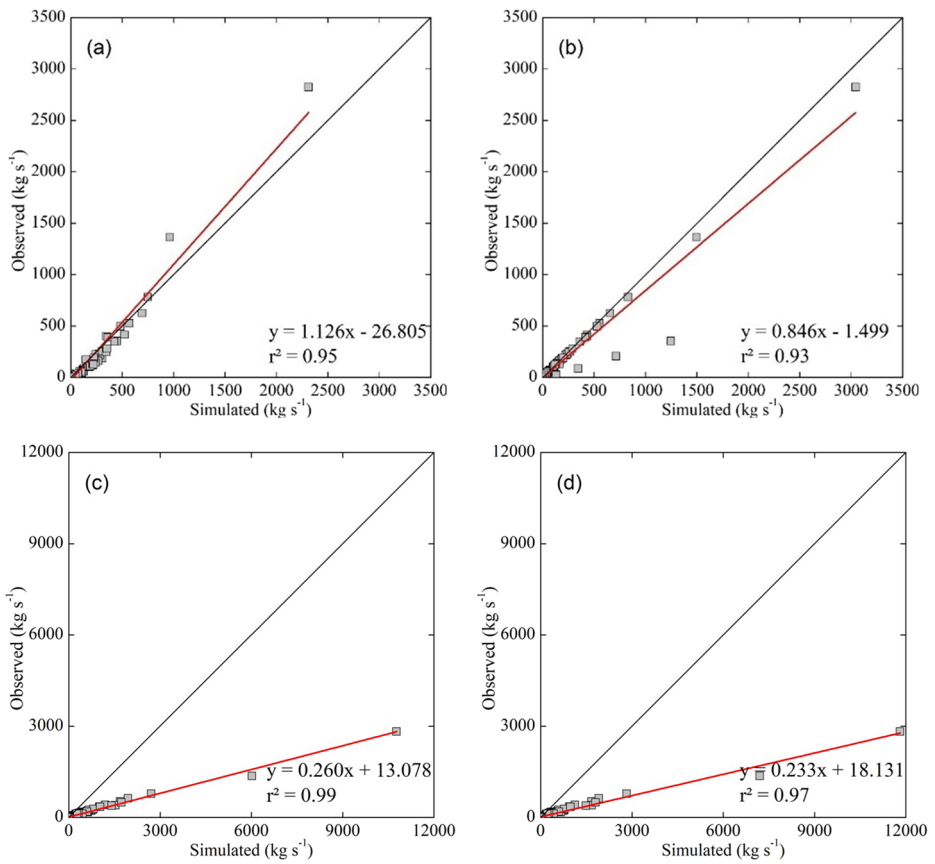


Fig. 35 Correlation of different SRC methods with monthly field measurements, Aliakmon River, Moni Illarion station: (a) simple rating curve, (b) different ratings for the dry and wet season of the year, (c) hydrographic classification, (d) broken line interpolation

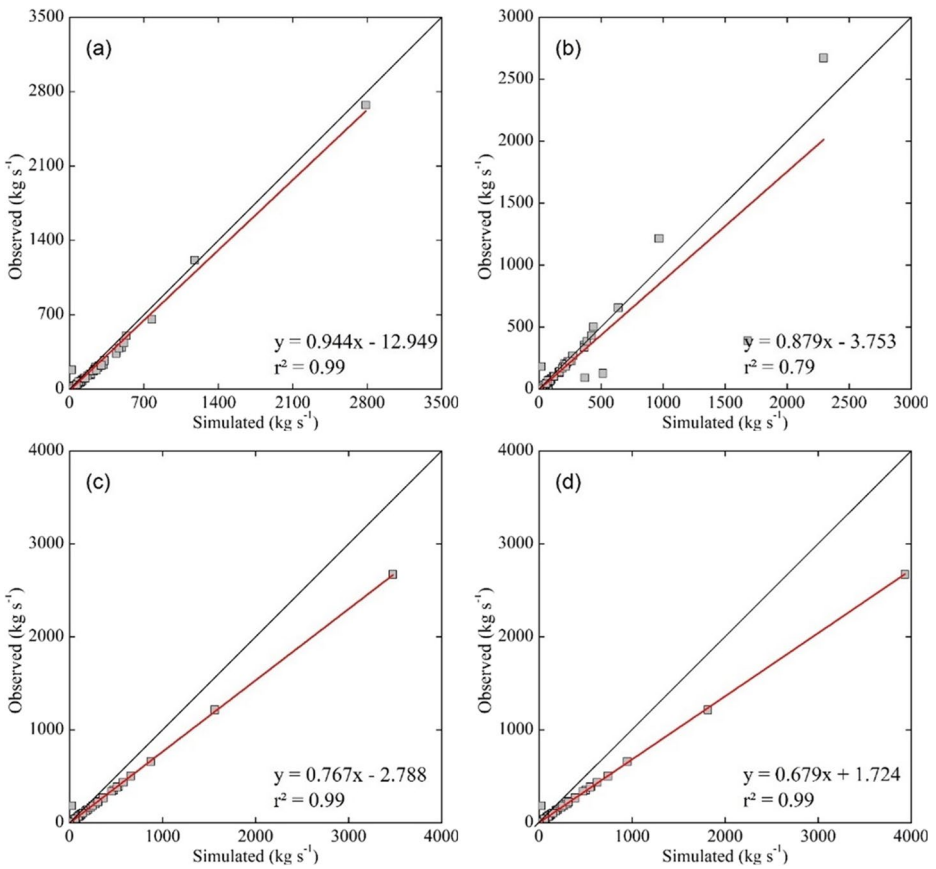


Fig. 36 Correlation of different SRC methods with monthly field measurements, Aliakmon River, Moni Prodromou station: (a) simple rating curve, (b) different ratings for the dry and wet season of the year, (c) hydrographic classification, (d) broken line interpolation

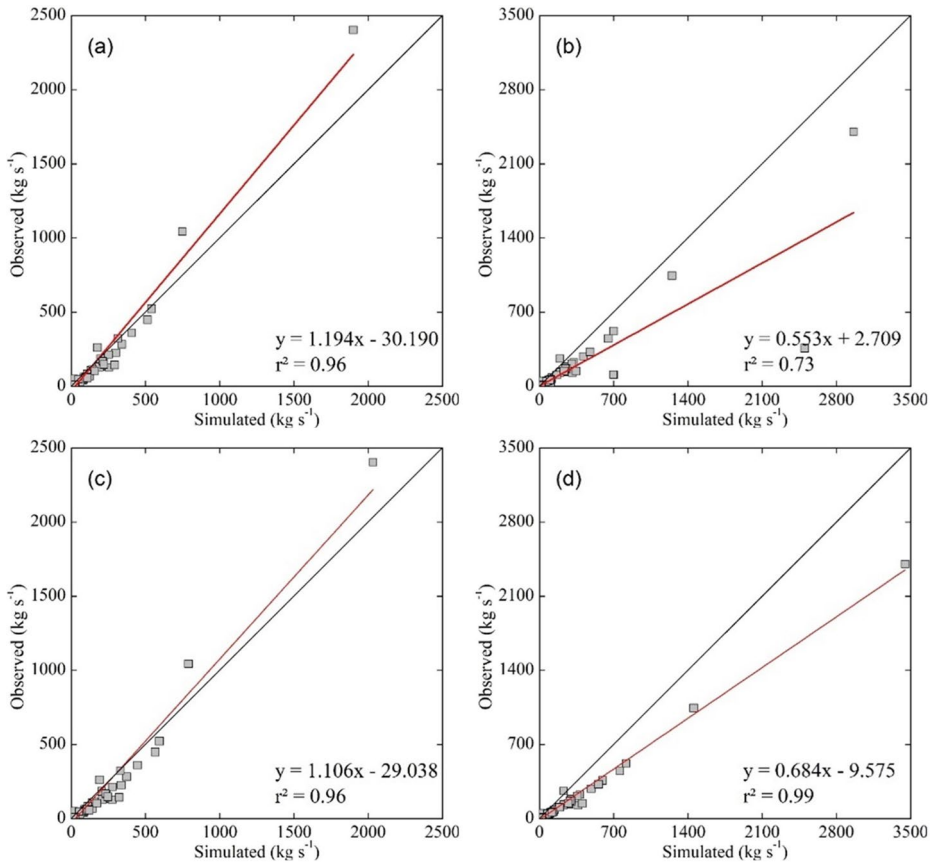


Fig. 37 Correlation of different SRC methods with monthly field measurements, Aliakmon River, Velventos station: (a) simple rating curve, (b) different ratings for the dry and wet season of the year, (c) hydrographic classification, (d) broken line interpolation

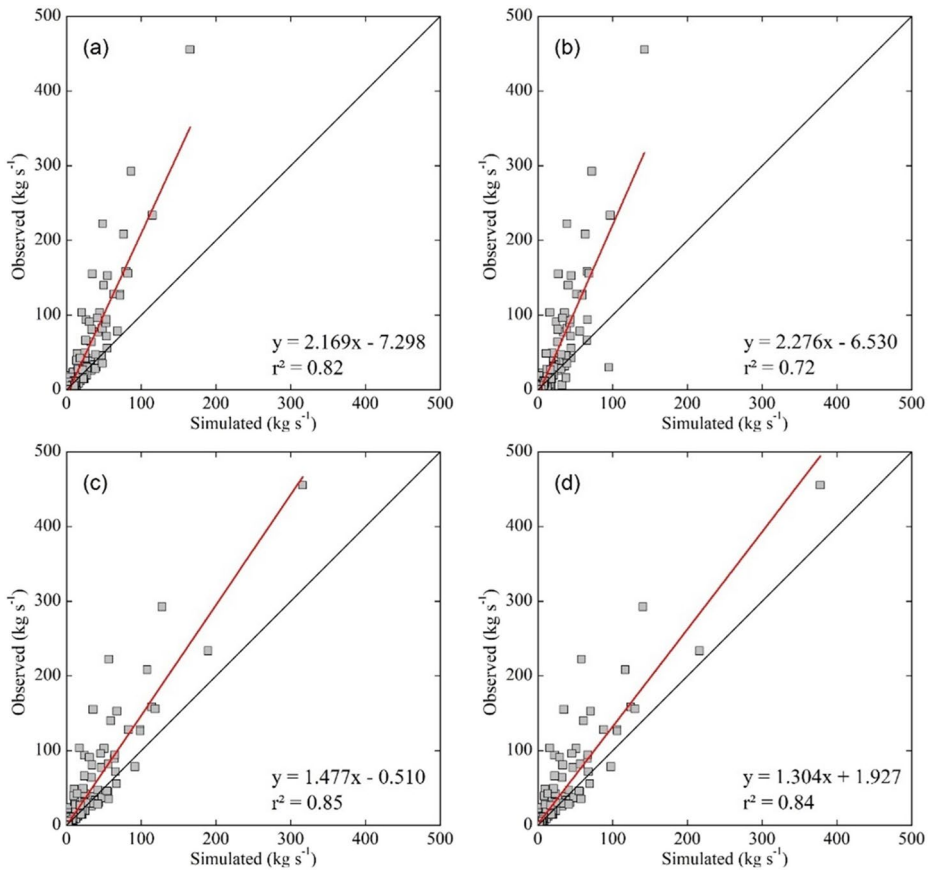


Fig. 38 Correlation of different SRC methods with monthly field measurements, upper Acheloos River, Avlaki dam station: (a) simple rating curve, (b) different ratings for the dry and wet season of the year, (c) hydrographic classification, (d) broken line interpolation

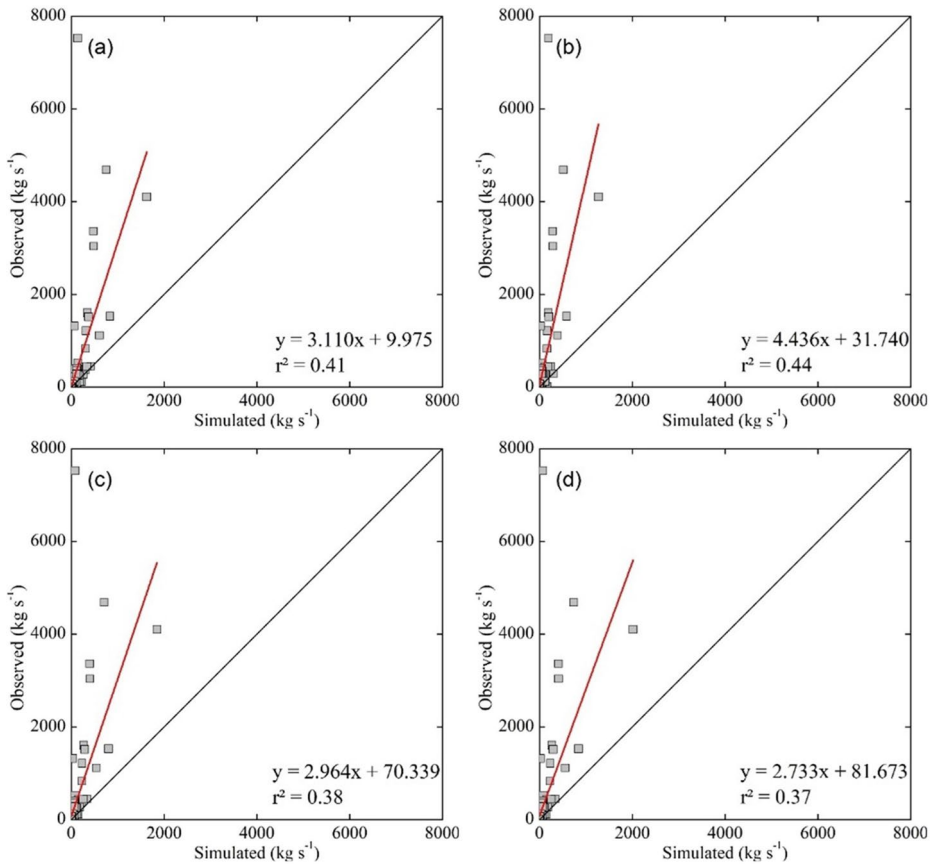


Fig. 39 Correlation of different SRC methods with monthly field measurements, Arachthos River, Arta bridge station: (a) simple rating curve, (b) different ratings for the dry and wet season of the year, (c) hydrographic classification, (d) broken line interpolation

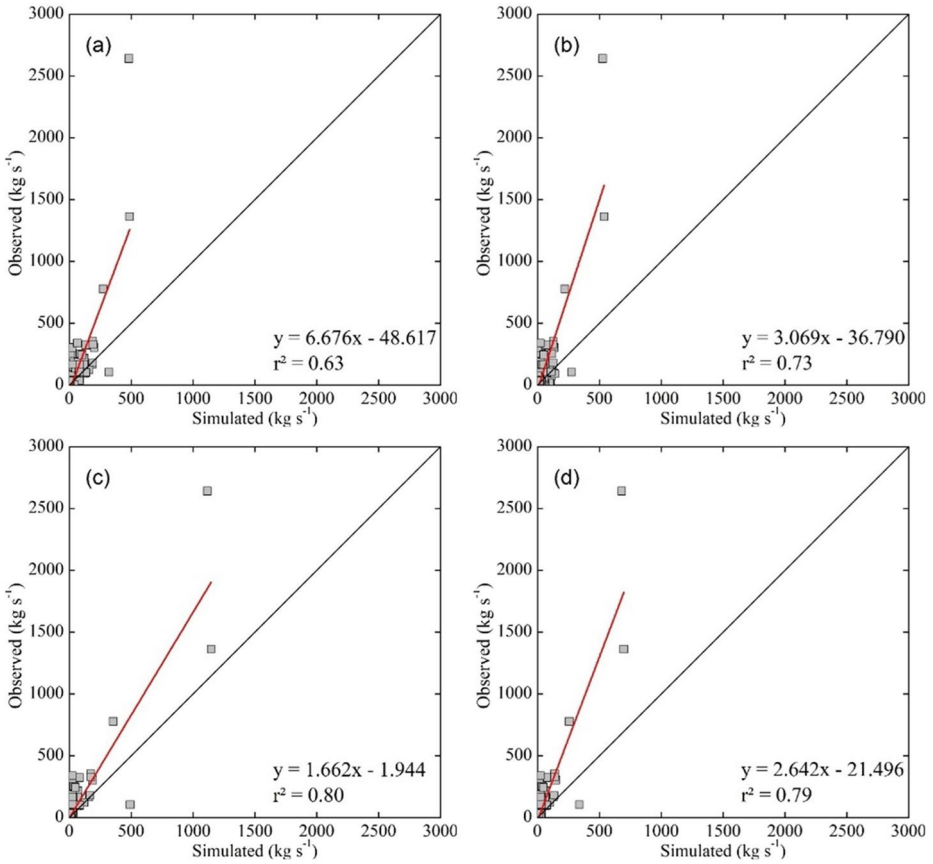


Fig. 40 Correlation of different SRC methods with monthly field measurements, Arachthos River, Plaka bridge station: (a) simple rating curve, (b) different ratings for the dry and wet season of the year, (c) hydrographic classification, (d) broken line interpolation

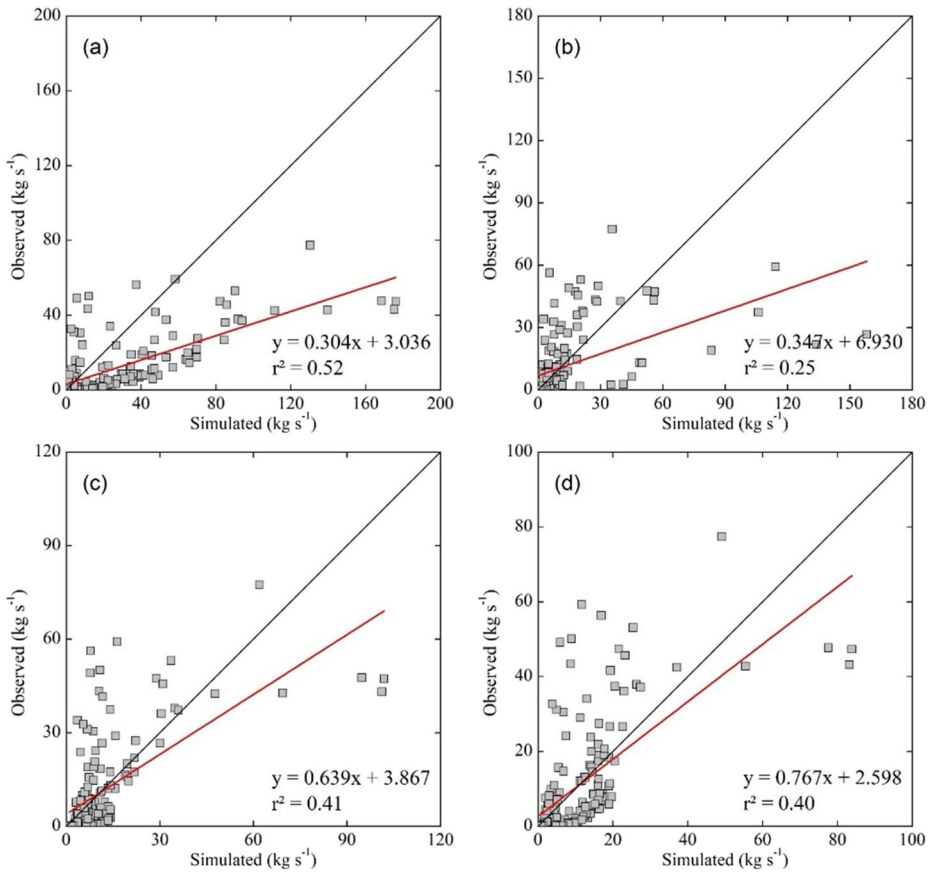


Fig. 41 Correlation of different SRC methods with monthly field measurements, Arachthos River, Tsimovo bridge station: (a) simple rating curve, (b) different ratings for the dry and wet season of the year, (c) hydrographic classification, (d) broken line interpolation

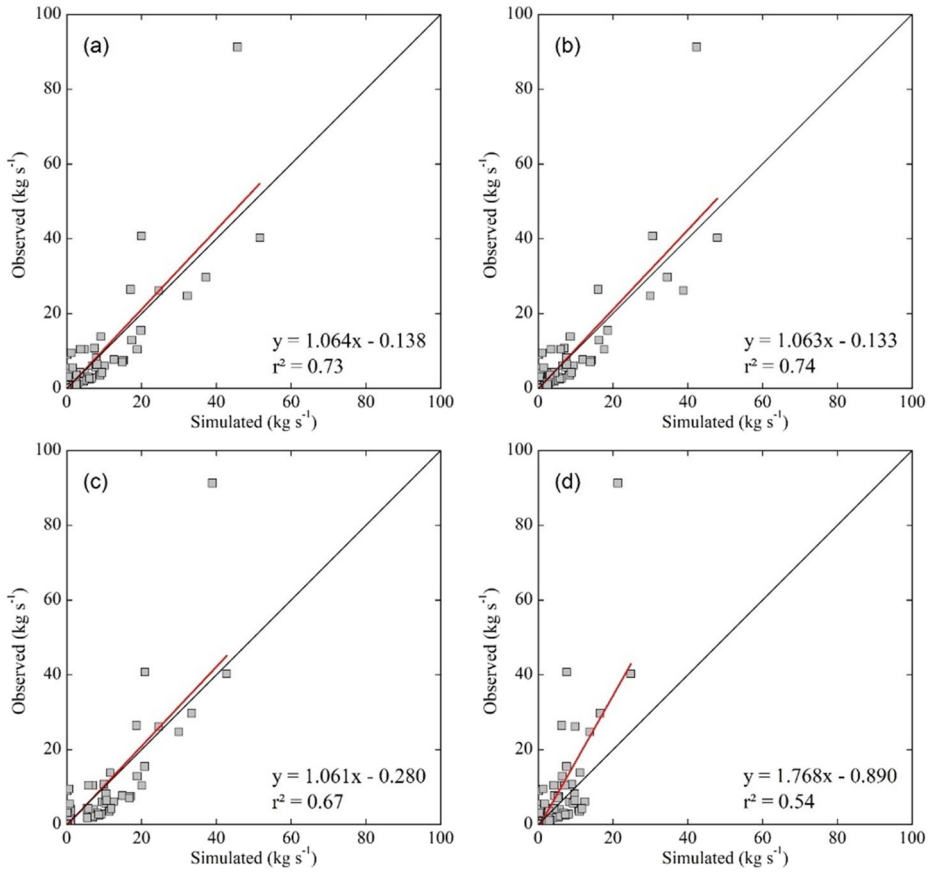


Fig. 42 Correlation of different SRC methods with monthly field measurements, Arachthos River, Gogo bridge station: (a) simple rating curve, (b) different ratings for the dry and wet season of the year, (c) hydrographic classification, (d) broken line interpolation

Acknowledgements The author wishes to thank the Greek Public Power Corporation (PPC) for providing the discharge, sediment discharge, and discharge-sediment discharge pair measurements.

Author Contributions EFTHIMIOU Nikolaos: Conceptualization, Methodology, Data curation, Formal analysis, Writing- Original draft preparation, Visualization, Supervision.

Funding Open access publishing supported by the National Technical Library in Prague. No funding was received for conducting this study.

Data Availability The data that support the findings of this study are available from the Greek Public Power Corporation (PPC). Restrictions apply to their availability, which were used under license for this study. Data are available from <https://www.dei.gr/el> with the permission of the Greek Public Power Corporation (PPC).

Declarations

Ethical Approval Ethics approval was not required for this study. Human subjects and/or animals are not involved in the study.

Consent to Participate A consent to participate was not required for this study.

Consent to Publish I, the undersigned, give my consent for the publication of identifiable details, which can include photograph(s) and/or videos and/or case history and/or details within the text ‘Suspended load estimation in data scarce rivers. The case of northwestern Greece.’ to be published in ‘Water Resources Management’.

Competing Interests The authors have no relevant financial or non-financial interests to disclose.

Open Access This article is licensed under a Creative Commons Attribution 4.0 International License, which permits use, sharing, adaptation, distribution and reproduction in any medium or format, as long as you give appropriate credit to the original author(s) and the source, provide a link to the Creative Commons licence, and indicate if changes were made. The images or other third party material in this article are included in the article’s Creative Commons licence, unless indicated otherwise in a credit line to the material. If material is not included in the article’s Creative Commons licence and your intended use is not permitted by statutory regulation or exceeds the permitted use, you will need to obtain permission directly from the copyright holder. To view a copy of this licence, visit <http://creativecommons.org/licenses/by/4.0/>.

References

- Achite M, Ouillon S (2007) Suspended sediment transport in a semiarid watershed, Wadi Abd, Algeria (1973–1995). *J Hydrol* 343:187–202. <https://doi.org/10.1016/j.jhydrol.2007.06.026>
- Arnold JG, Allen PM, Bernhardt G (1993) A comprehensive surface-groundwater flow model. *J Hydrol* 142(1–4):47–69. [https://doi.org/10.1016/0022-1694\(93\)90004-S](https://doi.org/10.1016/0022-1694(93)90004-S)
- Ashmore PE (1986) Suspended sediment transport in the Saskatchewan River basin. Report IWD-HQ-WRB-SS-86-9
- Asselman NEM (2000) Fitting and interpretation of sediment rating curves. *J Hydrol* 234(3–4):228–248. [https://doi.org/10.1016/S0022-1694\(00\)00253-5](https://doi.org/10.1016/S0022-1694(00)00253-5)
- Baiamonte G, Minacapilli M, Novara A, Gristina L (2019) Time scale effects and interactions of rainfall erosivity and cover management factors on vineyard soil loss erosion in the semi-arid area of southern Sicily. *Water* 11:978. <https://doi.org/10.3390/w11050978>
- Bailey G, King G, Sturdy D (1993) Active tectonics and land-use strategies: a palaeolithic example from northwest Greece. *Antiquity* 67(255):292–312. <https://doi.org/10.1017/S0003598X00045361>
- Balafoutis C (1977) Contribution to the study of Macedonia and Thrace climate. Dissertation, Aristotle University of Thessaloniki (in Greek)
- Benson MA (1965) Spurious correlation in hydraulics and hydrology. *J Hydr Eng Div-ASCE* 91(4):35–42

- Blanco MLR, Taboada-Castro MM, Palleiro L, Taboada-Castro MT (2010) Temporal changes in suspended sediment transport in an Atlantic catchment, NW Spain. *Geomorphology* 123:181–188. <https://doi.org/10.1016/j.geomorph.2010.07.015>
- Boyce RC (1975) Sediment routing with sediment-delivery ratios. In: Proceedings of the Sediment-Yield Workshop 'Present and Prospective Technology for Predicting Sediment Yields and Sources', 28–30 November 1972 Oxford, Miss. USDA Sedimentation Laboratory, Publication No. ARS-S-40, pp 61–65
- Bradu D, Mundlak Y (1970) Estimation in lognormal linear models. *J Am Stat Assoc* 65(329):198–211. <https://doi.org/10.1080/01621459.1970.10481074>
- Brandt SA (2000) Classification of geomorphological effects downstream of dams. *CATENA* 40(4):375–401. [https://doi.org/10.1016/S0341-8162\(00\)00093-X](https://doi.org/10.1016/S0341-8162(00)00093-X)
- Brown CB (1948) Perspective on sedimentation – purpose of conference. In: Proceedings of the Federal Inter-Agency Sedimentation Conference, 6–8 May, Denver Colorado. USDI, Washington (DC)
- Buyukyildiz M, Kumcu SY (2017) An estimation of the suspended sediment load using adaptive network based fuzzy inference system, support vector machine and artificial neural network models. *Water Resour Manag* 31:1343–1359. <https://doi.org/10.1007/s11269-017-1581-1>
- Canton Y, Solé-Benet A, de Vente J et al (2011) A review of runoff generation and soil erosion across scales in semiarid south-eastern Spain. *J Arid Environ* 75:1254–1261. <https://doi.org/10.1016/j.jaridenv.2011.03.004>
- Cerda A, Lavee H, Romero-Diaz A, Hooke J, Montanarella L (2010) Preface - soil erosion and degradation in Mediterranean-Type ecosystems. *Land Degrad Dev* 21(2):71–74 JRC56495. <https://doi.org/10.1002/ldr.968>
- Clark EHII, Havercamp JA, Chapman W (1985) Eroding soils: the off-farm impacts. The Conservation Foundation, Washington (DC)
- Cohn TA, Delong LL, Gilroy EJ, Hirsch RM, Wells DK (1989) Estimating constituent loads. *Water Resour Res* 25(5):937–942. <https://doi.org/10.1029/WR025i005p00937>
- Cohn TA, Caulder DL, Gilroy EJ, Zynjuk LD, Summers RM (1992) The validity of a simple statistical model for estimating fluvial constituent loads: an empirical study involving nutrient loads entering Chesapeake Bay. *Water Resour Res* 28:2353–2363. <https://doi.org/10.1029/92WR01008>
- Colby BR (1956) Relationship of sediment discharge to streamflow. USGS Open File Report
- Cordova JR, Gonzalez M (1997) Sediment yield estimation in small watersheds based on streamflow and suspended sediment discharge measurements. *Soil Technol* 11:57–69. [https://doi.org/10.1016/S0933-3630\(96\)00115-8](https://doi.org/10.1016/S0933-3630(96)00115-8)
- Cox NJ, Warburton J, Armstrong A, Holliday VJ (2008) Fitting concentration and load rating curves with generalized linear models. *Earth Surf Proc Land* 33:25–39. <https://doi.org/10.1002/esp.1523>
- Crowder DW, Demissie M, Markus M (2007) The accuracy of sediment loads when log transformation produces nonlinear sediment load discharge relationships. *J Hydrol* 336:250–268. <https://doi.org/10.1016/j.jhydrol.2006.12.024>
- De Girolamo AM, Pappagallo G, Lo Porto A (2015) Temporal variability of suspended sediment transport and rating curves in a Mediterranean river basin: the Celone (SE Italy). *CATENA* 128:135–143. <https://doi.org/10.1016/j.catena.2014.09.020>
- DiCenzo PD, Luk S (1997) Gully erosion and sediment transport in a small subtropical catchment. *CATENA* 29:161–176. [https://doi.org/10.1016/S0341-8162\(96\)00053-7](https://doi.org/10.1016/S0341-8162(96)00053-7)
- Dickinson WT (1981) Accuracy and precision of suspended loads. IAHS Publication No. 133. IAHS, Wallingford, pp 195–202
- Dijkman J (1978) Some characteristics of the USP–61 and Delft Bottle. Report No. 5–78. Delft University of Technology, The Netherlands
- Dijkman J (1981) Investigation of characteristic parameters of Delft Bottle. Report S362. Delft University of Technology, The Netherlands
- Douglas I (1971) Comments on the determination of fluvial sediment discharge. *Aust Geogr Stud* 9:172–176
- Duan N (1983) Smearing estimate: a nonparametric retransformation method. *J Am Stat Assoc* 78(383):605–610. <https://doi.org/10.1080/01621459.1983.10478017>
- Efthimiou N (2019) The role of sediment rating curve development methodology on river load modeling. *Environ Monit Assess* 191:108–126
- Efthimiou N, Lykoudi E, Psomiadis E (2020) Inherent relationship of the USLE, RUSLE Topographic Factor Algorithms and its impact on soil erosion modelling. *Hydrolog Sci J* 65(11):1879–1893. <https://doi.org/10.1080/02626667.2020.1784423>
- Efthimiou N, Markonis Y, Sklenicka P (2022) Magnitude–frequency analysis of coarse suspended sediment discharges in northwestern Greece. *Hydrolog Sci J* 67(7):1096–1113. <https://doi.org/10.1080/02626667.2022.2063726>
- Einstein HA (1948) Determination of rates of bed-load measurement. In: Proceedings of the Federal Inter-agency Sedimentation Conference. USDI, Washington (DC)

- Einstein HA (1950) The bed-load function for sediment transportation in open channel flows. Technical Bulletin No. 1026. USDA-SCS, Washington (DC)
- Einstein HA (1964) River sedimentation. In: Chow VT (ed) Handbook of applied hydrology, vol 17. McGraw-Hill, New York (NY), pp 35–67
- Ellison CA, Savage BE, Johnson GD (2014) Suspended-sediment concentrations, loads, total suspended solids, turbidity, and particle-size fractions for selected rivers. Minnesota, 2007 through 2011. Scientific investigations Report 2013–5205. USGS, Reston. <https://doi.org/10.3133/sir20135205>
- EUROSTAT (2014) Agri-environmental indicator – soil cover. https://ec.europa.eu/eurostat/statisticsexplained/index.php/Agri-environmental_indicator_-_soil_cover. Accessed 2 December 2023
- Everett JR, Morisawa M, Short MN (1986) Tectonic landforms. In: Short NM, Blair RW (eds) Geomorphology from space: a global overview of regional landforms. NASA, Washington (DC), pp 27–185
- Faust D, Schmidt M (2009) Soil erosion processes and sediment fluxes in a Mediterranean marl landscape, Campina De Cádiz, SW Spain. *Z Geomorphol* 53:247–265. <https://doi.org/10.1127/0372-8854/2009/0053-0247>
- Ferguson RI (1986) River loads underestimated by rating curves. *Water Resour Res* 22(1):74–76. <https://doi.org/10.1029/WR022i001p00074>
- Fleming G (1969) Mathematical simulation in hydrology and sediment transport. Strathclyde, UK
- Freund RJ, Wilson WJ, Sa P (2006) Regression analysis-statistical modeling of a response variable. Academic, Burlington
- Gao P (2008) Understanding watershed suspended sediment transport. *Prog Phys Geog* 32(3):243–263. <https://doi.org/10.1177/0309133308094849>
- Gao P, Puckett J (2012) A new approach for linking event-based upland sediment sources to downstream suspended sediment transport. *Earth Surf Proc Land* 37(2):169–179. <https://doi.org/10.1002/esp.2229>
- Gao P, Pasternack GB, Bali KM, Wallender WW (2007) Suspended-sediment transport in an intensively cultivated watershed in southeastern California. *CATENA* 69(3):239–252. <https://doi.org/10.1016/j.catena.2006.06.002>
- Gettel M, Gulliver JS, Kayhanian M, DeGroot G, Brand J, Mohsenic O, Erickson AJ (2011) Improving suspended sediment measurements by automatic samplers. *J Environ Monit* 13(10):2703–2709. <https://doi.org/10.1039/C1EM10258C>
- Gilbert KG (1914) The transportation of debris by running water. USGS Professional Paper 86. <https://doi.org/10.3133/pp86>. US Government Printing Office, Washington (DC)
- Glysson DG (1987) Sediment-transport curves. USGS Open-File Rep 87–218. <https://doi.org/10.3133/ofr87218>
- Gray JR, Gartner JW (2009) Technological advances in suspended-sediment surrogate monitoring. *Water Resour Res* 45(4). <https://doi.org/10.1029/2008WR007063>. W00D29
- Gregory KJ, Walling DE (1973) Drainage basin form and process. A geomorphological approach. Edward Arnold, London
- Gupta SK, Tyagi J, Sharma G, Jethoo AS, Singh PK (2019) An event-based sediment yield and runoff modeling using Soil Moisture Balance/Budgeting (SMB) method. *Water Resour Manag* 33:3721–3741. <https://doi.org/10.1007/s11269-019-02329-1>
- Gurnell AM (1987) Suspended sediment. In: Gurnell AM, Clark MJ (eds) Glacio-fluvial sediment. Transfer Wiley, Chichester, pp 305–354
- Guzman CD, Tilahun SA, Zegeye AD, Steenhuis TS (2013) Suspended sediment concentration–discharge relationships in the (sub-) humid Ethiopian highlands. *Hydrol Earth Syst Sc* 17:1067–1077. <https://doi.org/10.5194/hess-17-1067-2013>
- Hansen D, Bray D (1987) Generation of annual suspended sediment loads for the Kennebecasis using sediment rating curves. In: Proceedings of the 8th Canadian Hydrotechnology Conference, May 1987 Quebec. Canadian Society of Civil Engineers
- Hatzianastassiou N, Katsoulis B, Pnevmatikos J, Antakis V (2008) Spatial and temporal variation of precipitation in Greece and surrounding regions based on global precipitation climatology project data. *J Clim* 21:1349–1370. <https://doi.org/10.1175/2007JCLI11682.1>
- Herman EK, Toran L, White WB (2008) Threshold events in spring discharge: evidence from sediment and continuous water level measurement. *J Hydrol* 351:98–106. <https://doi.org/10.1016/j.jhydrol.2007.12.001>
- Horowitz AJ (2003) An evaluation of sediment rating curves for estimating suspended sediment concentrations for subsequent flux calculations. *Hydrol Process* 17(17):3387–3409. <https://doi.org/10.1002/hyp.1299>
- Hu B, Wang H, Yang Z, Sun X (2011) Temporal and spatial variations of sediment rating curves in the Changjiang (Yangtze River) basin and their implications. *Quatern Int* 230:34–43. <https://doi.org/10.1016/j.quaint.2009.08.018>

- Jain SK (2001) Development of integrated sediment rating curves using ANNs. *J Hydraul Eng* 127(1):30–37. [https://doi.org/10.1061/\(ASCE\)0733-9429\(2001\)127:1\(30\)](https://doi.org/10.1061/(ASCE)0733-9429(2001)127:1(30))
- Jansson MB (1996) Estimating a sediment rating curve of the Reventazon River at Palomo using logged mean loads within discharge classes. *J Hydrol* 183:227–241. [https://doi.org/10.1016/0022-1694\(95\)02988-5](https://doi.org/10.1016/0022-1694(95)02988-5)
- Jones KR (1981) Arid zone hydrology for agricultural development. FAO Irrigation and Drainage Paper No. 37. FAO Publications Division, Rome
- Juez C, Nadal-Romero E (2020) Long-term temporal structure of catchment sediment response to precipitation in a humid mountain badland area. *J Hydrol* 125723. <https://doi.org/10.1016/j.jhydrol.2020.125723>
- Juez C, Hassan MA, Franca MJ (2018) The origin of fine sediment determines the observations of suspended sediment fluxes under unsteady flow conditions. *Water Resour Res* 54(8):5654–5669. <https://doi.org/10.1029/2018WR022982>
- Karalis S, Karymbalis E, Mamassis N (2018) Models for sediment yield in mountainous Greek catchments. *Geomorphology* 322:76–88. <https://doi.org/10.1016/j.geomorph.2018.08.035>
- Kavian A, Dodangeh S, Abdollahi Z (2016) Annual suspended sediment concentration frequency analysis in Sefidroud basin, Iran. *Model Earth Syst Env* 2(1):1–10. <https://doi.org/10.1007/s40808-016-0101-2>
- Kennedy RG (1895) The prevention of silting in irrigation canals. Minutes of the Proceedings Institute of Civil Engineers 189:291–290
- Klein M (1984) Anti-clockwise hysteresis in suspended sediment concentration during individual storms: Holberck catchment; Yorkire, England. *CATENA* 11:251–257. [https://doi.org/10.1016/0341-8162\(84\)90014-6](https://doi.org/10.1016/0341-8162(84)90014-6)
- Koch RW, Smillie GM (1986) Bias in hydrologic prediction using log-transformed regression models. *Water Resour Bull* 22(5):717–723. <https://doi.org/10.1111/j.1752-1688.1986.tb00744.x>
- Kosmas C, Danalatos N, Kosmopoulou P (2001) Soil erosion in Greece. In: Boardman J, Poesen J (eds) *Soil erosion*. Wiley, Chichester, pp 279–288
- Kottek M, Grieser J, Beck C, Rudolf B, Rubel F (2006) World Map of the Köppen-Geiger climate classification updated. *Meteorol Z* 15(3):259–263. <https://doi.org/10.1127/0941-2948/2006/0130>
- Koulouri M, Giourga C (2007) Land abandonment and slope gradient as key factors of soil erosion in Mediterranean terraced lands. *CATENA* 69(3):274–281. <https://doi.org/10.1016/j.catena.2006.07.001>
- Koutsyiannis D (2000) Broken line smoothing: a simple method for interpolating and smoothing data series. *Environ Modell Softw* 15(2):139–149. [https://doi.org/10.1016/S1364-8152\(99\)00026-2](https://doi.org/10.1016/S1364-8152(99)00026-2)
- Koutsyiannis D, Tarla K (1987) Sediment yield estimations in Greece. *Technica Chronica A* –7(3):127–154 (in Greek)
- Kronvang B, Laubel A, Grant R (1997) Suspended sediment and particulate phosphorus transport and delivery pathways in an arable catchment, Gelbaek stream. *Denmark Hydrol Process* 11:627–642. [https://doi.org/10.1002/\(SICI\)1099-1085\(199705\)11:6%3C627::AID-HYP481%3E;3.CO;2-E](https://doi.org/10.1002/(SICI)1099-1085(199705)11:6%3C627::AID-HYP481%3E;3.CO;2-E)
- Kuhnle RA, Simon A (2000) Evaluation of sediment transport data for clean sediment TMDLs. USDA ARS, Oxford (MS)
- Kuhnle RA, Bingner RL, Foster GR, Grissinger EH (1996) Effect of land use changes on sediment transport in Goodwin Creek. *Water Resour Res* 32(10):3189–3196. <https://doi.org/10.1029/96WR02104>
- Kumar A, Kumar P, Singh VK (2019) Evaluating different machine learning models for runoff and suspended Sediment Simulation. *Water Resour Manag* 33:1217–1231. <https://doi.org/10.1007/s11269-018-2178-z>
- Lane EW (1937) Stable channels in erodible materials. *Trans ASCE* 102:123–142
- Lane EW (1955) Design of stable canals. *Trans ASCE* 120:1234–1260
- Lane EW, Kalinske A (1941) Engineering calculation of suspended sediment. *Trans AGU* 20(3):603–607. <https://doi.org/10.1029/TR022i003p00603>
- Laubel AR, Kronvang B, Larsen SE, Pedersen ML, Svendsen LM (2000) Bank erosion as a source of sediment and phosphorus delivery to small Danish streams. IAHS Publication No. 263. IAHS, Wallingford, pp 75–82
- Lecce SA, Pease PP, Gares PA, Wang J (2006) Seasonal controls on sediment delivery in a small coastal plain watershed, North Carolina, USA. *Geomorphology* 73(3–4):246–260. <https://doi.org/10.1016/j.geomorph.2005.05.017>
- Lenzi MA, Mao L, Comiti F (2003) Interannual variation of suspended sediment load and sediment yield in an alpine catchment. *Hydrolog Sci J* 48(6):899–915. <https://doi.org/10.1623/hysj.48.6.899.51425>
- Leopold LB, Maddock T (1953) The hydraulic geometry of stream channel and some physiographic implications. USGS Prof Paper 282–284. <https://doi.org/10.3133/pp252>. US Government Printing Office, Washington (DC)
- Lewis J (1996) Turbidity-controlled suspended sediment sampling for runoff-event load estimation. *Water Resour Res* 32(7):2299–2310. <https://doi.org/10.1029/96WR00991>
- Lindley ES (1919) Regime channels. In: Proceedings of the Punjab Engineering Congress, Punjab Engineering Society, Lahore, India 7:63–74

- Livadas GK (1976) Book 5: the climate of Greece. Lessons of climatology. Aristotle University, Thessaloniki, p 115. (in Greek)
- Lloyd D, Koenings JP, Laperriere JD (1987) Effects of turbidity in fresh waters of Alaska. *North Am J Fish Manag* 7(1):18–33. [https://doi.org/10.1577/1548-8659\(1987\)7%3C;18:EOTIFW%3E;2.0.CO;2](https://doi.org/10.1577/1548-8659(1987)7%3C;18:EOTIFW%3E;2.0.CO;2)
- Lohani AK, Goel NK, Bhatia KKS (2007) Deriving stage-discharge-sediment concentration relationships using fuzzy logic. *Hydrolog Sci J* 52(4):793–807. <https://doi.org/10.1623/hysj.52.4.793>
- Mahmood K (1987) Reservoir sedimentation: impact, extent and mitigation. Technical paper No.71. The World Bank, Washington (DC)
- Mao L, Carrillo R (2017) Temporal dynamics of suspended sediment transport in a glacierized Andean basin. *Geomorphology* 287:116–125. <https://doi.org/10.1016/j.geomorph.2016.02.003>
- Mao L, Cavalli M, Comiti F, Marchi L, Lenzi MA, Arattano M (2009) Sediment transfer processes in two alpine catchments of contrasting morphological settings. *J Hydrol* 364(1–2):88–98. <https://doi.org/10.1016/j.jhydrol.2008.10.021>
- Mariani PP, dos Reis Castro NM, Sari V, Schmitt TC, Pedrollo OC (2024) Different infiltration methods for SWAT model seasonal calibration of flow and sediment production. *Water Resour Manag* 38:303–322. <https://doi.org/10.1007/s11269-023-03671-1>
- Markonis Y, Batelis SC, Dimakos Y, Moschou EC, Koutsoyiannis D (2017) Temporal and spatial variability of rainfall over Greece. *Theor Appl Climatol* 130(1–2):217–232. <https://doi.org/10.1007/s00704-016-1878-7>
- Martinez-Mena M, Castillo V, Albaladejo J (2001) Hydrological and erosional response to natural rainfall in a semi-arid area of south-east Spain. *Hydrol Process* 15:557–571. <https://doi.org/10.1002/hyp.146>
- McBean EA, Al-Nassri S (1988) Uncertainty in suspended sediment transport curves. *J Hydraul Eng* 114(1):63–74. [https://doi.org/10.1061/\(ASCE\)0733-9429\(1988\)114:1\(63\)](https://doi.org/10.1061/(ASCE)0733-9429(1988)114:1(63))
- Meyer-Peter E, Müller R (1948) Formulas for bed-load transport. In: Proceedings of the 2nd meeting of the IAHSR, 7–9 June, Stockholm. <http://resolver.tudelft.nl/uuid:4fda9b61-be28-4703-ab06-43cdc2a21bd7>
- Migiros G, Stournaras G, Stamatis G et al (2008) Geological and tectonic study of the fissured rocks of the Hellenides and their hydrogeological pattern. In: Migiros G, Stamatis G, Stournaras G (eds) Proceedings of the 8th International Hydrogeological Congress of Greece – 3rd MEM Workshop on Fissured Rocks Hydrology, 8–10 October, Athens, 67–94
- Mimikou M (1982) An investigation of suspended sediment rating curves in western and northern Greece. *Hydrolog Sci J* 27(3):369–383. <https://doi.org/10.1080/02626668209491116>
- Molino B, De Vincenzo A, Mino A, Ambrosone L (2023) Long-term water management model for preserving sustainable useful capacity of reservoirs. *Water Resour Manag* 37:1789–1894. <https://doi.org/10.1007/s11269-023-03460-w>
- Moradinejad A (2024) Suspended load modeling of river using soft computing techniques. *Water Resour Manag* 38:1965–1986. <https://doi.org/10.1007/s11269-023-03722-7>
- Morgan RPC (2005) Soil erosion and conservation, 3rd edn. Blackwell Publishing Ltd, New Jersey
- Nadal-Romero E, Lasanta Martínez T, González-Hidalgo JC, de Luis M, García-Ruiz JM (2012) The effect of intense rainstorm events on the suspended sediment response under various land uses: the Aisa Valley Experimental Station. *Cuad De Investigacion Geografica* 38:27–47. <https://doi.org/10.18172/cig.1274>
- Nash JE, Sutcliffe JV (1970) River flow forecasting through conceptual models part I - A discussion of principles. *J Hydrol* 10(3):282–290. [https://doi.org/10.1016/0022-1694\(70\)90255-6](https://doi.org/10.1016/0022-1694(70)90255-6)
- Neal C, Neal M, Leeks GJL, Old G, Hill L, Wickham H (2006) Suspended sediment and particulate phosphorus in surface waters of the upper Thames Basin, UK. *J Hydrol* 330(1–2):142–154. <https://doi.org/10.1016/j.jhydrol.2006.04.016>
- Nicholas AP (2003) Modelling and monitoring flow and suspended sediment transport in lowland river flood plain environments. IAHS Publication No. 283. IAHS Press, Wallingford, pp 45–54
- Panagos P, Ballabio C, Borrelli P, Meusburger K (2016) Spatio-temporal analysis of rainfall erosivity and erosivity density in Greece. *CATENA* 137:161–172. <https://doi.org/10.1016/j.catena.2015.09.015>
- Panagos P, Matthews F, Patault E et al (2024) Understanding the cost of soil erosion: an assessment of the sediment removal costs from the reservoirs of the European Union. *J Clean Prod* 434:140183. <https://doi.org/10.1016/j.jclepro.2023.140183>
- Park J (1992) Suspended sediment transport in a mountainous catchment. *Sci Rep Inst Geoscience Univ Tsukuba A* 13:137–197
- Paschalidis G, Iordanidis I, Anagnostopoulos P (2021) Discharge and sediment transport modeling before and after the construction of a dam at the Inlet of a Basin. *Environ Processes* 8:1187–1212. <https://doi.org/10.1007/s40710-021-00534-y>
- Paul PK, Goswami A, Rudra RP, Goel PK, Daggupati P (2024) Exploring the trends in sediment and phosphorus concentrations and loads in part of the Canadian Great Lakes Basin. *Environ Processes* 11:30. <https://doi.org/10.1007/s40710-024-00710-w>

- Peters-Kümmerly BE (1973) Investigations into the composition and transport of suspended matter in some Swiss rivers. *Geogr Helv* 28(3):137–151 (in German). <https://doi.org/10.5194/gh-28-137-1973>
- Phillips JM, Webb BW, Walling DE, Leeks GJL (1999) Estimating the suspended sediment loads of rivers in the LOIS study area using infrequent samples. *Hydrol Process* 13(7):1035–1050. [https://doi.org/10.1002/\(SICI\)1099-1085\(199905\)13:7%3C:1035::AID-HYP788%3E;3.0.CO;2-K](https://doi.org/10.1002/(SICI)1099-1085(199905)13:7%3C:1035::AID-HYP788%3E;3.0.CO;2-K)
- Pineiro G, Perelman S, Guerschman JP, Paruelo JM (2008) How to evaluate models: observed vs. predicted or predicted vs. Observed? *Ecol Model* 216:316–322. <https://doi.org/10.1016/j.ecolmodel.2008.05.006>
- Poesen J, Hooke J (1997) Erosion, flooding and channel management in Mediterranean environments of southern Europe. *Prog Phys Geogr* 21(2):157–199. <https://doi.org/10.1177/030913339702100201>
- Polykretis C, Alexakis D, Grillakis MG, Manoudakis S (2020) Assessment of Intra-annual and Inter-annual variabilities of Soil Erosion in Crete Island (Greece) by incorporating the dynamic nature of R and C-Factors in RUSLE Modeling. *Remote Sens-Basel* 12:2439. <https://doi.org/10.3390/rs12152439>
- Poulos S, Collins M, Evans G (1996) Water-sediment fluxes of Greek rivers, southeastern Alpine Europe: annual yields, seasonal variability, delta formation and human impact. *Z Geomorphol* 40(2):243–261. <https://doi.org/10.1127/zfg/40/1996/243>
- Prestegard KL (1988) Morphological controls on sediment delivery pathways. IAHS Publication No. 174. IAHS, Wallingford, pp 533–540
- Ramalingam S, Chandra V (2019) Experimental investigation of water temperature influence on suspended sediment concentration. *Environ Processes* 6:511–523. <https://doi.org/10.1007/s40710-019-00371-0>
- Rasmussen PP, Gray JR, Glysson D, Ziegler AC (2009) Guidelines and procedures for computing time-series suspended-sediment concentration and loads from in-stream turbidity-sensor and streamflow data. *USGS Techniques Methods* 3–C4
- Richards RP, Holloway J (1987) Monte Carlo studies of sampling strategies for estimating tributary loads. *Water Resour Res* 23(10):1939–1948. <https://doi.org/10.1029/WR023i010p01939>
- Rieger WA, Olive LJ, Gippel CJ (1988) Channel sediment behaviour as a basis for modelling delivery processes. IAHS Publication No. 174. IAHS, Wallingford, pp 541–548
- Roberts G (1997) The influence of sampling frequency on streamflow chemical loads. *J Chart Inst Water E* 11:114–118. <https://doi.org/10.1111/j.1747-6593.1997.tb00101.x>
- Rodrigo-Comino J, Senciales JM, Ramos MC et al (2017) Understanding soil erosion processes in Mediterranean sloping vineyards (Montes De Málaga, Spain). *Geoderma* 296:47–59. <https://doi.org/10.1016/j.geoderma.2017.02.021>
- Rovira A, Batalla RJ (2006) Temporal distribution of suspended sediment transport in a Mediterranean basin: the Lower Tordera (NE SPAIN). *Geomorphology* 79(1–2):58–71. <https://doi.org/10.1016/j.geomorph.2005.09.016>
- Ryan SE, Porth LS (2007) A tutorial on the piecewise regression approach applied to bedload transport data. General Technical Report RMRS-GTR-189. USDA, Fort Collins. <https://doi.org/10.2737/RMRS-GTR-189>
- Schleiss AJ, Franca MJ, Juez C, De Cesare G (2016) Reservoir sedimentation. *J Hydraul Res* 54(6):595–614. <https://doi.org/10.1080/00221686.2016.1225320>
- Schmidt S, Alewell C, Meusbürger K (2018) Mapping spatio-temporal dynamics of the cover and management factor (C-factor) for grasslands in Switzerland. *Remote Sens Environ* 211:89–104. <https://doi.org/10.1016/j.rse.2018.04.008>
- Schoklitsch A (1930) Manual of hydraulic engineering, 2nd edn. Springer, Vienna. (in German)
- Seeger M, Errea M-P, Arnáez J, Martí C, García-Ruiz JM (2004) Catchment soil moisture and rainfall characteristics as determinant factors for discharge/suspended sediment hysteretic loops in a small headwater catchment in the Spanish Pyrenees. *J Hydrol* 288:299–311. <https://doi.org/10.1016/j.jhydrol.2003.10.012>
- Sharma N, Zakaullah Md, Tiwari H, Kumar D (2015) Runoff and sediment yield modeling using ANN and support vector machines: a case study from Nepal watershed. *Model Earth Syst Env* 1(3):1–8. <https://doi.org/10.1007/s40808-015-0027-0>
- Singh KP, Durgunoglu A (1989) Developing accurate and reliable stream sediment yields. IAHS Publication No. 184. IAHS Press, Wallingford, pp 193–99
- Singh KP, Stenger R (2018) Indirect methods to Elucidate Water flows and Contaminant Transfer Pathways through Meso-scale catchments. – *Rev Environ Processes* 5:683–706. <https://doi.org/10.1007/s40710-018-0331->
- Sivakumar B, Wallender WW (2004) Deriving high-resolution sediment load data using a nonlinear deterministic approach. *Water Resour Res* 40. <https://doi.org/10.1029/2004WR003152>
- Sloff CJ (1991) Reservoir sedimentation: a literature survey. Communications on Hydraulic and Geotechnical Engineering. Report No. 91–2. Delft University of Technology, The Netherlands

- Steegeen A, Govers G, Nachtergaele J, Takken I, Beuselinck L, Poesen J (2000) Sediment export by water from an agricultural catchment in the Loam Belt of central Belgium. *Geomorphology* 33(1–2):25–36. [https://doi.org/10.1016/S0169-555X\(99\)00108-7](https://doi.org/10.1016/S0169-555X(99)00108-7)
- Steiger J, Gurnell AM, Ergenzinger P, Snelder D (2001) Sedimentation in the riparian zone of an incising river. *Earth Surf Proc Land* 26:91–108. [https://doi.org/10.1002/1096-9837\(200101\)26:1%3C;91::AID-ESP164%3E;3.0.CO;2-U](https://doi.org/10.1002/1096-9837(200101)26:1%3C;91::AID-ESP164%3E;3.0.CO;2-U)
- Sui J, Jackson P, Fang D (2005) Investigation of the sediment budget of a reach of the Yellow River in the Loess Plateau. IAHS Publication No. 291. IAHS, Wallingford, pp 172–181
- Syvitski JP, Morehead MD, Bahr DB, Mulder T (2000) Estimating fluvial sediment transport: the rating parameters. *Water Resour Res* 36(9):2747–2760. <https://doi.org/10.1029/2000WR900133>
- Syvitski JPM, Vörösmarty CJ, Kettner AJ, Green P (2005) Impact of humans on the flux of terrestrial sediment to the global coastal ocean. *Science* 308(5720):376–380. <https://doi.org/10.1126/science.1109454>
- Tanaka T, Marui A, Yasuhara M, Takayama S (1983) Reconnaissance study on suspended sediment discharge during a storm event. *Annual Rep Inst Geoscience Univ Tsukuba* 9:32–35
- USEPA (1996) National Water Quality Inventory Report to Congress. <https://www.epa.gov/waterdata/1996-national-water-quality-inventory-report-congress>. Accessed 9 January 2024
- USEPA (2017) National Water Quality Inventory Report to Congress. <https://www.epa.gov/waterdata/2017-national-water-quality-inventory-report-congress>. Accessed 6 January 2024
- van Rompaey AJJ, Verstraeten G, Van Oost K, Govers G, Poesen J (2001) Modelling mean annual sediment yield using a distributed approach. *Earth Surf Proc Land* 26(11):1221–1236. <https://doi.org/10.1002/esp.275>
- Walling DE (1977) Limitations of the rating curve technique for estimating suspended sediment loads, with particular reference to British rivers. *Proceedings of the Paris Symposium 'Erosion and Solid Matter Transport in Inland Waters'*. IAHS Publication No. 122 (pp. 34–48). IAHS Press, Wallingford
- Walling DE (1984) The sediment yields of African rivers. In: Walling DE, Foster SSD, Wurzel P (eds) *Challenges in African Hydrology*. *Proceedings of the Harare Symposium*. IAHS Publ. no. 144. pp 265–283
- Walling DE, Webb BW (1988) The reliability of rating curve estimates of suspended sediment yield: some further comments. In: *Proceedings of the Porto Alegre Symposium 'Sediment budgets'*, 11–15 December, Porto Alegre, Brazil. IAHS Publication No. 174, pp 337–350
- Waters TF (1995) *Sediments in streams: sources, biological effects and control*. American Fisheries Society, Bethesda
- Williams GP (1989) Sediment concentration versus water discharge during single hydrologic events in rivers. *J Hydrol* 111(1–4):89–106. [https://doi.org/10.1016/0022-1694\(89\)90254-0](https://doi.org/10.1016/0022-1694(89)90254-0)
- Woodward JC (1995) Patterns of erosion and suspended sediment yield in Mediterranean river basins. In: Foster IDL, Gurnell AM, Webb BW (eds) *Sediment and water quality in river catchments*. Wiley, Chichester, pp 365–389
- Wren DG, Barkdoll BD, Kuhnle RA, Derrow RW (2000) Field techniques for suspended-sediment measurement. *J Hydraul Eng* 126:97–104. [https://doi.org/10.1061/\(ASCE\)0733-9429\(2000\)126:2\(97\)](https://doi.org/10.1061/(ASCE)0733-9429(2000)126:2(97))
- Wright S, Parker G (2004) Flow resistance and suspended load in sand-bed rivers: simplified stratification model. *J Hydraul Eng* 130(8):796–805. [https://doi.org/10.1061/\(ASCE\)0733-9429\(2004\)130:8\(796\)](https://doi.org/10.1061/(ASCE)0733-9429(2004)130:8(796))
- Yang G, Chen Z, Yu F, Wang Z, Zhao Y, Wang Z (2007) Sediment rating parameters and their implications: Yangtze River, China. *Geomorphology* 85:166–175. <https://doi.org/10.1016/j.geomorph.2006.03.016>
- Yang L, Liu S, Tsoka S, Papageorgiou LG (2016) Mathematical programming for piecewise linear regression analysis. *Expert Syst Appl* 44:156–167. <https://doi.org/10.1016/j.eswa.2015.08.034>
- Zahiri J, Mollaei Z, Ansari MR (2020) Estimation of suspended sediment concentration by M5 Model Tree based on hydrological and Moderate Resolution Imaging Spectroradiometer (MODIS) Data. *Water Resour Manag* 34:3725–3737. <https://doi.org/10.1007/s11269-020-02577-6>